Chapter 1

Introduction

Aircraft flight accidents often result in disastrous consequences. This is why a major concern of aircraft companies is to prevent structural failures caused by environmental or fatigue problems (I. Trendafilova, 2005).

In flexible structures, a dangerous phenomenon encounters, called flutter, which subject to aerodynamic forces (Burnside, Joseph E., 2011). In this oscillatory condition, unsteady aerodynamics excites the structure natural frequencies at the airstream speed. This includes aircraft, bridges and buildings. Moreover, the interaction between the stiffness, aerodynamics and the structural inertial forces cause flutter. In aircrafts, with an increase in the speed of the air stream, inadequacy of the structural damping may increase to suppress the motion excited by the airstream forces which increase due to impartation of the aerodynamic energy to the structure. Structural failure can occur due to this vibration can cause. Hence, to design an aircraft wing, considering flutter characteristics is an essential part (Chad Herbert *et al*. 2011).

Additionally, the interaction between the motion of an aircraft structure and the aerodynamic load can also cause flutter. Sometimes, the instability in flutter may affect aircraft performance or even lead to the structural failure (L.Librescu, and P.Marzocca, 2002). Earlier, local stiffening and mass balancing were applied as traditional and passive ways of avoiding flutter. However, these methods are usually insufficient as they add mass to the structure (Zhoa, 2009).

In early 1970s, active flutter suppression as a new method was developed to overcome the insufficiency of the previous techniques so aircrafts can fly at a greater velocity than the flutter velocity.

“In active flutter suppression, flutter is suppressed through the pitching motions of the control surfaces actuated by an onboard automatic control system.” (Zhoa, 2009)

Afterwards, many advanced control strategies were developed and applied in the flutter suppression control systems design (Zhoa, 2009), such as robust control (J.H.Han, and J.Tani, 2006), optimal control (D.Borglund, and J.Kuttenkeuler, 2002), and adaptive control (M.Andrighettoni, and P.Mantegazza, 1998).

Furthermore, active vibration control has been applied to aircraft to increase performance, extending the operational region and decreasing structural mass (Kanai, K., 1985).

Another strategy which has been widely used in active vibration control is Positive Position Feedback (PPF) (Nima Mahmoodi, *et al*. 2010), for aerospace applications (Goh and Caughey, 1985). In this method, piezoelectric sensors and actuators are used for vibration control (Fanson and Caughey, 1990). Adaptive approaches have been included to PPF to improve the efficiency of the controller (Hu, 2008).

Aircraft experience many types of vibrations. Vibrations may be reciprocating, oscillating, or losing a position or state of equilibrium for any periodic motion of an elastic or rigid body. Generally, passengers only notice minor vibrations, such as noise and flexing of the wings, which are common and completely safe. However, there can be more serious, irregular vibrations. Aircraft engineers continue to study these vibrations improving performance and safety.

Linear differential equation models with constant coefficients were employed in many previously used models on vibration analysis (R Whalley, and M Ebrahimi, 1998). There are many design procedures available for these systems with single or multiple inputs and outputs, such as the time domain procedures by Collar A. R. and Simpson, A. (1987) and the frequency response methods discussed by Rao, S. S. (1986).

Attempts to validate any model for design purposes or analysis are necessary when model variations are introduced due to physical alterations such as pressure, temperature and velocity. Generally, a very time consuming procedure called linearization is used by selecting and evaluating the system model according to the desired steady state conditions. When many parameters are variable, it is almost impracticable to obtain the performance for all possible combinations of the parameters. Usually, design analysis is based on the worst case conditions models. Nevertheless, considering controller analysis in accordance with worst case situations is risky and unsafe as stability of the performance may not be assured (R Whalley, and M Ebrahimi, 1998).

Unfortunately, wing model's variations are usually complicated and extremely nonlinear and vary due to physical alterations such as velocity, temperature and pressure. Furthermore, the demand for high performance aircraft requires precise design, analysis and simulation studies in order to achieve specification requirements.

In the following analysis, this issue will be further discussed. The purpose of designing a controller for a wing arrangement will be demonstrated using multivariable system techniques to provide the desired operational performance enabling the regulation of flutter during low speed flight conditions.

There are many techniques such as least effort regulation (R Whalley, and M Ebrahimi, 1999), optimal control (Kalman R.E., 1960), and the Inverse Nyquist Array method (Rosenbrock, 1969) for aircraft wing controller design. In this paper, the design of the system will be based on least or minimum effort regulation by minimizing a performance index. The procedure includes two steps: an inner loop design and an outer loop design. The inner loop design provides the flexibility to improve the dynamic response of the wing system. The outer loop design is employed to provide specified disturbance suppression conditions and specified steady state output decoupling (R Whalley, and M Ebrahimi, 1999).

Simple transformation techniques enabling the establishment of a conventional pre and feedback compensator structure will be applied.

Additionally, the Nyquist array method will be investigated for this wing arrangement, for energy consumption and gain comparison purposes. In order to apply single input single output control method, the system transfer function matrix must be diagonally dominant. For this purpose, Gershgorin's band theorem will be used.

Eventually, the energy dissipation by these controllers will be computed and compared in order to prove that Least effort controller dissipates the least energy for this wing arrangement.

In general, this dissertation is organized as follows:

Chapter one gives an introduction regarding the flutter occurring in aircraft wings and the control strategies that can be applied for regulation purposes. It includes a brief summary of previous work.

Chapter two provides a literature review considering flutter and the control of aircraft wings. It addresses the subject of various control strategies applied to wing models such as optimal control (D.Borglund, and J.Kuttenkeuler, 2002), robust control (J.H.Han, and J.Tani, 2006) and adaptive control (M.Andrighettoni, and P.Mantegazza, 1998).

Chapter three concerns the introduction and analysis for aircraft wing models. The computation of the transfer function matrix for a wing assembly is also included.

Chapter four includes the Least Effort control strategy and the complete approach to obtain the inner and outer loop controllers. Inner loop calculations for a wing model at zero airstream velocity are also included.

Chapter five contains the design procedure for the compensator network for this wing arrangement. A mathematical derivation and analysis is included.

Chapter six includes an outline of the Nyquist array method for this wing model using a pre-compensator and proportional control. The Gershgorin’s band theorem is also included.

Chapter seven shows and discusses the results of the simulation for the Least effort control strategy.

Chapter eight contains the disturbance suppression results for the Least effort control strategy. The energy dissipation of the system model for various gain ratios for the Least effort control strategy is also included.

Chapter nine shows and discusses the results of the simulation for the Nyquist array method. The energy dissipation comparison of the system model for the Least effort control strategy and the Nyquist array method is also included.

Chapter ten presents a complete comparison study concerning the difficulties of each strategy.

Chapter eleven concludes the research and discusses the advantages and disadvantages of the selected methods for control purposes. In addition, a recommendation for future work is stated.

Chapter 2

Literature Review

Flutter is a dynamic instability condition, described in details by Theodorsen (1935)**,** and reported in 1916 (Kehoe, M. W., 1995) that can cause mechanical failure of aircraft wings. As aircraft design techniques develop by using lighter materials, in order to improve aircraft stability and fuel consumption, active flutter suppression becomes extremely important (Jeffrey M. Barker *et al.* 1999).

"Scientists and engineers studied flutter and developed theories for the cause and mathematical tools to analyze the behavior. In the 1920s and 1930s, unsteady aerodynamic theory was developed. Closed-form solutions to simple problems were studied in the 1940s and 1950s. In the next thirty years, strip theory aerodynamics, beam structural models, unsteady lifting surface methods (e.g. double-lattice) and finite element models expanded analysis capabilities. The advent of digital computers has further supported the development of other powerful methods. Disciplines involved in analyzing flutter include aerodynamics, structural finite element modeling, control theory and structural dynamics." (Chad Herbert *et al.* 2011)

To determine the performance of the aeroelastic systems, different techniques have been applied for structural modeling considering their own limitations. Structural modeling starts with simple models such as mass-spring model and continues to higher dimension models where analytical computational strategies or Finite Element method have been applied (Karpouzian G, and Librescu L., 1996) and (H. Haddadpour, and R.D. Firouz-Abadi, 2006).

The National Aeronautics and Space Administration (NASA) is one of the most important research centers in the design, control and development of high performance aircraft wings. In 1986, the U.S. Navy and NASA designed an oblique wing for an aircraft and implemented active control using Linear Quadratic Gaussian design techniques. A method of modal residualization was used to reduce the order of the controller used for flutter suppression from 24th order to 7th order (Burken *et al.* 1986).

The design process for this research involved (Burken *et al.* 1986):

1. Formulation of the state space model including independent wing actuators and s-plane approximations of the unsteady aerodynamics
2. Determination of full state optimal control law
3. Determination of robust feedback control law
4. Formulation of reduced order control law
5. Evaluation of a practical control law

An organized study for active flutter suppression of a high aspect-ratio wing with multiple control surfaces was presented (Zhoa, 2009) and (Barzegari, Mohammad M. 2012). Finite element methods were used to model the wing structure. Doublet lattice methods (E.Albano, and W.P.Rodden, 1969) were applied to model unsteady aerodynamic loads effecting on the leading and trailing edge control surfaces. The modal transformation of the structural equations and a minimum state approximation of an aerodynamic influence coefficient matrix were employed to construct the open loop equations with input delays. To suppress flutter of the time delayed system models, a dynamic controller was designed using H_∞ control theory framework, as shown in figure 2.1.

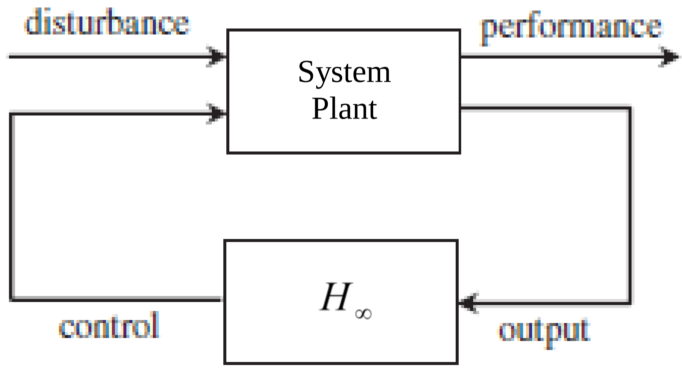

Figure 2.1, Block diagram of system plant with feedback controller H_∞ (Zhoa, 2009)

"The modern approach to characterizing closed-loop performance objectives is to measure the size of certain closed-loop transfer function matrices using various matrix norms. Matrix norms provide a measure of how large output signals can get for certain classes of input signals. Optimizing these types of performance objectives over the set of stabilizing controllers is the main thrust of recent optimal control theory, such as H_2 and H_∞ control." (Zhoa, 2009)

"In practical situations, the delay-independently stable region is usually a very small part of the parameter space of system. If the system parameters do not fall into the delay-independent stable region, the real part of at least one characteristic root changes its sign when the time delay varies. That is, the stability of the controlled system cannot keep unchanged with an increase of time delay. Such a change of stability with time delay is referred to as the stability switch." (Zhoa, 2009)

The stability of the closed loop system was tested by tracing the eigenvalues of the system. To demonstrate the suitability of the calculated critical time delay values, "(time delays at which the eigenvalues become purely imaginary are called critical time delays generate potential points for a stability switch of the system)" (Zhoa, 2009), a time delay can be gradually increased to see the changes in the stability of the system. For this purpose, time delays τ of 0.02, 0.03 and 0.0325 sec were tested, respectively. As shown in figure 2.2, the closed loop system is stable for both $\tau =$ 0.02,0.03 sec whereas instability arises for $\tau = 0.0325$ sec (Zhoa, 2009).

It was discovered that applying the infinitesimal generator approximation for the solution operator matrix for the eigenvalues of the system was useful to get the right critical time delay $\tau_c = 0.0315$ sec, at which the system became unstable (Zhoa, 2009).

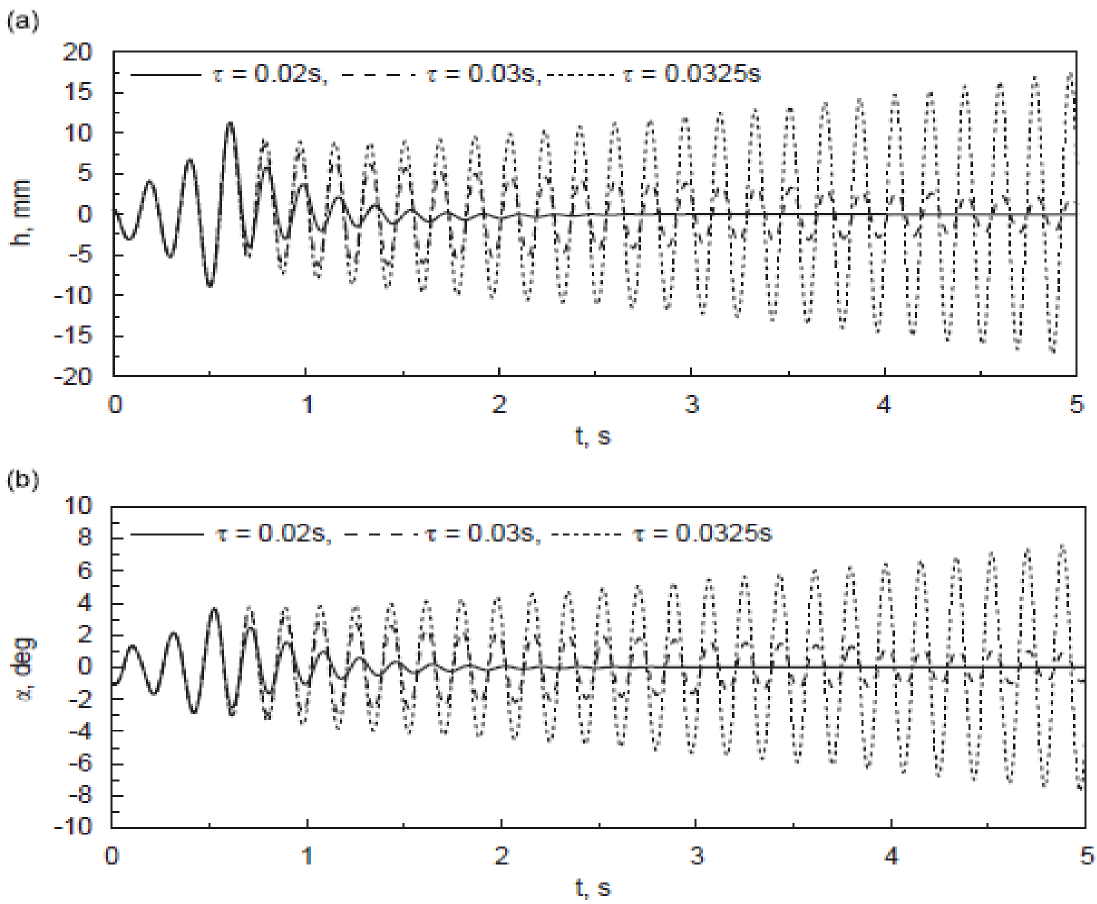

Figure 2.2, Time responses of the system at different time delays (a) vertical bending h deflection and (b) torsional angle of the elastic axis α (Zhoa, 2009)

Another research achieved successful results for vibration attenuation similar to (Zhoa, 2009) by designing a gain scheduled controller using linear fractional transformations. This method is a continuation of H_∞ control for systems that vary with measurable parameters such as Mach number, (speed of an object in relation to the speed of sound), and dynamic pressure. Time domain simulations showed the stability of the closed loop where both dynamic pressure and Mach number were allowed to vary whilst disturbances were existed. The closed loop system stability in the operating region was achieved by applying an optimized linear controller and the linear fractional gain-scheduled controller (Jeffrey M. Barker *et al.* 1999).

It was stated: “There are two main performance objectives for any flutter suppression system. The first is to extend the flutter boundary, that is, to use feedback control to stabilize the wing over a larger region of operating conditions. Secondarily, flutter control is used to suppress vibrations in the operating region where the wing is open loop stable. By allowing the controller to depend explicitly on Mach number and dynamic pressure, attaining improved closed-loop performance and stability should be possible.” (Jeffrey M. Barker *et al.* 1999)

Accordingly, parametric uncertainties were considered in both pitch stiffness and damping for adaptive control design to suppress limit cycle oscillations. Firstly, in accordance with partial feedback linearization for the wing section having a single trailing edge control surface, an adaptive controller was derived, as shown in figure 2.3. Simulation results showed that the damping uncertainty is proportional to control efficiency. Secondly, adaptive control was implemented using a structured model for an aeroelastic system with both trailing edge and leading edge control surfaces (Daochun Li *et al.* 2008).

For this purpose, a Structured Model Reference (SMR) using adaptive control law was derived. This method has been implemented for a specific structure by Akella and Junkins (1998), and used for suppressing the flutter of an aeroelastic system (J. Ko *et al.* 1998). Besides, considering the damping uncertainty, simulation results showed that the SMR adaptive controller was useful in the free, low air velocity. However, at higher velocities the positive effect of the controller reduced although the damping uncertainty caused the closed loop system flutter velocity to be greater (Daochun Li *et al.* 2008).

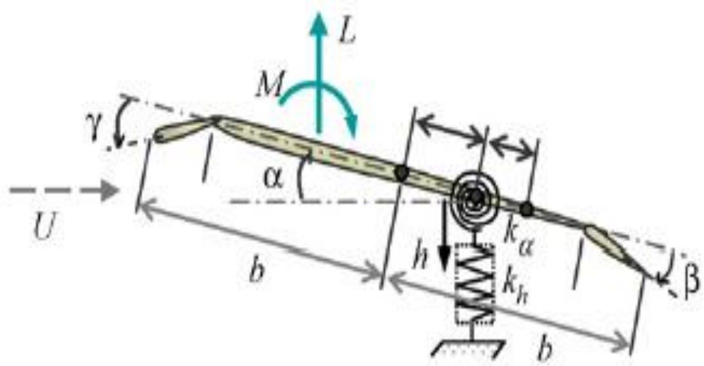

Figure 2.3, Aeroelastic model with leading and trailing edge control surfaces (Daochun Li *et al.* 2008)

In 2006, flutter was modeled using a simple spring mass system with two degree of freedom and aerodynamics forcing, as shown in figure 2.4, where K_h and K_a are representative of the bending and torsional stiffness of the wing about its elastic axis. For this purpose, the equation of motion for a 2-D wing model was derived to represent flutter prediction, as shown by Theodorson and Garrik (1940), for a straight wing of large span by giving it the inertial and geometric characteristics for the cross-section (Karthik Palaniappan *et al.* 2006).

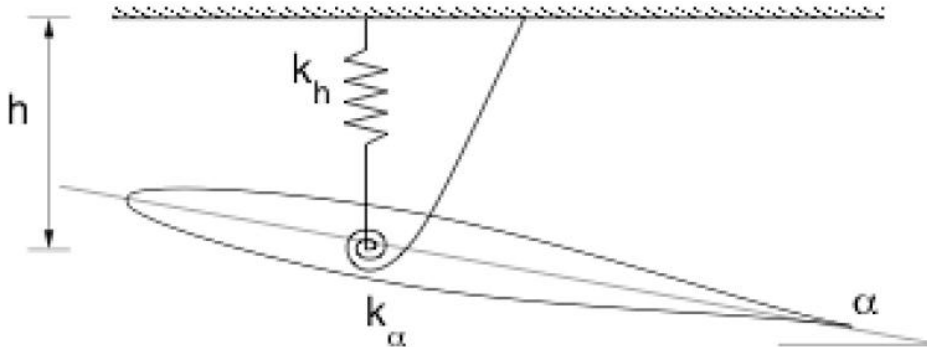

Figure 2.4, Typical Section Wing Model Geometry
(Karthik Palaniappan *et al.* 2006)

The dynamics of the system were represented in State Space form. An Adjoint method (Antony Jameson, 1988, and Siva Nadarajah, 2003) was used to obtain sensitivity matrix of the state vectors, with respect to the control variables. The objective of the problem was to control the given system to produce a final value of the state vector. For optimization purpose, the function including a positive definite weighting matrix was minimized (Karthik Palaniappan *et al.* 2006).

Moreover, to control flutter, regulation by means of air suction and blowing was used. This was based on deriving a feedback control law from a linearized model and solving the Riccati equation for the aero-structural system. The feedback matrix derived was tested on a nonlinear model and was found to effectively control the flutter (Karthik Palaniappan *et al.* 2006).

A new design approach called 'Reciprocal State Space' framework was introduced for vibration control problems of an aircraft wings where the state derivatives can be measured and fed back directly. Finite element methods and State Space were used for modeling the aircraft wing as shown in figure 2.5 (Yuan-Wei Tseng, and Rama K. Yedavalli, 1997).

Information on acceleration, velocity and displacement were obtained and fed back by applying integrators and accelerometers. In this framework to improve closed loop performance, the state and its derivative and integral may be fed back. Since accelerometers are widely used, this technique is useful in structural control (Yuan-Wei Tseng, and Rama K. Yedavalli, 1997).

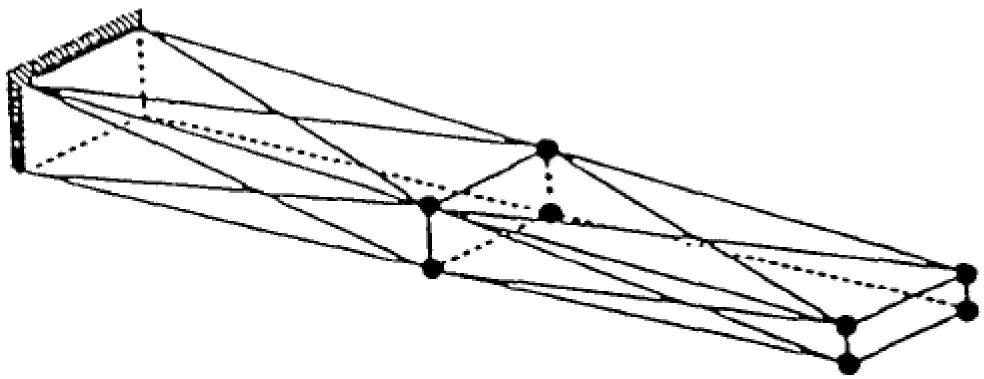

Figure 2.5, The wing box Finite Element model
(Yuan-Wei Tseng, and Rama K. Yedavalli, 1997)

“Recently, frequency-based least-squares (LS) estimators have found wide application in identifying aircraft flutter parameters. However, the frequency methods are often known to suffer from numerical difficulties when identifying a continuous-time model, especially, of broader frequency or higher order models.” (Tang Wei *et al.* 2008)

“A numerically robust LS estimator based on vector orthogonal polynomial is proposed to solve the numerical problem of multivariable systems and applied to the flutter testing. The key idea of this method is to represent the frequency response function (FRF) matrix, by a right matrix fractional description (RMFD) model, and expand the numerator and denominator polynomial matrices on a vector orthogonal basis.” (Tang Wei *et al.* 2008)

Consequently, an ideal numerical condition was achieved for linear least-squares estimator. Eventually, this method was verified by a flutter test on a wing model in a wind tunnel as shown in figure 2.6 and real flight flutter test of an aircraft (Tang Wei *et al.* 2008).

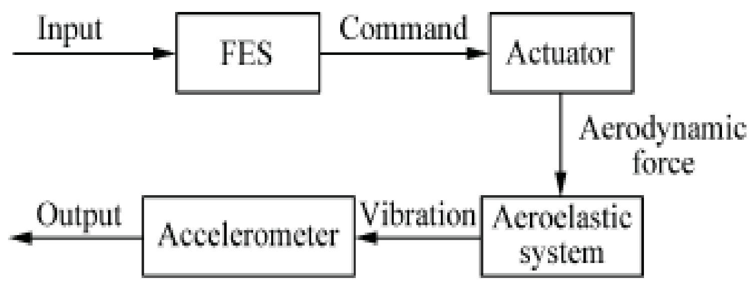

Figure 2.6, Flutter test schematic diagram
(Tang Wei *et al.* 2008)

Figure 2.6 depicts the typical setup of the flutter test. It is equipped with a flutter excitation system (FES), which is operated for structural excitation to insert programmed digital signals such as actuator sweep commands to the control system. The responses were measured by accelerometers located in the aircraft wingtips. In practice, the input signal for excitation is known beforehand and is free from noise. For simplicity, only the errors in the output were considered (Tang Wei *et al.* 2008).

In the past three decades, with the quick development of both control systems strategy and actuator techniques, an increase of interests in the active control of aircraft wing flutter was noticeable (Mingli Yu, and Haiyan Hu, 2012). The earlier hydraulic types of actuators for control surfaces were mainly used, as reviewed in Waszak and Fung (1996). Various new actuators have been implemented, with the improvement of practical materials and new theories such as using high performance linear motors to achieve the active flutter control for huge wings using wind tunnel, by Borglund, and Kuttenkeuler (2002).

Obtaining the transient response of systems from frequency response data was one of Rosenbrock's interests (Rosenbrock, 1958). Afterward, the multivariable control systems theory in the frequency domain was introduced. His papers include the transformations of linear constant system equations, the reduction of system matrices, and linear system theory (Rosenbrock, 1967). He presented the Nyquist and Inverse Nyquist Array method for multivariable control systems design which was done by reducing the system coupling assuring the diagonally dominance of the transfer function matrix model in 1969. Thereafter, single input single output theory could be simply applied.

Gershgorin's band theorem was used to investigate stability and diagonally dominance for the system transfer function matrix (Gershgorin, 1931). It states that, the system transfer function is diagonally dominant when the union of Gershgorin's bands does not enclose the origin of the complex plane. Additionally, when the union of Gershgorin's bands does not enclose the (-1,0) point, closed loop stability is attained (Munro, 1972).

The main problem of using Nyquist and Inverse Nyquist Array method is that of achieving diagonal dominance for the square system transfer function matrix. Many suggestions had been introduced regarding this problem such as an optimal constant diagonal scaling matrix which was suggested by Mees (1981) and Psedudo-diagonalisation technique by Hawkins (1972). Moreover, spectral factorization technique for decoupling the system, and then compensator relaxation would result in diagonally dominance (R Whalley, 1978).

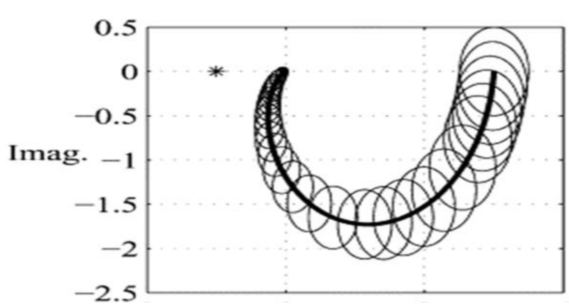

Figure 2.7, Gershgorin's bands

In last decades, the conventional Inverse Nyquist Array (INA) method was used by many engineers for the improvement of controllers for many processes (Koudstaal *et al.* 1981) and (Grujic, 1995). From a design point of view, such controllers seem acceptable, although instability in the closed loop performance may appear when modelling errors are existed. The robustness cannot be detected by INA, and may affect the diagonal dominance and significantly cause instability in the performance of multivariable control systems. Therefore, Arkun *et al.* (1984) presented Robust INA control methodology.

Dejan D. Ivezic´, and Trajko B. Petrovic (2003) used Robust Inverse Nyquist Array method for a milling circuit control design. The transfer function matrix of the system model was derived from the milling circuit diagram in equation 2.1 below.

$$\tilde{\mathbf{P}} = \begin{bmatrix} \tilde{\mathbf{P}}_{11} & \tilde{\mathbf{P}}_{12} \\ \tilde{\mathbf{P}}_{21} & \tilde{\mathbf{P}}_{22} \end{bmatrix} = \begin{pmatrix} \dfrac{-0.9362 \cdot e^{-350s}}{1164s+1} & \dfrac{(10.252s + 2.819 \cdot 10^{-3}) \cdot e^{-200s}}{80218s^2 + 652s + 1} \\ \dfrac{36.49}{792s+1} & \dfrac{1.1405}{179s+1} \end{pmatrix};$$

$$y = \tilde{\mathbf{P}}u; \qquad y = [y_1 y_2]^T; \quad u = [u_1 u_2]^T \qquad 2.1$$

The goal of their paper was to construct a practical system model. As the real environment varies due to disturbances and time, the control system is required to be able to resist these changes. For this purpose, the uncertainties with 10%, equation 2.2, were added to the transfer function matrix to be assumed for real process. Therefore, a set of transfer function matrix were obtained instead of single transfer function matrix, as approximations of the uncontrolled plant, which could cover all other transfer function matrices (Dejan D. Ivezic´, and Trajko B. Petrovic, 2003).

$$\mathbf{P} = \begin{bmatrix} \mathbf{P}_{11} & \mathbf{P}_{12} \\ \mathbf{P}_{21} & \mathbf{P}_{22} \end{bmatrix}$$

$$= \begin{bmatrix} \dfrac{-k_1 \cdot 0.9362 \cdot e^{-k_2 \cdot 350 \cdot s}}{1 + k_3 \cdot 1164 \cdot s} & \dfrac{(k_4 \cdot 2.819 \cdot 10^{-3} + k_5 \cdot 10.252 \cdot s) \cdot e^{-k_6 \cdot 200 \cdot s}}{1 + k_7 \cdot 652 \cdot s + k_8 \cdot 80218 \cdot s^2} \\ \dfrac{k_{10} \cdot 36.49}{1 + k_9 \cdot 792 \cdot s} & \dfrac{k_{12} \cdot 1.1405}{1 + k_{11} \cdot 179 \cdot s} \end{bmatrix}$$

$$k_i \in [0.9,\ 1.1], i = 1, \ldots, 12 \qquad 2.2$$

The uncertainty was easier to describe in terms of uncertainty in each elements of the transfer function matrix because the process model was obtained from experimental identification of the system. To satisfy the relation below, the upper boundary of additive uncertainty for each element in the transfer matrix was defined as:

$$|\mathbf{P}_{ij} - \tilde{\mathbf{P}}_{ij}| \leq |e_{ij}|, \forall i,\ j$$

for any change of uncertainty parameters which proves independency of each element in plant P, but confined to a disk with a specific radius in the Nyquist plane as shown in figure 2.8 (Dejan D. Ivezic´, and Trajko B. Petrovic, 2003).

The following notation will be used, as INA method requires inverse values of transfer matrixes defined above. (Symbol ^ denotes inversion):

$$\hat{\tilde{\mathbf{P}}} = \tilde{\mathbf{P}}^{-1}$$

$$\hat{\mathbf{P}} = \mathbf{P}^{-1}$$

$$\hat{\mathbf{E}} = \hat{\mathbf{P}} - \hat{\tilde{\mathbf{P}}} = (\tilde{\mathbf{P}} + \mathbf{E})^{-1} - \tilde{\mathbf{P}}^{-1}$$

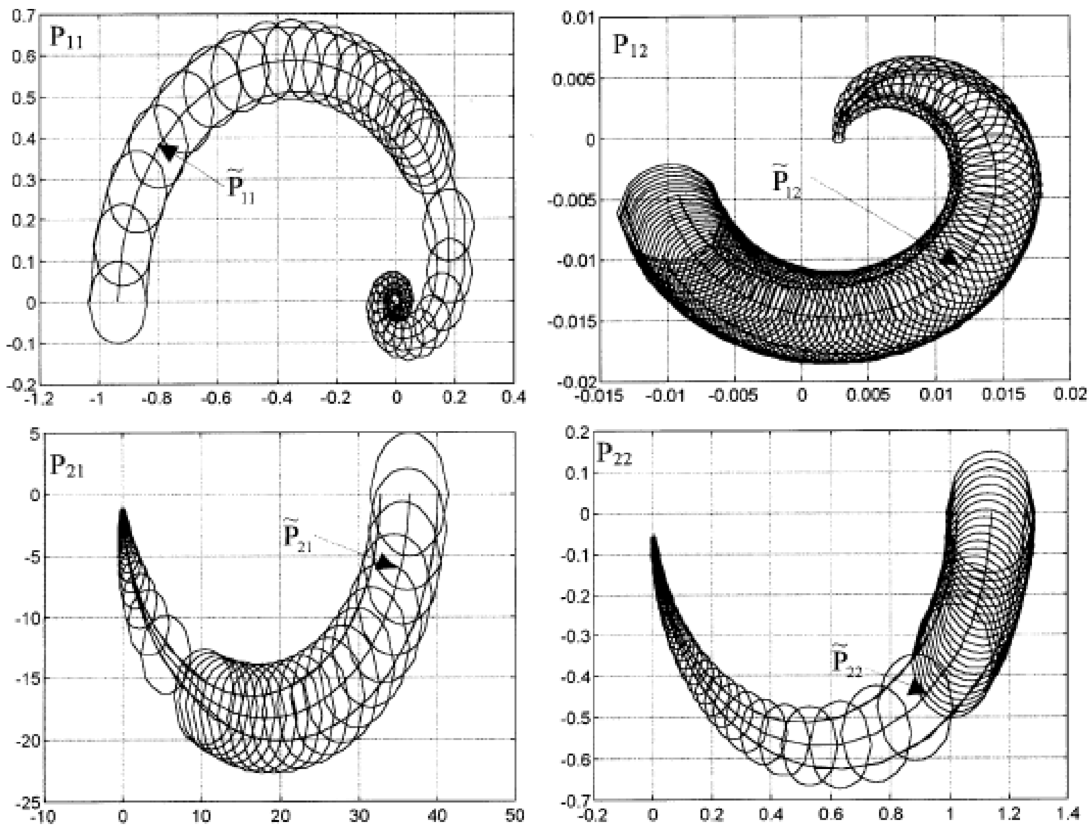

Figure 2.8, Uncertainties imposed for the Nyqist array of the nominal $\tilde{P}$ and perturbed P transfer matrix elements

(Dejan D. Ivezic´, and Trajko B. Petrovic, 2003)

The feedback system was constructed using model in figure 2.9 with a pre-compensator transfer function matrix which includes two matrices as below:

$$\mathbf{K} = \mathbf{K}_1 \mathbf{K}_2$$

where these must be selected so that the robust dominance feature of the system is assured as following:

$$\hat{Q} = \hat{\mathbf{K}}_1 \hat{\mathbf{P}} = \tilde{Q} + Q_E = \hat{\mathbf{K}}_1 \hat{\tilde{\mathbf{P}}} + \hat{\mathbf{K}}_1 \hat{\mathbf{E}}$$

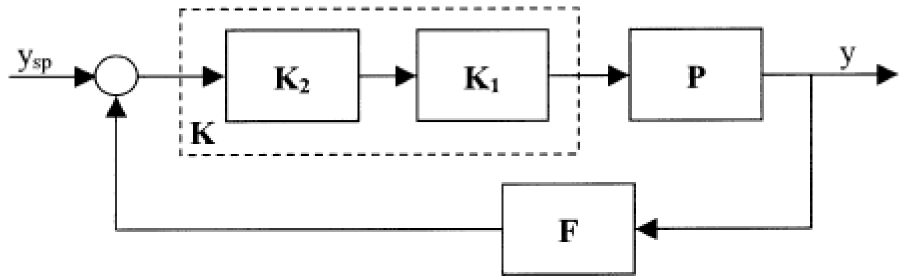

Figure 2.9, The standard multivariable feedback system

(Dejan D. Ivezic´, and Trajko B. Petrovic, 2003)

The first step for the robust INA controller design was providing diagonally dominance for the system as the Gershgorin’s row bands showed that the uncompensated system was not diagonally row dominant. The pre-compensator was calculated but this did not result to a stable, proper transfer function matrix. Adding post-compensators and solving optimization problems, as given in Arkun et al. (1984), were also tried by the authors to achieve column dominance but this also failed. Therefore, diagonally dominance investigation of the closed loop system was essential. The obtained compensators are as follows:

$$\mathbf{K}_1 = \begin{bmatrix} \left(\dfrac{-7219}{79}\right)\left(\dfrac{792s+1}{179s+1}\right) & 0 \\ \dfrac{204657}{70} & \left(\dfrac{36156}{53}\right)\left(\dfrac{\frac{4287}{14}s+1}{\frac{8145}{109}s+1}\right) \end{bmatrix}$$

$$\mathbf{F} = \begin{bmatrix} f_1 & 0 \\ 0 & f_2 \end{bmatrix} = \begin{bmatrix} 0.003 & 0 \\ 0 & 0.1 \end{bmatrix}$$

Appropriate dominance was achieved as robust Ostrowski row bands of the closed loop system can be seen in figure 2.10.

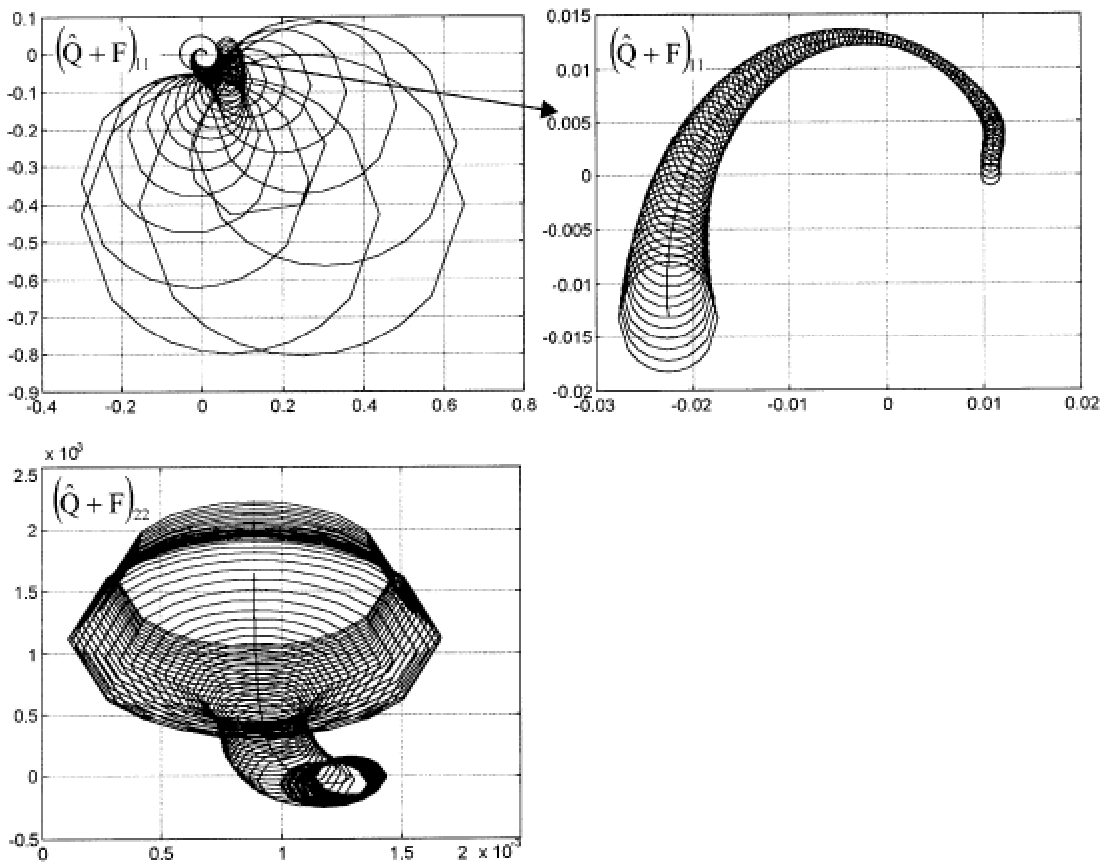

Figure 2.10, Diagonal elements INA with robust Ostrowski bands for compensated closed system

(Dejan D. Ivezic´, and Trajko B. Petrovic, 2003)

The second step was designing the single-input single-output SISO controllers for the diagonal transfer function obtained above. Achieving certain dynamic performances such as no overshoot and no steady-state error was the purpose of designing these controllers as below:

$$\mathbf{K}_2 = \begin{bmatrix} 1 + \dfrac{1}{150 \cdot s} & 0 \\ 0 & 0.3 + \dfrac{1}{500 \cdot s} \end{bmatrix}$$

In order to obtain the performance of the proposed robust controller, computer simulations were performed. The transient responses of the closed loop system using robust INA and some other methods such as classical PI controller, decentralized (DC) controller, RINA controller and previously designed Grujic´ (1995) INA controller were shown and compared in figures 2.11 and 2.12 (Dejan D. Ivezic´, and Trajko B. Petrovic, 2003).

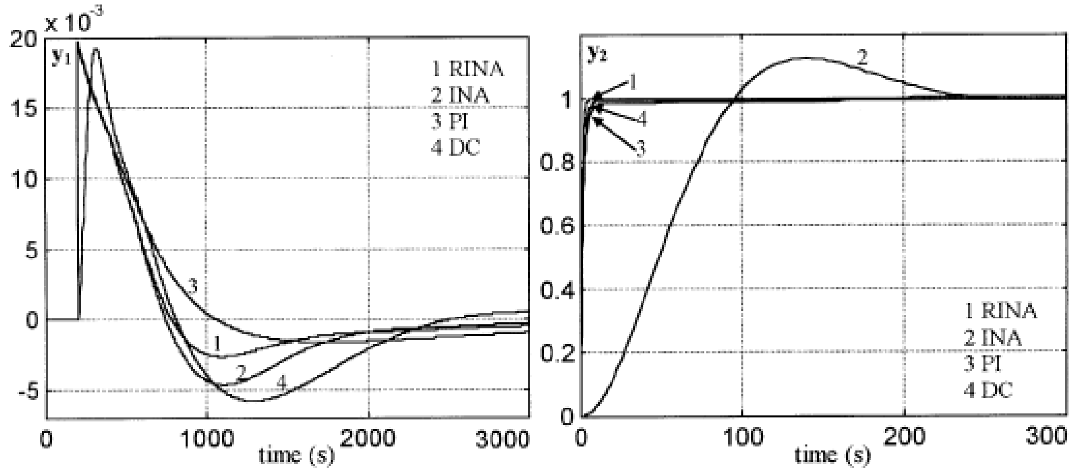

Figure 2.11, Transient responses of nominal plant following a unity step signal on second input (Dejan D. Ivezic´, and Trajko B. Petrovic, 2003)

Here the responses for the second input are only shown. The time responses of the nominal plant are shown in figure 2.12. The INA and RINA controllers responses for the closed loop system following a step signal, on second input show better performances in comparison with the DC and PI controllers where the dominance concept effect is noticeable in the system behavior. The presence of the time delays in the diagonal elements of the transfer matrix, whilst applying INA and RINA controllers for small amplitudes, prevents the realization of first output zero time responses following a step input on the second reference. A better performance was achieved by RINA controller than INA controller where the settling time is nearly 100 times shorter with no overshoot and similar behavior as DC and PI controllers (Dejan D. Ivezic´, and Trajko B. Petrovic, 2003).

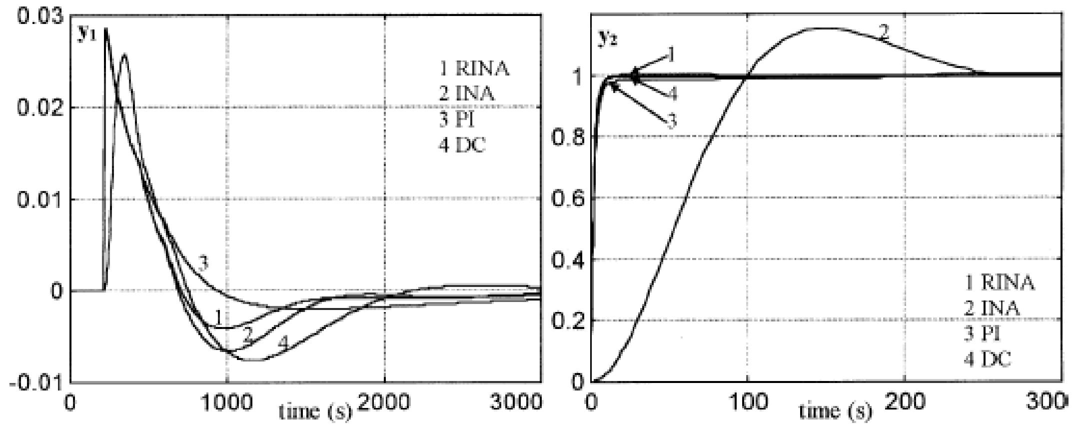

Figure 2.12, Transient responses of perturbed plant following a step signal on second input (Dejan D. Ivezic´, and Trajko B. Petrovic, 2003)

The worst case assumption time responses were computed for satisfactory verification of the robust responses and shown in figure 2.12. The perturbation plant model for selected combinations of maximal model parameters is:

$$\mathbf{P} = \begin{bmatrix} \dfrac{-1.1 \cdot 0.9362 \cdot e^{-1.1 \cdot 350 \cdot s}}{1 + 0.9 \cdot 1164 \cdot s} & \dfrac{(0.9 \cdot 2.819 \cdot 10^{-3} + 1.1 \cdot 10.252 \cdot s) \cdot e^{-1.1 \cdot 200 \cdot s}}{1 + 1.1 \cdot 652 \cdot s + 0.9 \cdot 80218 \cdot s^2} \\ \dfrac{1.1 \cdot 36.49}{1 + 0.9 \cdot 792 \cdot s} & \dfrac{0.9 \cdot 1.1405}{1 + 1.1 \cdot 179 \cdot s} \end{bmatrix}$$

"In real cases, uncertainties will be smaller, so that corresponding time responses will have similar features, though less distinctive." (Dejan D. Ivezic´, and Trajko B. Petrovic, 2003)

The closed loop system transient responses with perturbed plant and with RINA controller have similar performances as with the nominal plant as shown in figure 2.12. It is reasonably obvious that the plant model uncertainties were added in the design procedure (Dejan D. Ivezic´, and Trajko B. Petrovic, 2003).

In the classical INA design, avoiding uncertainties of the system is a disadvantage. The INA controller responses are slower with greater overshoots in comparison with the RINA controller. The reason is that the INA method considers only the nominal plant in providing the dominance of the system model. For that reason, the system dominance can be seriously damaged by changes in the nominal model (Dejan D. Ivezic´, and Trajko B. Petrovic, 2003).

The transient response of the closed loop system with RINA controller is better compared to the ones with DC and PI controllers and a perturbed plant. In addition, their responses are more satisfactory than the responses of INA controller compared to their poor responses in the nominal case (Dejan D. Ivezic´, and Trajko B. Petrovic, 2003).

Additionally, most aircraft have the control surface at the trailing edge of each wing. In 1998, the research of controlling the trailing edge was done by R Whalley, and M Ebrahimi (1998).

Figure 2.13 shows the cross section of the wing system that has been used in (R Whalley, and M Ebrahimi, 1998) to control the trailing edge of the aircraft. The inputs of this system were leading and trailing edge forces and the outputs were leading and trailing edge displacements.

As it can be seen, there was no point of employing leading edge aileron flaps. Therefore, a single input, trailing edge force, and two outputs, trailing edge and leading edge deflections, realization was used for the regulation problem (R Whalley, and M Ebrahimi, 1998).

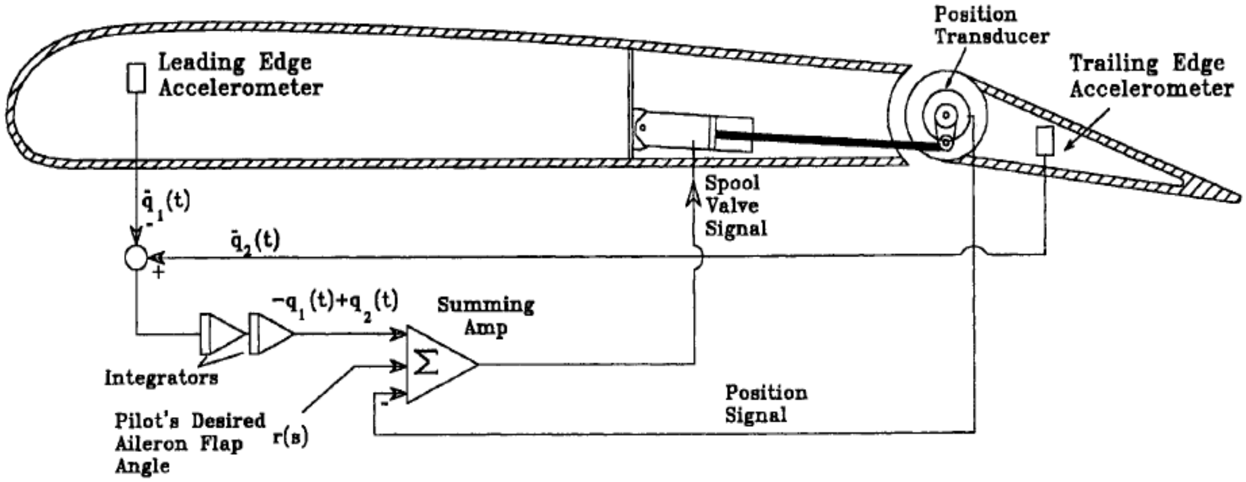

Figure 2.13, Cross section diagram of the wing system
(R Whalley, and M Ebrahimi, 1998)

The model for this wing arrangement was used by Frazer *et al.* (1963). Stability was investigated directly by tracing the roots of the characteristic equation of the transfer function of this system which was the determinant of the impedance transfer function for various values of velocity. It was clear that for this wing arrangement, flutter occurred at low airstream velocities. Furthermore, the poles of the system varied with changes in velocity, as shown in figure 2.14 (R Whalley, and M Ebrahimi, 1998).

Additionally, the controllability properties of the model were examined in order to ensure that all of the system's vibrational modes could be affected by controlled inputs through the trailing edge flaps. Similarly, the investigation of observability would be essential if only one output measurement was available, so that not all the vibrational modes could appear in this output. This consideration was important for the reason that "If an unobservable mode of vibration is slow, for example, or even unstable then it could not be measured and hence controlled by regenerative feedback." (R Whalley, and M Ebrahimi, 1998)

The controllability test proved to be positive across the desired speed range by applying the spectral factorization for the transfer function matrix and observability was simultaneously guaranteed, as both outputs were observable to feedback the system (R Whalley, and M Ebrahimi, 1998).

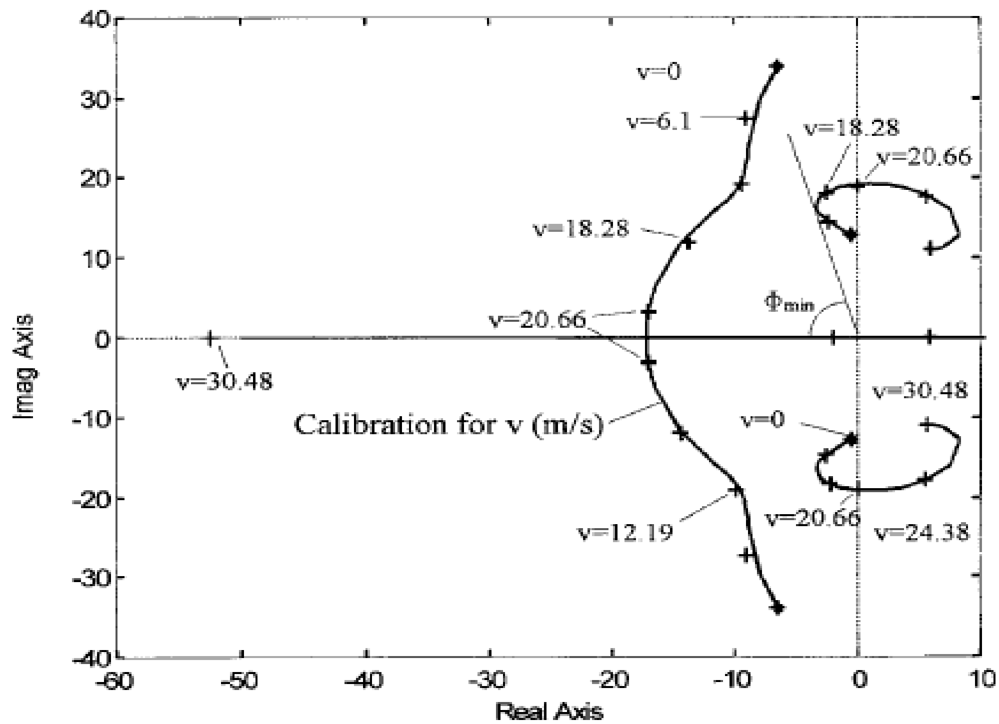

Figure 2.14, Pole velocity variations of the open loop wing model
(R Whalley, and M Ebrahimi, 1998)

To stabilize and reduce the variation in the deflections of this wing model, a restoring force was introduced. For example, to obtain corrective action, if roll control was utilized for the flap mechanism, then the wing force would increase proportionally to velocity squared. The following control law would show this effect:

$$f(s) = \begin{bmatrix} \alpha_1 \\ \alpha_2 \end{bmatrix} \left[r(s) - \begin{pmatrix} -1 & 1 \end{pmatrix} v^2 q(s) \right]$$

where $f(s)$ is the percentage changes of the leading edge and trailing edge, $q(s)$ is leading edge and trailing edge deflections and v is the wing steady state air velocity.

In order to find the displacements difference, this arrangement for control law was constructed. The values for α_1 and α_2 depend on the dimensions of the flaps. Furthermore, it was obtained by R Whalley and M Ebrahimi (1998) that the difference in the leading edge and trailing edge displacements can cause oscillatory behaviour for the wing assembly.

“Oscillatory flutter behaviour has its origins in repeated deflection differences at the leading and trailing edges, which increase cumulatively.” (R Whalley, and M Ebrahimi, 1998)

A control law was constructed in order to restore the forces which are proportional to the difference, in the leading edge and trailing edge deflections. The control law was tested on this wing model successfully. This approach provided a significant improvement in the wing performance. The wing was stable in the time and frequency domain responses at higher speeds and remained nearly similar to the open loop analysis at lower speeds (R Whalley, and M Ebrahimi, 1998).

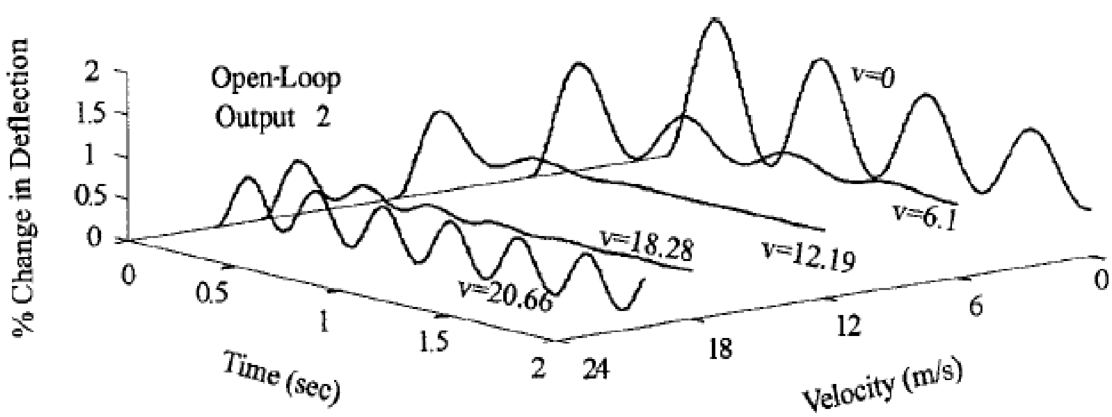

Figure 2.15, The open loop step response for the trailing edge deflection (R Whalley, and M Ebrahimi, 1998)

The open loop and closed loop time responses for this research have been shown in figures 2.15 and 2.16.

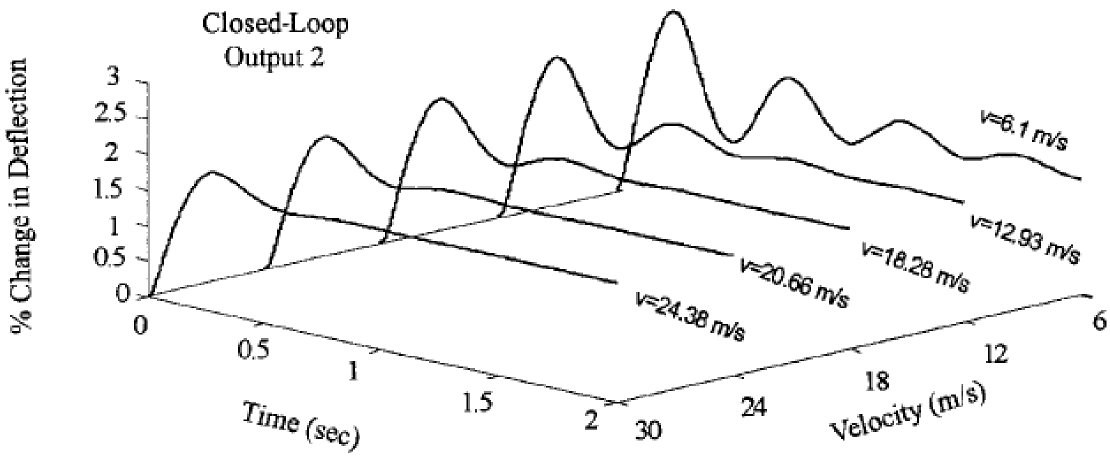

Figure 2.16, The closed loop step response for the trailing edge deflection
(R Whalley, and M Ebrahimi, 1998)

This paper is continuous of the work of R Whalley and M Ebrahimi (1998) with two inputs (leading and trailing edge forces) and two variable outputs (leading and trailing edge deflections) and the control surface is applied on both outputs whereas in R Whalley and M Ebrahimi's paper (1998), only the trailing edge had a control surface. In addition, Least effort control strategy is applied to control this MIMO (multiple input – multiple output) wing model instead of simple SIMO (single input – multiple output) feedback controller. Furthermore, the Nyquist array method is applied for comparison purposes.

Chapter 3

Research Methodology

Basically large variations are experienced by wing structures due to their frictional and stiffness factors which are proportional to the airstream velocity. According to equation 3.1, frictional parameter occurs in proportion to aircraft velocity and stiffness parameter occurs in proportion to aircraft velocity squared. Furthermore, there is a characteristic which is independent of the air velocity, and dependent of the damping, mass-inertia and stiffness features (R Whalley, and M Ebrahimi, 1998).

General transformed wing models with zero initial conditions could be formed as following, as shown by Collar, and Simpson (1987):

$$[A_n(s) + vBs + v^2C]q(s) = f(s) + \delta(s) \qquad 3.1$$

where

$A_n(s) =$ impedance matrix model relating leading and trailing edge characteristics

$B =$ damping ratio matrix

$C =$ stiffness matrix

$q(s)$ is the transformed output vector.

The transformed input force vector and the disturbance vector are given by $f(s)$ and $\delta(s)$ respectively.

The quadratic matrix below which has two degree of freedom is independent of velocity. Upon transformed, the model becomes:

$$A_2(s) = A_0 s^2 + A_1 s + A_2$$

where

A_0 = inertia matrix

A_1 = matrix of friction

A_2 = stiffness matrix

3.1. Analysis of the Wing Model

The scaled transformed wing matrix equation, from Frazer *et al*. (1963), with zero initial conditions, is:

$$[A_2(s) + vBs + v^2 C]q(s) = f(s) + \delta(s) \qquad 3.2$$

where $q(s)$ the transformed output vector (the leading and trailing edge deflections) and the input vectors of $f(s)$ as applied input force and $\delta(s)$ as applied disturbance force, where:

$$A_2(s) = A_0 s^2 + A_1 s + A_2 \qquad 3.3$$

with

$$A_0 = \begin{bmatrix} 5.443 & 2.907 \\ 2.907 & 4.743 \end{bmatrix}$$

$$A_1 = \begin{bmatrix} 29 & -9 \\ -9 & 9 \end{bmatrix}$$

$$A_2 = \begin{bmatrix} 2502.7 & -614.7 \\ -614.7 & 1487.7 \end{bmatrix} \qquad 3.4$$

The damping and stiffness matrices, as given in equation 3.5, are dependent of airstream velocity:

$$B = \begin{bmatrix} 0.4466 & 0.9076 \\ -0.3456 & 0.8064 \end{bmatrix}$$

$$C = \begin{bmatrix} -0.633 & 0.633 \\ -0.144 & 0.144 \end{bmatrix} \tag{3.5}$$

The percentage of the transformed leading and trailing edge deflections are:

$$q(s) = \begin{bmatrix} \%q_1(s) & \%q_2(s) \end{bmatrix}^T$$

and the percentage of applied forces at leading and trailing edges and disturbances, are as follows, respectively:

$$f(s) = \begin{bmatrix} \%f_l(s) & \%f_t(s) \end{bmatrix}^T$$

$$\delta(s) = \begin{bmatrix} \%\delta_1(s) & \%\delta_2(s) \end{bmatrix}^T$$

The maximum values of inputs, outputs and disturbance for this wing model in percentage terms, given by equation 3.2, are as below:

$$q_1(t) = q_2(t) = 0.254 \text{ mm}$$

$$f_l(t) = f_t(t) = 444.8 \text{ N}$$

$$v_{\max} = 60.96 \text{ m/s}$$

The transfer function of the wing model can be found by inverting equation 3.2 and substituting for $A_2(s)$ from equation 3.3 as follows:

$$[A_2(s) + vBs + v^2C]q(s) = f(s) + \delta(s)$$

$$q(s) = [\left(A_0 s^2 + A_1 s + A_2\right) + svB + v^2C]^{-1}\left(f(s) + \delta(s)\right)$$

$$q(s) = [A_0 s^2 + \left(A_1 + vB\right)s + \left(A_2 + v^2C\right)]^{-1}\left(f(s) + \delta(s)\right)$$

The transfer function of the wing model becomes:

$$G(s) = [A_0 s^2 + \left(A_1 + vB\right)s + \left(A_2 + v^2C\right)]^{-1} \qquad 3.6$$

The open loop block diagram of the wing model is shown in figure 3.1 below.

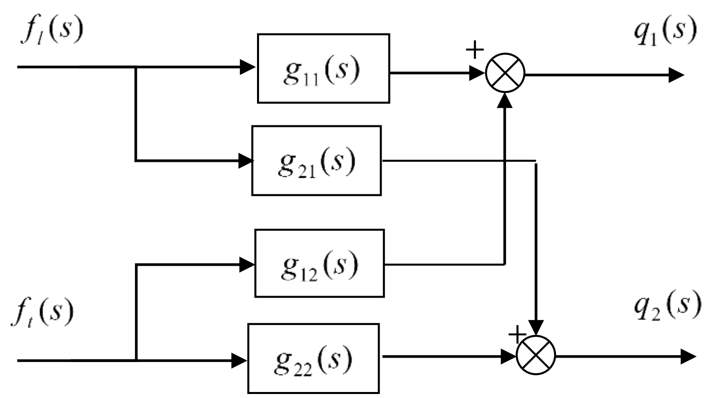

Figure 3.1, Open loop block diagram of the wing model

Then, substituting for A_0, A_1, A_2, B and C from equations 3.4 and 3.5 in equation 3.6 yields:

$$G(s) = \begin{bmatrix} 5.443s^2 + (29 + 0.4466v)s + (2502.7 - 0.633v^2) & 2.907s^2 - (9 - 0.9076v)s - (614.7 - 0.633v^2) \\ 2.907s^2 - (9 + 0.3456v)s - (614.7 - 0.144v^2) & 4.743s^2 + (9 + 0.8064v)s + (1487.7 + 0.144v^2) \end{bmatrix}^{-1}$$

After inverting the previous equation, the general transfer function matrix for the system is given by:

$$G(s) = \frac{\begin{bmatrix} 4.743s^2 + (9+0.8064v)s + (1487.7+0.144v^2) & -\left(2.907s^2 - (9-0.9076v)s - (614.7-0.633v^2)\right) \\ -\left(2.907s^2 - (9+0.3456v)s - (614.7-0.144v^2)\right) & 5.443s^2 + (29+0.4466v)s + (2502.7-0.633v^2) \end{bmatrix}}{\Delta(s)}$$

where

$$\Delta(s) = 17.365s^4 + 238.86s^3 + 2.372\times10^4 s^2 + 5.46\times10^4 s + 3.456\times10^6 + \left(5.164s^3 + 31.564s^2 + 2966s\right)v + \left(-3s^2 + 2.88s - 280.737\right)v^2 + 0.11v^3 s \qquad 3.7$$

To apply the least effort control method for this wing arrangement, the numerator of the transfer function should be reduced to a first degree polynomial and the transient and steady state responses of the system model must be preserved. For this purpose, factors having s^2 in the numerator in equation 3.7 have been eliminated and this results in equation 3.8 below. The denominator is unchanged as a characteristic equation of the system. To verify this, zero velocity is chosen for the system model. The open loop time responses have been shown before and after neglecting the s^2 factors from the numerator of $G_0(s)$ in figures 5.1 and 5.2 where the correspondence is excellent. In view of this, the reduced model is given by:

$$G(s) = \frac{\begin{bmatrix} (9+0.8064v)s + (1487.7+0.144v^2) & (9-0.9076v)s + \left(614.7-0.633v^2\right) \\ (9+0.3456v)s + \left(614.7-0.144v^2\right) & (29+0.4466v)s + (2502.7-0.633v^2) \end{bmatrix}}{\Delta(s)}$$

where

$$\Delta(s) = 17.365s^4 + 238.86s^3 + 2.372\times10^4 s^2 + 5.46\times10^4 s + 3.456\times10^6 + \left(5.164s^3 + 31.564s^2 + 2966s\right)v + \left(-3s^2 + 2.88s - 280.737\right)v^2 + 0.11v^3 s \qquad 3.8$$

Substituting zero for v in equation 3.7 yields in:

$$G_0(s) = \frac{\begin{bmatrix} 4.743s^2 + 9s + 1487.7 & -\left(2.907s^2 - 9s - 614.7\right) \\ -\left(2.907s^2 - 9s - 614.7\right) & 5.443s^2 + 29s + 2502.7 \end{bmatrix}}{\Delta_0(s)}$$

where

$$\Delta_0(s) = 17.365s^4 + 238.86s^3 + 2.372\times10^4 s^2 + 5.46\times10^4 s + 3.456\times10^6 \qquad 3.9$$

After eliminating the factors having s^2 from the numerator in equation 3.9, the transfer function becomes:

$v = 0$

$$G_0(s) = \frac{\begin{bmatrix} 9s + 1487.7 & 9s + 614.7 \\ 9s + 614.7 & 29s + 2502.7 \end{bmatrix}}{\Delta_0(s)}$$

where

$$\Delta_0(s) = 17.365s^4 + 238.86s^3 + 2.372\times10^4 s^2 + 5.46\times10^4 s + 3.456\times10^6 \qquad 3.10$$

As mentioned earlier, to apply the least effort method to this system, the factors having s^2 were neglected. Equations 3.9 and 3.10 are the transfer function matrix equations before and after eliminating the factors having s^2. The open loop system models, figures A.1 and A.2 in the Appendix, were simulated in MATLAB. Figures 7.1 and 7.2 show that the behaviour of the open loop system after approximation, at zero velocity, have been changed only slightly. Therefore equation 3.10 for the system model was used to apply the least effort control method.

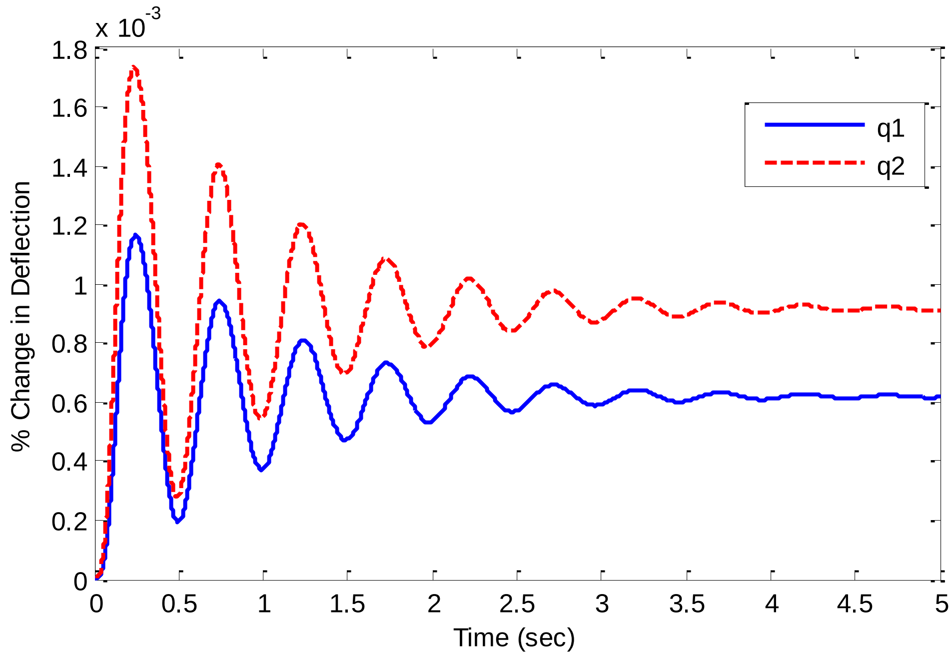

Figure 3.2, Open loop step responses for transfer function in equation 3.9

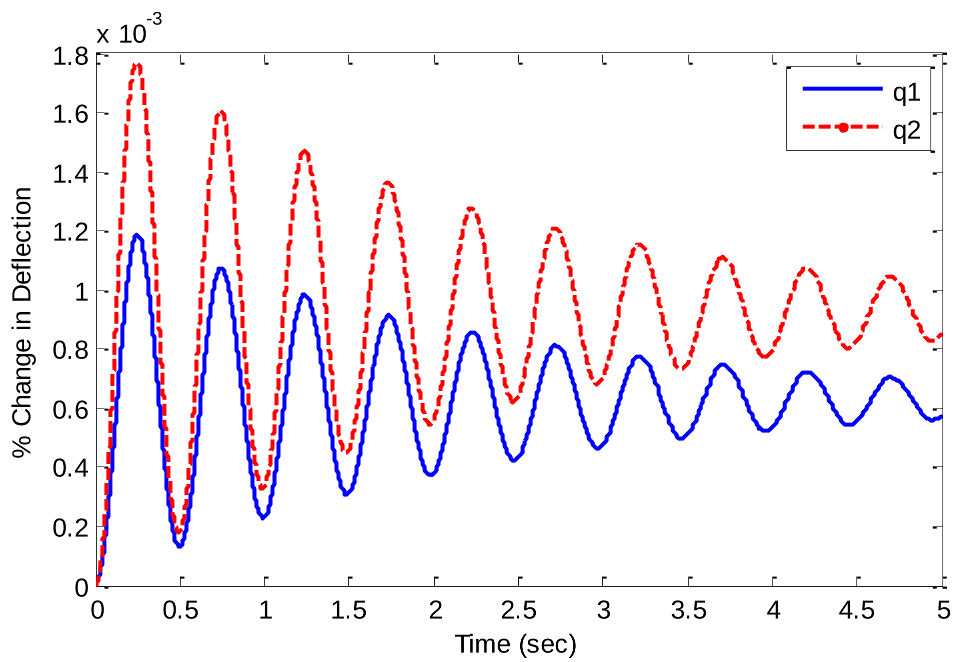

Figure 3.3, Open loop step responses for transfer function in equation 3.10

Chapter 4

Least Effort Control Strategy

In the design procedure, a dual loop approach will be applied as shown in figure 4.2. The inner loop is employed to achieve desired dynamics and satisfactory disturbance recovery. The outer loop is employed to achieve the required steady state by generating a pre and feedback compensator structure for the closed loop system (R Whalley, and M Ebrahimi, 1999).

The Laplace transformed transfer function for the open loop system is given by $G(s)$.

The open loop system model is:

$$y(s) = G(s)u(s) + \delta(s) \qquad , y(s) = q(s) = \left[q_1(s) \quad q_2(s)\right]^T \qquad , u(s) = f(s) = \left[f_l(s) \quad f_t(s)\right]^T$$

and the control (feedback) law for the system is:

$$u(s) = \underbrace{k(s)\left[\bar{r}(s) - h(s)y(s)\right]}_{\substack{\text{Inner loop} \\ \text{(Dynamics)}}} + \underbrace{P\left[r(s) - Fy(s)\right]}_{\substack{\text{Outer loop} \\ \text{(Steady state)}}}$$

As shown in figure 4.1, the inner loop controller is:

$$u(s) = k(s)\left[\bar{r}(s) - h(s)y(s)\right]$$

and the outer loop controller is:

$$P\left[r(s) - Fy(s)\right]$$

An outer loop gain matrix F is proposed to restrict output interaction as follows:

$$F = Diag(f_1, f_2) \qquad , f_1 = f_2 = f \qquad , 0 < f < 1$$

With $\bar{r}(s) = 0$, the closed loop system equation becomes:

$$y(s) = \left(I + G(s)\langle k(s) \times h(s)\rangle + PF\right)^{-1}\left(G(s)\Pr(s) + \delta(s)\right) \qquad 4.1$$

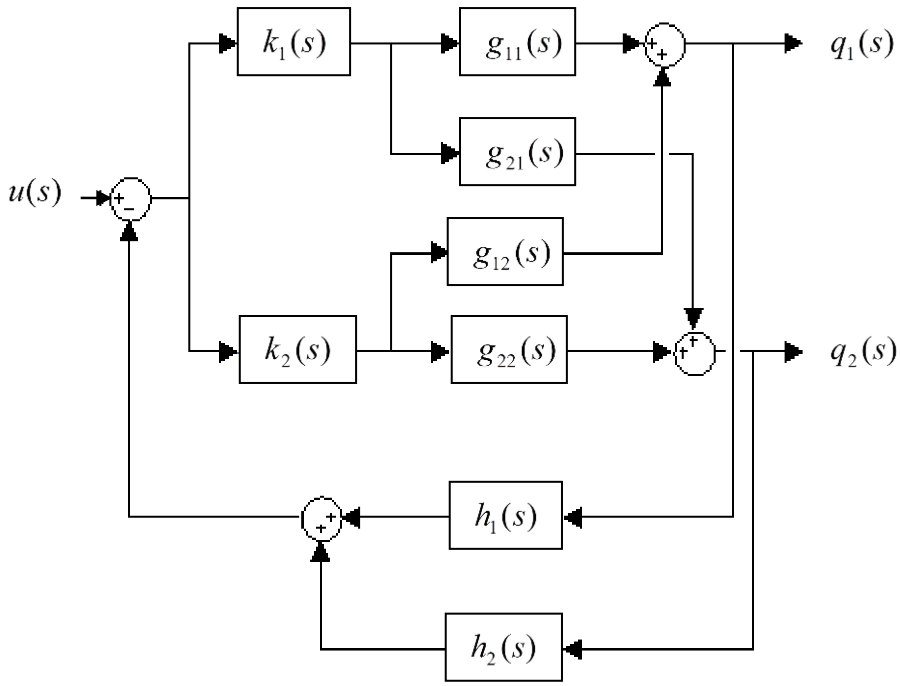

Figure 4.1, Inner loop block diagram for the system model

The steady-state relationship is:

$$y(0) = S_s r(0) \qquad 4.2$$

For zero interaction, the steady state matrix should be:

$$S_s = I_m$$

Combining equations 4.1 and 4.2 with $\delta(s) = 0$ results in:

$$P = \left[G^{-1}(0) + k(0) \times h(0)\right] S_s \left[I - FS_s\right]^{-1} \qquad 4.3$$

Figure 4.2 shows the block diagram for the outer loop controllers.

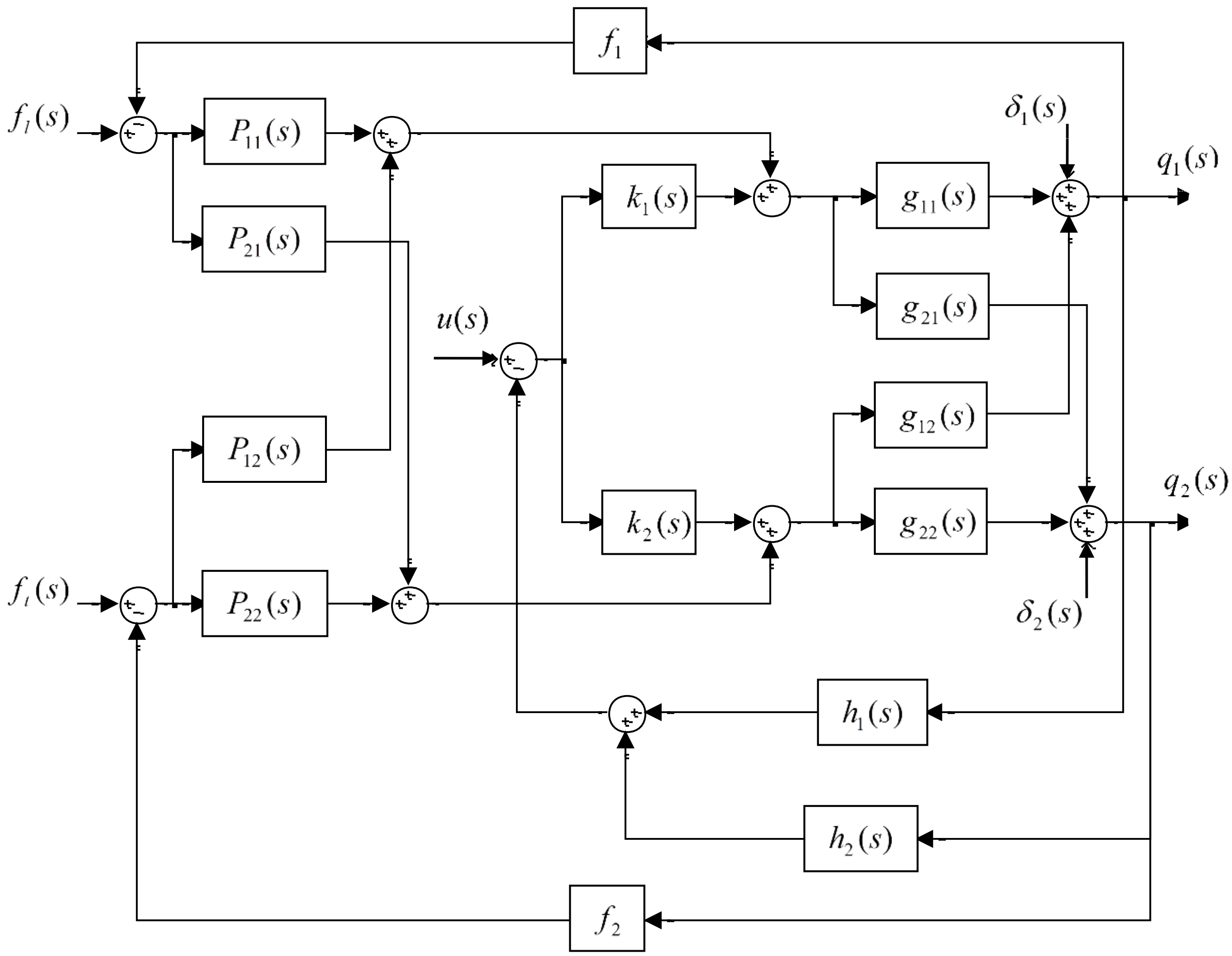

Figure 4.2, Block diagram for inner and outer loop controllers

For implementation purposes, a conventional pre and feedback compensator structure as shown in figure 4.3 could be employed yielding:

$$y(s) = (I + G(s)K(s)H(s))^{-1}(G(s)K(s)r(s) + \delta(s)) \quad 4.4$$

Comparing equation 4.1 with 4.4, evidently:

$$K(s) = P \quad 4.5$$

and:

$$H(s) = P^{-1}k(s) \times h(s) + F \qquad 4.6$$

$H(s)$ and $K(s)$ are constant and full rank matrices, respectively.

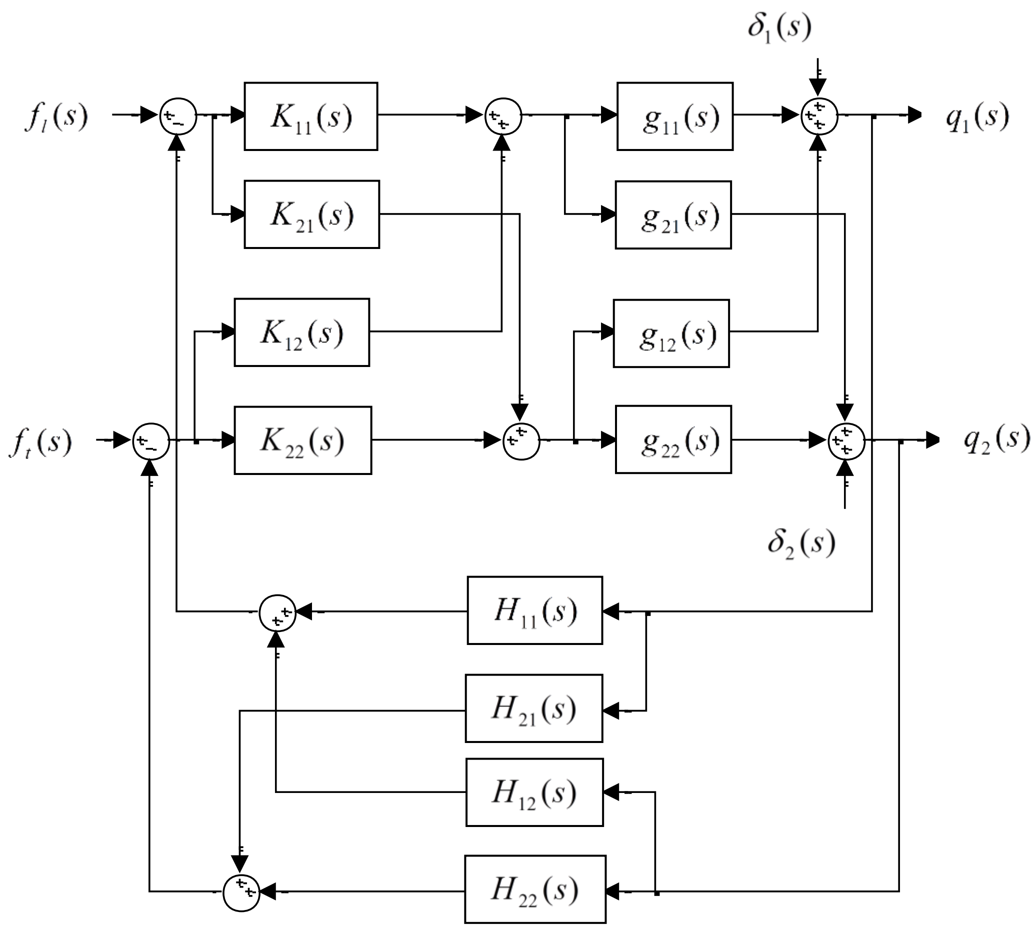

Figure 4.3, Conventional multivariable feedback structure block diagram

4.1. Inner Loop Control Strategy

The complete equation for the system can be written as below:

$$y(s) = \left(I + G(s)\langle k(s) \times h(s)\rangle\right)^{-1}\left(G(s)k(s)\bar{r}(s) + \delta(s)\right)$$

where

$$k(s) = [k_1 \quad k_2]^T$$
$$h(s) = [h_1 \quad h_2]$$

The characteristic equation can be computed from the determinant of $[I + G(s)\langle k(s) \times h(s)\rangle]$ as following, as $\langle k(s) \times h(s)\rangle$ is a rank one matrix.

$$\det[I + G(s)\langle k(s) \times h(s)\rangle] = 1 + h(s)G(s)k(s) = 1 + [h_1 \quad h_2]\frac{\begin{bmatrix} g_{11}(s) & g_{12}(s) \\ g_{21}(s) & g_{22}(s) \end{bmatrix}}{\Delta(s)}\begin{bmatrix} k_1 \\ k_2 \end{bmatrix}$$

$$= 1 + \left(\frac{k_1\left(h_1 g_{11}(s) + h_2 g_{21}(s)\right) + k_2\left(h_1 g_{12}(s) + h_2 g_{22}(s)\right)}{\Delta(s)}\right)$$

Hence:

$$\det[I + G(s)\langle k(s) \times h(s)\rangle] = 1 + \frac{[g_{11}(s) \quad g_{21}(s) \quad g_{12}(s) \quad g_{22}(s)]}{\Delta(s)}\begin{bmatrix} k_1 h_1 \\ k_1 h_2 \\ k_2 h_1 \\ k_2 h_2 \end{bmatrix}$$

Let $k_2 = nk_1$.

If

$$\frac{h(s)A(s)k(s)}{\Delta(s)} = \frac{\left[g_{11}(s) \quad g_{21}(s) \quad g_{12}(s) \quad g_{22}(s)\right]}{\Delta(s)} \begin{bmatrix} k_1 h_1 \\ k_1 h_2 \\ n k_1 h_1 \\ n k_1 h_2 \end{bmatrix}$$

and

$$h(s)A(s)k(s) = b(s) = b_{\circ}(s + x)$$

then

$$\left[g_{11}(s) \quad g_{21}(s) \quad g_{12}(s) \quad g_{22}(s)\right] \begin{bmatrix} k_1 h_1 \\ k_1 h_2 \\ n k_1 h_1 \\ n k_1 h_2 \end{bmatrix} = b_{\circ}(s + x) \qquad 4.7$$

Rearranging equation 4.7 results in:

$$k_1 (1 \quad s) Q(n) \begin{bmatrix} h_1 \\ h_2 \end{bmatrix} = (1 \quad s) b_{\circ} \begin{bmatrix} x \\ 1 \end{bmatrix} \Rightarrow k_1 Q(n) \begin{bmatrix} h_1 \\ h_2 \end{bmatrix} = b_{\circ} \begin{bmatrix} x \\ 1 \end{bmatrix}$$

Let $k_1 = 1$ then the inner loop controllers can be calculated from the following equations.

$$k(s) = \begin{bmatrix} k_1 \\ k_2 \end{bmatrix} = \begin{bmatrix} 1 \\ n \end{bmatrix}$$

$$\left[h(s)\right]^T = \begin{bmatrix} h_1 \\ h_2 \end{bmatrix} = Q^{-1}(n) \begin{bmatrix} x \\ 1 \end{bmatrix} b_{\text{o}} \qquad 4.8$$

To find the characteristic equation and the appropriate gain ratio n, the determinant of $\left[I + G(s)\langle k(s) \times h(s)\rangle\right]$ is equated to zero.

$$\det\left[I + G(s)\langle k(s) \times h(s)\rangle\right] = 0$$

Hence:

$$1+\frac{h(s)A(s)k(s)}{\Delta(s)}=1+\frac{\left[g_{11}(s)\quad g_{21}(s)\quad g_{12}(s)\quad g_{22}(s)\right]}{\Delta(s)}\begin{bmatrix} k_1h_1 \\ k_1h_2 \\ nk_1h_1 \\ nk_1h_2 \end{bmatrix}=1+\frac{b_\circ(s+x)}{\Delta(s)}=0$$

The characteristic equation is:

$$\frac{b_\circ(s+x)}{\Delta(s)}=-1 \qquad 4.9$$

Under closed loop conditions, detection of the minimum control effort with the constraint that the controller model produces a particular zero is essential, to provide a minimum effort performance index (Sahar Tavalla, 2011).

The control energy cost is proportional to:

$$E(t)=\int_0^T\left(u_1^{\,2}(t)+u_2^{\,2}(t)\right)dt=\int_0^T\left(\sum_{i=1}^{m}k_i^{\,2}\sum_{j=1}^{m}h_j^{\,2}y_j^{\,2}(t)\right)dt \qquad 4.10$$

Hence minimizing:

$$J(n)=\sum_{i=1}^{m}h_i^{\,2}\sum_{j=1}^{m}k_j^{\,2}$$

would minimize the control energy required to suppress the resulting arbitrary disturbance changes.

Since $k_2=nk_1$ and $\begin{bmatrix} h_1 \\ h_2 \end{bmatrix}=Q^{-1}(n)\begin{pmatrix} x \\ 1 \end{pmatrix}b_\circ$, the performance index $J(n)$ becomes:

$$J(n)=k_1^2\left(1+n^2\right)\left(h_1^2+h_2^2\right)=\left(1+n^2\right)b^T\left(Q^{-1}(n)\right)^TQ^{-1}(n)b \qquad 4.11$$

In order to find the extremum values of the gain ratios n, the performance index derivative, $\frac{dJ(n)}{dn}$, is equated to zero.

The block diagram for computing the energy dissipation for this system, equation 4.10, is shown in figure 4.4 below.

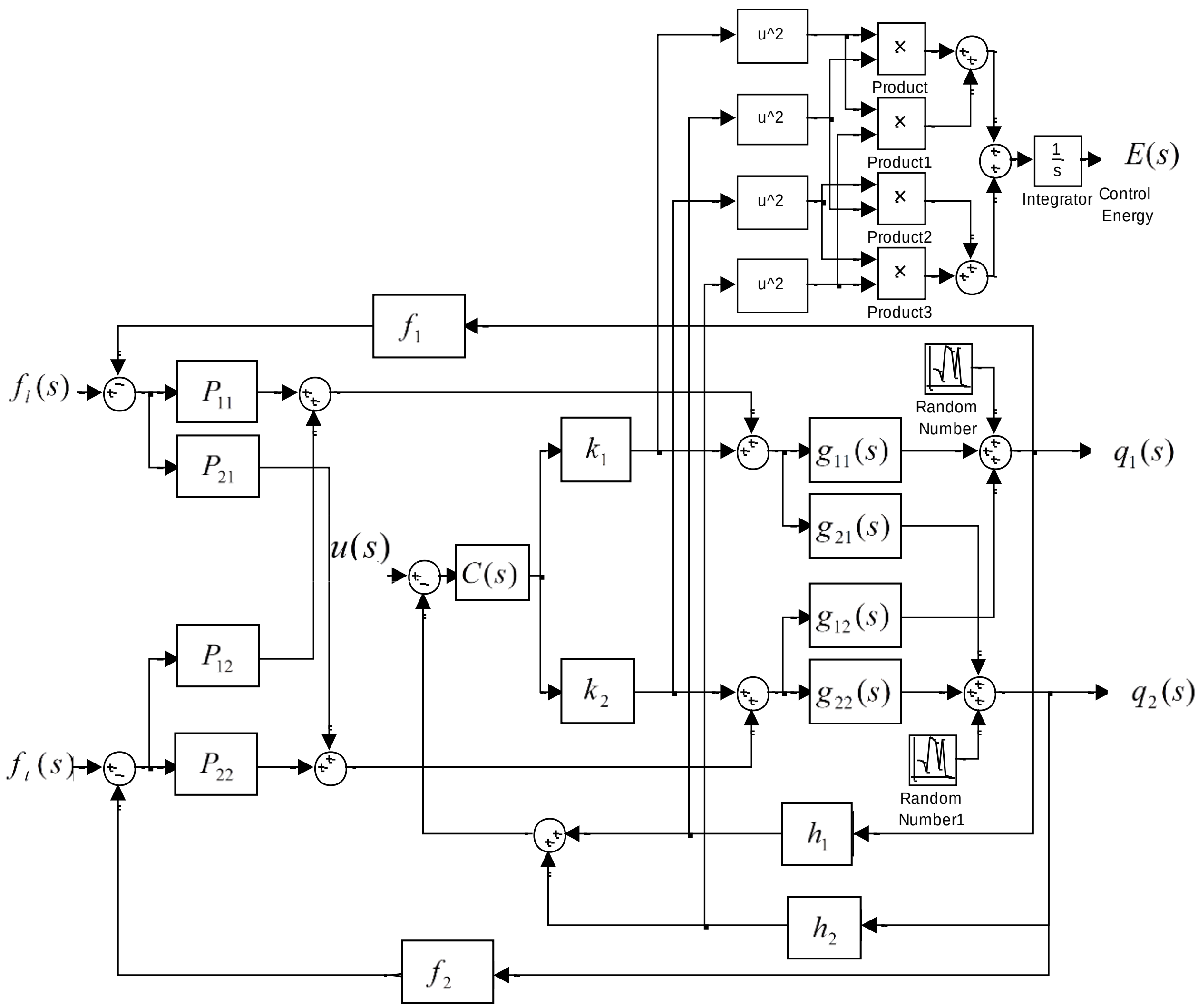

Figure 4.4, Block diagram of the system model including the energy dissipation following random disturbances

4.2. Inner Loop Calculations for the Wing Model at Zero Airstream Velocity

According to equation 3.10, the open loop transfer function matrix for the wing model, at zero velocity is:

$$v = 0$$

$$G_0(s) = \frac{\begin{bmatrix} 9s + 1487.7 & 9s + 614.7 \\ 9s + 614.7 & 29s + 2502.7 \end{bmatrix}}{\Delta_0(s)}$$

$$\Delta_0(s) = 17.365s^4 + 238.86s^3 + 2.372 \times 10^4 s^2 + 5.46 \times 10^4 s + 3.456 \times 10^6$$

The equation for the Root Locus from equation 4.9 is:

$$\frac{b_\circ (s + x)}{\Delta_0(s)} = -1$$

If $x = 0.1$ and $b_\circ = 1$

then the Root Locus equation for this system model becomes:

$$\frac{(s + 0.1)}{\left(17.365s^4 + 238.86s^3 + 2.372 \times 10^4 s^2 + 5.46 \times 10^4 s + 3.456 \times 10^6\right)} = -1$$

Hence:

$$\frac{(0.057587)(s + 0.1)}{\left(s^2 + 0.895s + 161.5\right)\left(s^2 + 12.86s + 1193\right)} = -1 \qquad 4.12$$

Figure 4.5 shows the Root Locus plot for the equation 4.12.

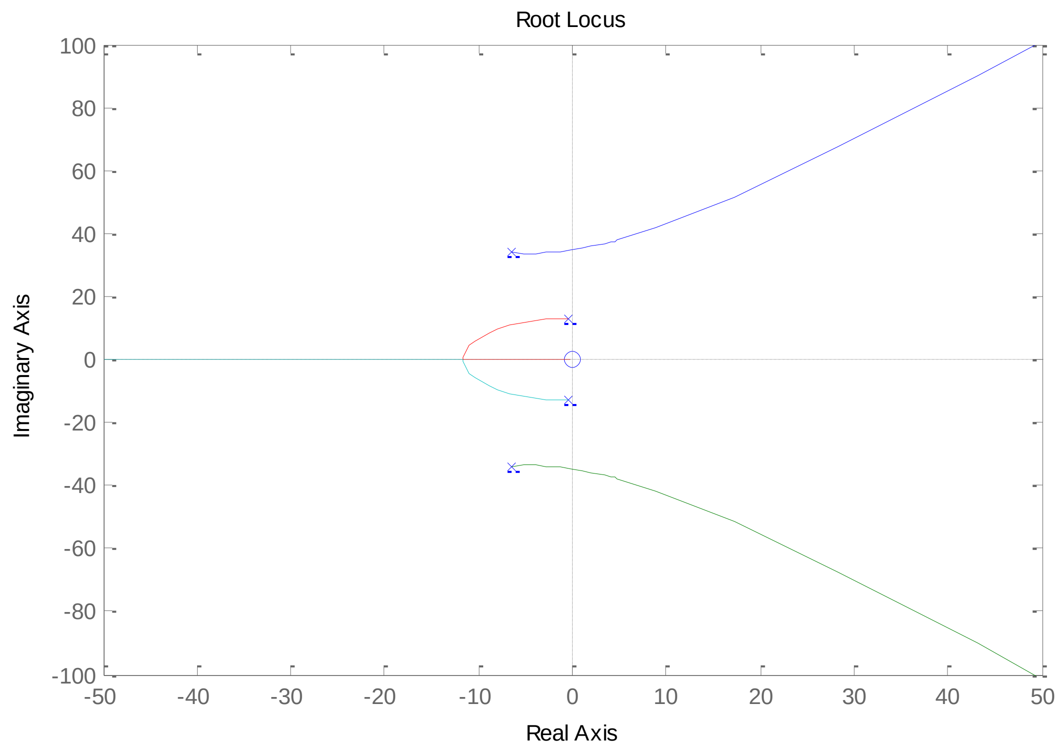

Figure 4.5, Root Locus plot for the inner loop system

An appropriate $b_{\circ}$ can be chosen, as shown in figure 4.6, to achieve an acceptable response for the inner loop.

$$0.0575875 b_{\circ} = \frac{\prod |POLES|}{\prod |ZEROS|} = \frac{(P1)(P2)(P3)(P4)}{(Z1)}$$
$$= \frac{(45.3391)(22.543)(24.6951)(5.5468)}{(12.7635)}$$

Hence:

$$b_{\circ} = 1.0969 \times 10^{4} / 0.0575875$$

As it can be seen, the calculated value for $b_{\circ}$ for an acceptable response is high.

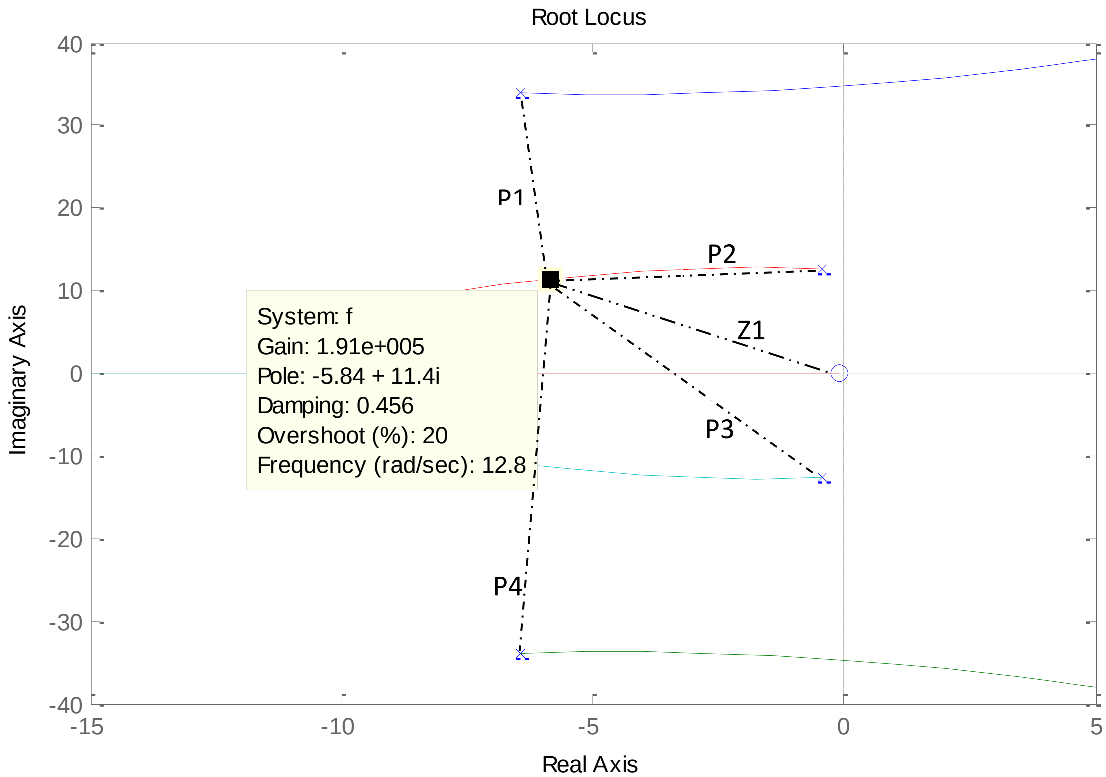

Figure 4.6, Root Locus to find the proper $b_\circ$

As mentioned in the previous section, after calculating the suitable $b_\circ$, the gain ratio n must be calculated to obtain the inner loop controller. In order to find n, the coefficient matrix $Q(n)$ should be obtained from equation 4.7 as following.

$$\begin{bmatrix} g_{11}(s) & g_{21}(s) & g_{12}(s) & g_{22}(s) \end{bmatrix} \begin{bmatrix} k_1 h_1 \\ k_1 h_2 \\ nk_1 h_1 \\ nk_1 h_2 \end{bmatrix} = b_\circ (s+x) = b_\circ \begin{pmatrix} 1 & s \end{pmatrix} \begin{bmatrix} x \\ 1 \end{bmatrix}$$

Substituting (0.1) for x:

$$\begin{bmatrix} 9s+1487.7 & 9s+614.7 & 9s+614.7 & 29s+2502.7 \end{bmatrix} \begin{bmatrix} k_1 h_1 \\ k_1 h_2 \\ nk_1 h_1 \\ nk_1 h_2 \end{bmatrix} = b_\circ (s+0.1)$$

Hence:

$$k_1(1 \quad s)\begin{bmatrix} 1487.7 & 614.7 & 614.7 & 2502.7 \\ 9 & 9 & 9 & 29 \end{bmatrix}\begin{bmatrix} k_1h_1 \\ k_1h_2 \\ nk_1h_1 \\ nk_1h_2 \end{bmatrix} = (1 \quad s)\begin{bmatrix} 0.1 \\ 1 \end{bmatrix} b_\circ$$

and

$$k_1 Q(n)\begin{bmatrix} h_1 \\ h_2 \end{bmatrix} = b_\circ \begin{bmatrix} x \\ 1 \end{bmatrix}$$

If

$$k_1 = 1, \begin{bmatrix} h_1 \\ h_2 \end{bmatrix} = Q^{-1}(n)\begin{bmatrix} x \\ 1 \end{bmatrix} b_\circ$$

then

$$k_1 \begin{bmatrix} 614.7n + 1487.7 & 2502.7n + 614.7 \\ 9n + 9 & 29n + 9 \end{bmatrix}\begin{bmatrix} h_1 \\ h_2 \end{bmatrix} = b_\circ \begin{bmatrix} 0.1 \\ 1 \end{bmatrix} \qquad 4.13$$

The coefficient matrix and its inverse will be:

$$Q(n) = \begin{bmatrix} 614.7n + 1487.7 & 2502.7n + 614.7 \\ 9n + 9 & 29n + 9 \end{bmatrix}$$

$$\Rightarrow Q^{-1}(n) = \frac{\begin{bmatrix} 29n + 9 & -(2502.7n + 614.7) \\ -(9n + 9) & 614.7n + 1487.7 \end{bmatrix}}{10^4(-0.4698n^2 + 2.0619n + 0.7857)}$$

Let

$$k_1 = 1$$
$$b_\circ = (1.0969 \times 10^4 / 0.057587)$$

then equation 4.13 becomes:

$$\begin{bmatrix} h_1 \\ h_2 \end{bmatrix} = \frac{\begin{bmatrix} 29n+9 & -(2502.7n+614.7) \\ -(9n+9) & 614.7n+1487.7 \end{bmatrix}}{10^4\left(-0.4698n^2+2.0619n+0.7857\right)} \begin{bmatrix} 0.1 \\ 1 \end{bmatrix} \left(1.0969 \times 10^4 / 0.057587\right) \qquad 4.14$$

Substituting for b and $Q(n)$ in the performance index equation for $J(n)$, in equation 4.11 yields:

$J(n) =$

$$b_o{}^2\left(1+n^2\right)\begin{bmatrix} 0.1 \\ 1 \end{bmatrix}^T \frac{\begin{bmatrix} 29n+9 & -(9n+9) \\ -(2502.7n+614.7) & 614.7n+1487.7 \end{bmatrix}\begin{bmatrix} 29n+9 & -(2502.7n+614.7) \\ -(9n+9) & 614.7n+1487.7 \end{bmatrix}}{\left(10^4\left(-0.4698n^2+2.0619n+0.7857\right)\right)^2}\begin{bmatrix} 0.1 \\ 1 \end{bmatrix}$$

$$J(n) = \frac{\left(1+n^2\right)\left(10^6\left(6.6258n^2+4.864n+2.5873\right)\right)}{\left(10^4\left(-0.4698n^2+2.0619n+0.7857\right)\right)^2}$$

Hence:

$$J(n) = \frac{6.6258n^4+4.894n^3+9.2131n^2+4.894n+2.5873}{0.2207n^4-1.9374n^3+3.5132n^2+3.2401n+0.6173}$$

To find the minimum of $J(n)$, $\frac{dJ(n)}{dn}$ must be equated to zero.

Hence:

$$\frac{dJ(n)}{dn} = -13.9169n^5+42.4889n^4+64.7537n^3+36.7589n^2-6.8049n-5.362=0$$

The roots of above equation are:

$n = 4.2777, -0.5956 \pm 0.5691i, -0.3814$

Figure 4.7 shows the graph for the performance index with its minimum when:

$n = 0.3298$

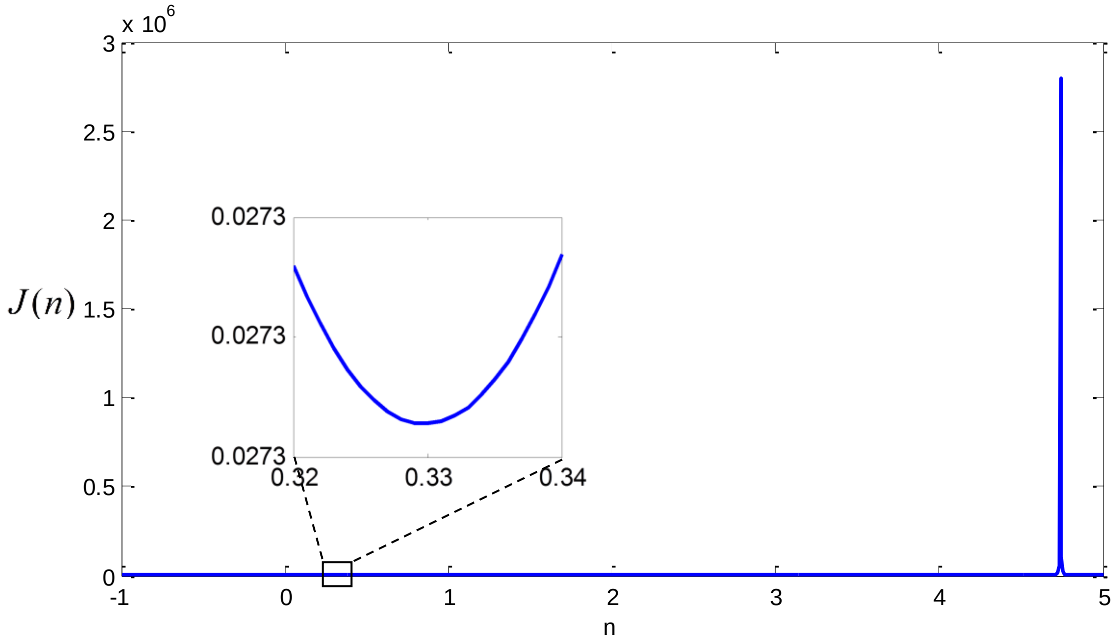

Figure 4.7, Performance Index $J(n)$ against gain ratio n

Substituting for n in $h(s)$ and $k(s)$ in equations 4.8 and 4.14 results in:

$$\begin{bmatrix} k_1 \\ k_2 \end{bmatrix} = \begin{bmatrix} 1 \\ 0.3298 \end{bmatrix} \qquad 4.15$$

$$\begin{bmatrix} h_1 & h_2 \end{bmatrix} = \begin{bmatrix} -0.09 & 0.1057 \end{bmatrix} \left(1.0969 \times 10^4 / 0.057587 \right) \qquad 4.16$$

After finding the inner loop controller, the outer loop controller using equation 4.3 is given by:

$$P = \left[G^{-1}(0) + k(0) \times h(0) \right] S_s \left[I - FS_s \right]^{-1}$$

Substituting $(s=0)$ to find $G_0(0)$ in equation 3.10 yields:

$$G_0(0)=\frac{\begin{bmatrix}1487.7 & 614.7\\ 614.7 & 2502.7\end{bmatrix}}{3.456\times10^6}$$

Hence:

$$G_0^{-1}(0)=\begin{bmatrix}2502.7 & -614.7\\ -614.7 & 1487.7\end{bmatrix}$$

Using equations 4.15 and 4.16 results in:

$$\langle k(0)\times h(0)\rangle =$$

$$\begin{bmatrix}1\\ 0.3298\end{bmatrix}\times\begin{bmatrix}-0.09 & 0.1057\end{bmatrix}b_o=\begin{bmatrix}-0.09 & 0.1057\\ -0.0297 & 0.0349\end{bmatrix}\left(1.0969\times10^4/0.057587\right)$$

If

$$S_s=(0.1)I_2$$
$$F=diag(f,f)$$

then

$$S_s\left[I-FS_s\right]^{-1}=(0.1)I_2\big/(1-f)$$

Substituting in equation 4.2:

$$P=\frac{\begin{bmatrix}-1464.02 & 1951.87\\ -504.24 & 813.53\end{bmatrix}}{(1-f)}$$

If $f = 0$

then: $P = \begin{bmatrix} -1464.02 & 1951.87 \\ -504.24 & 813.53 \end{bmatrix}$ 4.17

If $f = 0.5$

then: $P = \begin{bmatrix} -2928.04 & 3903.74 \\ -1008.48 & 1627.06 \end{bmatrix}$ 4.18

At higher values than $f = 0.5$, the system responses exhibit large overshoots, high frequency characteristics which should not be acceptable in practice.

Chapter 5

Compensator Design

The purpose of compensator design is usually to satisfy both transient and steady state responses. Compensators are used to modify the response of a control system in order to accommodate set design specifications.

To design the compensator, the transfer function of the system, in equation 3.10 has been written as:

$$G_0(s) = \frac{(0.057587)\begin{bmatrix} 9s+1487.7 & 9s+614.7 \\ 9s+614.7 & 29s+2502.7 \end{bmatrix}}{\left(s^2+0.895s+161.5\right)\left(s^2+12.86s+1193\right)}$$

The poles of the system can be calculated by equating the characteristic equation which is the denominator of the transfer function to zero. This system has four complex poles at:

$$\begin{cases} s = -0.4475 \pm 12.6991i \\ s = -6.4301 \pm 33.9359i \end{cases}$$

To eliminate oscillatory effects of the two complex poles closest to the imaginary axis, the following compensator has been designed for this system. The compensator network is a second order active filter network, given by equation 5.1, shown in figure 5.1.

$$C(s) = \frac{\left(s^2+0.895s+161.5\right)}{\left(s^2+25.5s+162.5\right)} \qquad 5.1$$

The zeros and poles of the compensator are:

$$\begin{cases} zeros = -0.4475 \pm 12.6991i \\ poles = -12.5, -13 \end{cases}$$

The compensator equation and the required conditions are:

$$C(s) = \frac{\left(s^2 + b_1 s + b_2\right)}{\left(s^2 + a_1 s + a_2\right)} \tag{5.2}$$

$$\begin{cases} a_1 = \dfrac{1}{R_1 C_1} \\ a_2 = \dfrac{1}{R_2 R_4 C_1 C_2} \\ b_1 = \left(1 - \dfrac{R_1 R_7}{R_3 R_8}\right)(a_1) \qquad \left(b_1 \langle a_1\right) \\ b_2 = \left(1 - \dfrac{R_2 R_7}{R_3 R_9}\right)(a_2) \qquad \left(b_2 \langle a_2\right) \end{cases} \tag{5.3}$$

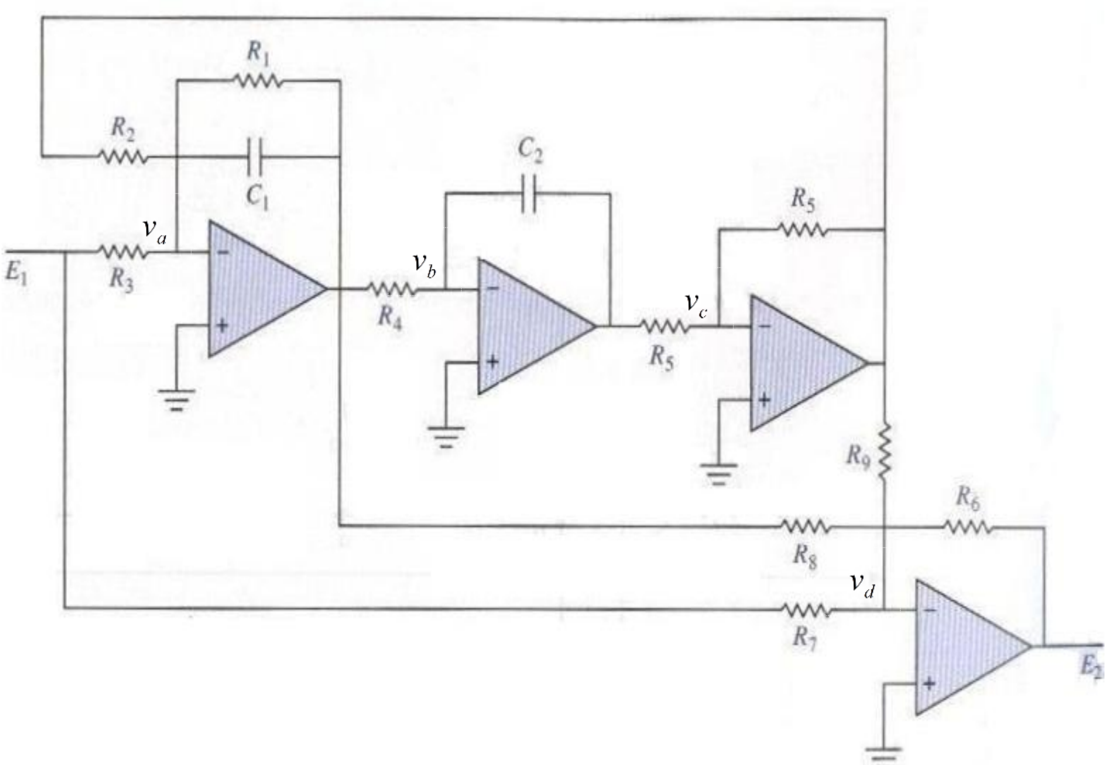

Figure 5.1, Compensator circuit diagram

The parameters of this network can be calculated after comparing equation 5.1 with equations 5.2 and 5.3 which are shown in table 1 below.

a_1	25.5
a_2	162.5
b_1	0.895
b_2	161.5
R_1	1.96078 kΩ
R_2	5 kΩ
R_3	79.96801 kΩ
R_4	3.0769 kΩ
R_5	10 kΩ
R_6	9.842 kΩ
R_7	9.842 kΩ
R_8	0.2501 kΩ
R_9	100 kΩ
C_1	20 μF
C_2	20 μF

Table 1, Parameters of the compensator network

The analytical derivation for this network is as follows. The equations for the four nodes at v_a, v_b, v_c and v_d can be written as below:

As $R_1 \parallel C_1$, then: $Z_1 = \frac{R_1 (1/C_1 s)}{R_1 + (1/C_1 s)} = \frac{R_1}{R_1 C_1 s + 1}$

First node at v_a :

$$* \begin{cases} \frac{V_c}{V_b} = -\frac{R_5}{R_5} = -1 \\ \frac{V_b}{V_a} = -\frac{1}{R_4 C_2 s} \end{cases}$$

Hence:

$$\frac{V_c}{V_a} = \frac{1}{R_4 C_2 s}$$

Second node at v_b :

$$* \frac{V_a}{Z_1} + \frac{V_c}{R_2} + \frac{E_1}{R_3} = 0$$

Hence:

$$-\frac{E_1}{R_3} = V_a \left(\frac{R_1 C_1 s + 1}{R_1} \right) + V_a \left(\frac{1}{R_4 C_2 s} \right) = V_a \left(\frac{R_1 R_2 R_4 C_1 C_2 s^2 + R_2 R_4 C_2 s + R_1}{R_1 R_2 R_4 C_2 s} \right)$$

Third node at v_c :

$$* \frac{V_c}{R_9} + \frac{V_a}{R_8} + \frac{E_1}{R_7} + \frac{E_2}{R_6} = 0$$

Hence:

$$-\left(\frac{E_1}{R_7} + \frac{E_2}{R_6} \right) = \frac{V_a}{R_9 R_4 C_2 s} + \frac{V_a}{R_8} = V_a \left(\frac{R_4 R_9 C_2 s + R_8}{R_4 R_8 R_9 C_2 s} \right)$$

Combining the previous node equations results in:

$$\frac{E_1/R_3}{\left(E_1/R_7+E_2/R_6\right)}=\frac{V_a\left(\dfrac{R_1R_2R_4C_1C_2s^2+R_2R_4C_2s+R_1}{R_1R_2R_4C_2s}\right)}{V_a\left(\dfrac{R_4R_9C_2s+R_8}{R_4R_8R_9C_2s}\right)}$$

Hence:

$$\frac{E_1}{\left(E_1/R_7+E_2/R_6\right)}=\frac{R_1R_2R_3R_4R_8R_9C_1C_2s^2+R_2R_3R_4R_8R_9C_2s+R_1R_3R_8R_9}{R_1R_2R_4R_9C_2s+R_1R_2R_8}$$

If

$$X_1=R_1R_2R_3R_4R_8R_9C_1C_2s^2+R_2R_3R_4R_8R_9C_2s+R_1R_3R_8R_9$$
$$X_2=R_1R_2R_4R_9C_2s+R_1R_2R_8$$

then

$$\frac{E_1}{\left(E_1/R_7+E_2/R_6\right)}=\frac{X_1}{X_2}$$

and

$$E_1X_2=\frac{E_1X_1}{R_7}+\frac{E_2X_1}{R_6},\qquad \frac{E_2}{E_1}=\frac{R_6}{R_7}\left(\frac{X_2R_7-X_1}{X_1}\right)$$

Substituting for X_1 and X_2 yields in:

$$\frac{E_2}{E_1}=$$
$$\frac{R_6}{R_7}\left(\frac{\left(R_1R_2R_4R_9C_2s+R_1R_2R_8\right)R_7-\left(R_1R_2R_3R_4R_8R_9C_1C_2s^2+R_2R_3R_4R_8R_9C_2s+R_1R_3R_8R_9\right)}{R_1R_2R_3R_4R_8R_9C_1C_2s^2+R_2R_3R_4R_8R_9C_2s+R_1R_3R_8R_9}\right)$$

and

$$\frac{E_2}{E_1} = -\frac{R_6}{R_7}\left(\frac{s^2 + \left(\frac{1}{R_1C_1} - \frac{R_7}{R_3R_8C_1}\right)s + \left(\frac{1}{R_2R_4C_1C_2} - \frac{R_7}{R_3R_4R_9C_1C_2}\right)}{s^2 + \frac{1}{R_1C_1}s + \frac{1}{R_2R_4C_1C_2}}\right)$$

The transfer function of this network will be as shown in equation 5.4 below which is matched with equations 5.2 and 5.3.

$$\frac{E_2}{E_1} = -\frac{R_6}{R_7}\left(\frac{s^2 + \left(1 - \frac{R_1R_7}{R_3R_8}\right)\left(\frac{1}{R_1C_1}\right)s + \left(1 - \frac{R_2R_7}{R_3R_9}\right)\left(\frac{1}{R_2R_4C_1C_2}\right)}{s^2 + \frac{1}{R_1C_1}s + \frac{1}{R_2R_4C_1C_2}}\right) \qquad (R_6 = R_7) \qquad 5.4$$

5.1. Inner and Outer Loop Design for the System with Compensator

After combining equations 3.10 and 5.3, the new transfer function of the system $G(s)$ will be:

$$G(s) = C(s)G_0(s) = \left(\frac{s^2 + 0.895s + 161.5}{s^2 + 25.5s + 162.5}\right)\frac{(0.057587)\begin{bmatrix} 9s + 1487.7 & 9s + 614.7 \\ 9s + 614.7 & 29s + 2502.7 \end{bmatrix}}{(s^2 + 0.895s + 161.5)(s^2 + 12.86s + 1193)}$$

$$G(s) = \frac{\begin{bmatrix} 85.6722(1 + 0.006s) & 35.3987(1 + 0.0146s) \\ 35.3987(1 + 0.0146s) & 144.123(1 + 0.116s) \end{bmatrix}}{(s^2 + 25.5s + 162.5)(s^2 + 12.86s + 1193)}$$

let

$$\Delta(s) = (s^2 + 25.5s + 162.5)(s^2 + 12.86s + 1193) \qquad 5.5$$

The inner loop block diagram of the system with compensator is shown in figure 5.2.

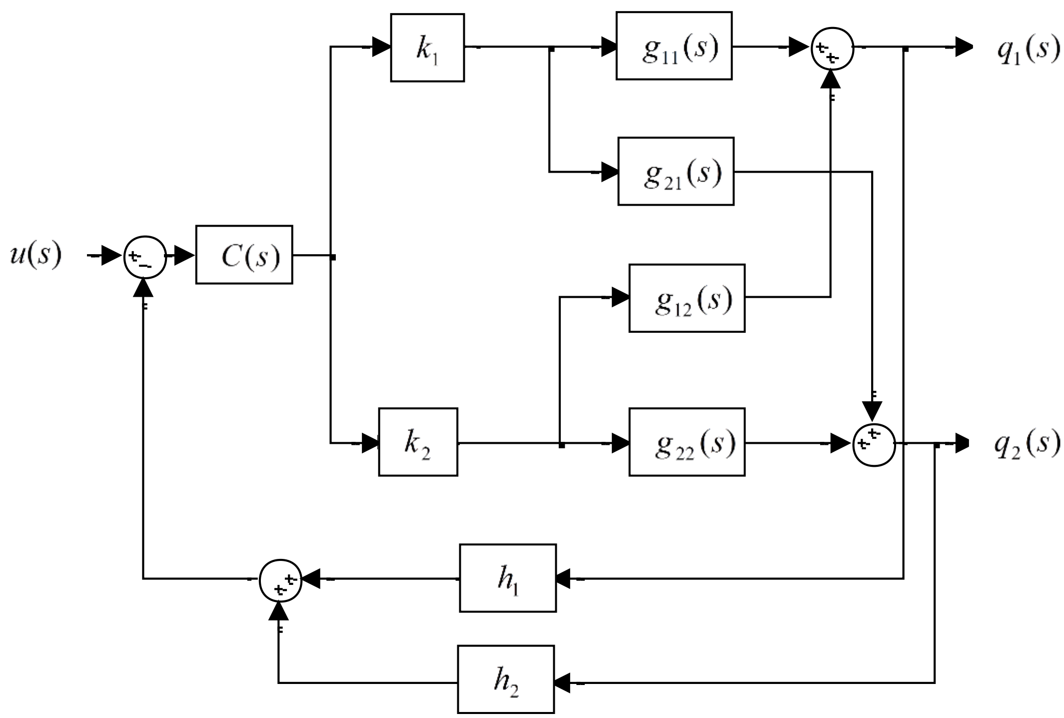

Figure 5.2, Inner loop system block diagram with compensator

Same procedure as used in previous sections for inner loop controllers can be applied for the new system model as follows, from equation 4.5:

$$[g_{11}(s) \quad g_{21}(s) \quad g_{12}(s) \quad g_{22}(s)]\begin{bmatrix} k_1 h_1 \\ k_1 h_2 \\ nk_1 h_1 \\ nk_1 h_2 \end{bmatrix} = b_\circ (s+x) = b_\circ (1 \quad s)\begin{bmatrix} x \\ 1 \end{bmatrix}$$

The controller generated zero is selected initially at $(x=-6)$ in order to increase the separation from the imaginary axis.

$$
[0.5183s+85.6722, \quad 0.5183s+35.3987, \quad 0.5183s+35.3987, \quad 1.67s+144.123]\begin{bmatrix} k_1h_1 \\ k_1h_2 \\ nk_1h_1 \\ nk_1h_2 \end{bmatrix}
$$

$$
= b_o(s+6)
$$

Hence:

$$
k_1(1 \quad s)\begin{bmatrix} 85.6722 & 35.3987 & 35.3987 & 144.123 \\ 0.5183 & 0.5183 & 0.5183 & 1.67 \end{bmatrix}\begin{bmatrix} k_1h_1 \\ k_1h_2 \\ nk_1h_1 \\ nk_1h_2 \end{bmatrix} = (1 \quad s)\begin{bmatrix} 6 \\ 1 \end{bmatrix} b_{\circ}
$$

let

$$
k_1 Q(n)\begin{bmatrix} h_1 \\ h_2 \end{bmatrix} = b_{\circ}\begin{bmatrix} x \\ 1 \end{bmatrix} \text{ and } k_1 = 1
$$

then

$$
\begin{bmatrix} h_1 \\ h_2 \end{bmatrix} = Q^{-1}(n)\begin{bmatrix} x \\ 1 \end{bmatrix} b_{\circ}
$$

$$
\begin{bmatrix} 35.3987n+85.6722 & 144.123n+35.3987 \\ 0.5183n+0.5183 & 1.67n+0.5183 \end{bmatrix}\begin{bmatrix} h_1 \\ h_2 \end{bmatrix} = b_{\circ}\begin{bmatrix} 6 \\ 1 \end{bmatrix}
$$

The coefficient matrix and its inverse for the system model with compensator at zero velocity will be:

$$
Q(n) = \begin{bmatrix} 35.3987n+85.6722 & 144.123n+35.3987 \\ 0.5183n+0.5183 & 1.67n+0.5183 \end{bmatrix}
$$

and

$$Q^{-1}(n)=\frac{\begin{bmatrix}1.67n+0.5183 & -(144.123n+35.3987)\\ -(0.5183n+0.5183) & 35.3987n+85.6722\end{bmatrix}}{(-15.5831n^2+68.3736n+26.0568)}$$

Let

$k_1=1$
$b_\circ=1$

then

$$\begin{bmatrix}h_1\\ h_2\end{bmatrix}=\frac{\begin{bmatrix}1.67n+0.5183 & -(144.123n+35.3987)\\ -(0.5183n+0.5183) & 35.3987n+85.6722\end{bmatrix}}{(-15.5831n^2+68.3736n+26.0568)}\begin{bmatrix}6\\ 1\end{bmatrix} \quad 5.6$$

Substituting for b and $Q(n)$ in performance index equation $J(n)$ in equation 4.11 yields in:

$$J(n)=(1+n^2)\begin{bmatrix}6 & 1\end{bmatrix}$$
$$\frac{\begin{bmatrix}1.67n+0.5183 & -(0.5183n+0.5183)\\ -(144.123n+35.3987) & 35.3987n+85.6722\end{bmatrix}\begin{bmatrix}1.67n+0.5183 & -(144.123n+35.3987)\\ -(0.5183n+0.5183) & 35.3987n+85.6722\end{bmatrix}}{(-15.5831n^2+68.3736n+26.0568)^2}\begin{bmatrix}6\\ 1\end{bmatrix}$$

$$J(n)=\frac{1.9026n^4+1.4186n^3+2.7389n^2+1.4186n+0.8363}{0.2428n^4-2.1309n^3+3.8629n^2+3.5632n+0.679} \quad 5.7$$

As mentioned earlier, to find the minimum value of $J(n)$, $\frac{dJ(n)}{dn}$ must be equated to zero, where:

$$\frac{dJ(n)}{dn} =$$
$$-4.3987n^6 + 13.3691n^5 + 30.621n^4 + 20.5105n^3 + 12.5152n^2 - 2.7417n - 2.0167 = 0$$

After finding the roots of the previous equation which are:

n = 4.7406, -1.2184, -0.2411 ± 0.7622i, 0.3521, -0.3527

the minimum occurs when:

$$n = 0.3521$$

Figure 5.3 shows the graph for the performance index in equation 5.7 and the minimum of it.

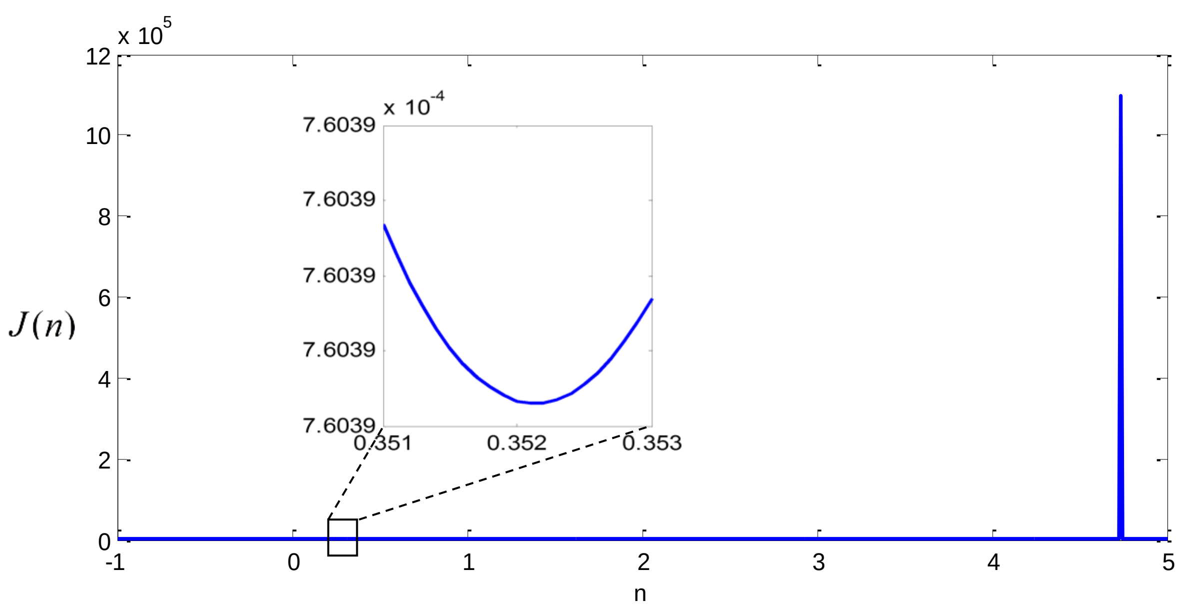

Figure 5.3, Performance Index $J(n)$ against gain ratio n

Substituting for the calculated n in $h(s)$ and $k(s)$ in equations 4.8 and 5.6 results in:

$$k(s) = \begin{bmatrix} k_1 \\ k_2 \end{bmatrix} = \begin{bmatrix} 1 \\ 0.3521 \end{bmatrix}$$

$$h(s) = \begin{bmatrix} h_1 & h_2 \end{bmatrix} = \begin{bmatrix} -1.6495 & 1.9488 \end{bmatrix} \tag{5.8}$$

After finding the inner loop controllers, the outer loop controllers have been obtained as follows using equation 4.3. From equation 5.5:

$$G(s) = \frac{\begin{bmatrix} 85.6722(1+0.006s) & 35.3987(1+0.0146s) \\ 35.3987(1+0.0146s) & 144.123(1+0.116s) \end{bmatrix}}{\left(s^2 + 25.5s + 162.5\right)\left(s^2 + 12.86s + 1193\right)}$$

If $s = 0$, then:

$$G(0) = \frac{\begin{bmatrix} 85.6722 & 35.3987 \\ 35.3987 & 144.123 \end{bmatrix}}{(162.5)(1193)}$$

and

$$G^{-1}(0) = \begin{bmatrix} 2518.44409 & -618.56641 \\ -618.56641 & 1497.05908 \end{bmatrix}$$

$$\langle k(0) \times h(0) \rangle = \begin{bmatrix} 1 \\ 0.3521 \end{bmatrix} \times \begin{bmatrix} -1.6495 & 1.9488 \end{bmatrix} = \begin{bmatrix} -1.6495 & 1.9488 \\ -0.58078 & 0.68617 \end{bmatrix}$$

If

$$S_s = \begin{bmatrix} 1 & 0.1 \\ 0.1 & 1 \end{bmatrix}$$

$$F = diag(f, f) \quad , 0 \langle f \langle 1$$

then:

$$S_s[I - FS_s]^{-1} = \frac{\begin{bmatrix} 1-0.99f & 0.1 \\ 0.1 & 1-0.99f \end{bmatrix}}{\left(1.01f^2 - 2f + 1\right)}$$

Substituting for P in equation 4.3:

$$P = \frac{\begin{bmatrix} 2516.79459 & -616.61761 \\ -619.14719 & 1497.74525 \end{bmatrix}\begin{bmatrix} 1-0.99f & 0.1 \\ 0.1 & 1-0.99f \end{bmatrix}}{\left(1.01f^2 - 2f + 1\right)} \qquad 5.9$$

If (0.55) is selected for f, then:

$$P = \begin{bmatrix} 5.2806\times10^3 & -145.5411 \\ -639.8245 & 3.0169\times10^3 \end{bmatrix} \qquad 5.10$$

The inner and outer loop controller block diagram of the system with compensator is shown in figure 5.4 below.

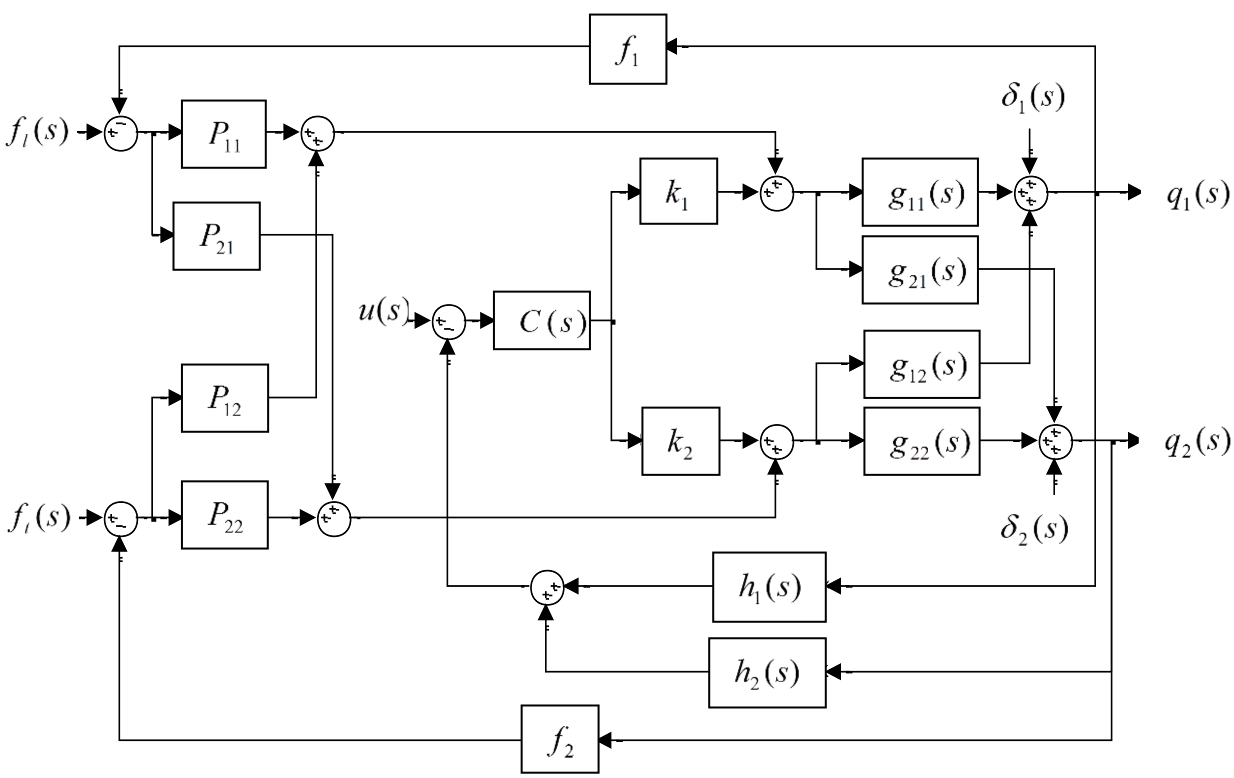

Figure 5.4, Block diagram for inner and outer loop controllers

For implementation purposes, as the values for P are high in equation 5.10, the gains have to be distributed between forward and feedback path. The blocks that have to be changed are shown in figure 5.5. As it can be seen, the forward gain of $(1/100)$ has been included in the model, the outer loop forward path gain P is divided by (100) and the outer loop feedback gain f is multiplied by (100). Thus, the new values for P and f become:

$$P = \begin{bmatrix} 52.806 & -1.455411 \\ -6.398245 & 30.169 \end{bmatrix} \tag{5.11}$$

$$f = 55 \tag{5.12}$$

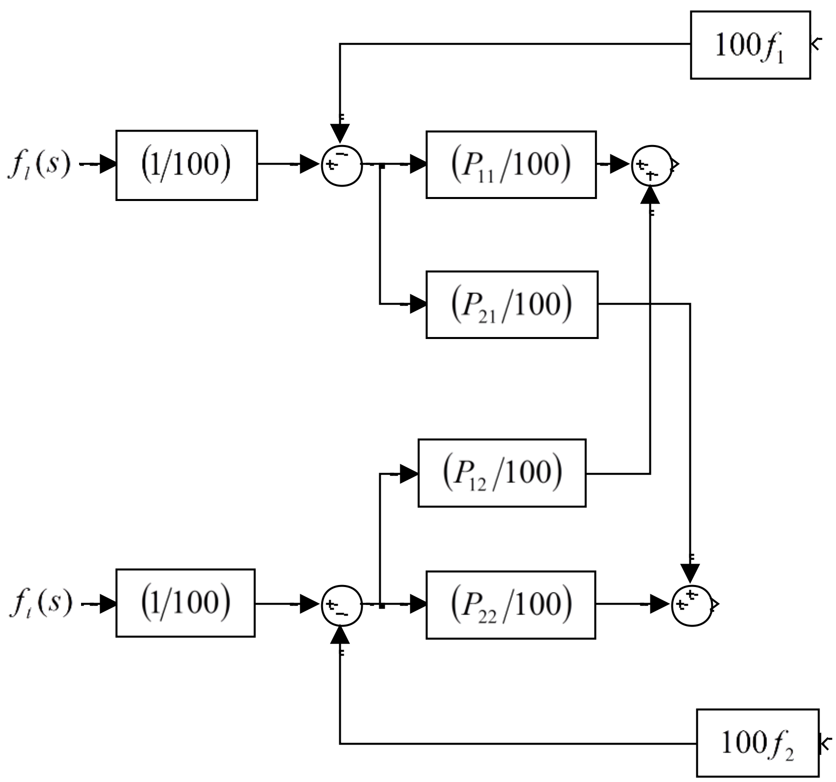

Figure 5.5, The block diagram changes in figure 5.4
for implementation purposes

Using equations 4.4, 4.5, 4.6 and 5.10, the conventional multivariable feedback structure can be constructed in figure 5.6.

$K(s)$ and $H(s)$ are calculated for $f = 0.55$ as below:

$$K(s) = \begin{bmatrix} 5.2806\times10^{3} & -145.5411 \\ -639.8245 & 3.0169\times10^{3} \end{bmatrix} \quad 5.13$$

$$H(s) = \begin{bmatrix} -3.1954\times10^{-4} & 0.5503 \\ -0.5502 & 3.075\times10^{-4} \end{bmatrix} \quad 5.14$$

It is noticeable that the values for $K(s)$ are high in equation 5.13. The same procedure is applied to distribute the gains between $K(s)$ and $H(s)$. The blocks that have to be changed are shown in figure 4.5. As it can be seen, the forward path gain of $(1/100)$ has been included in the model, the outer loop feedback gain $K(s)$ has been divided by (100) and the outer loop feedback gain $H(s)$ is multiplied by (100). Thus, the new values for $K(s)$ and $H(s)$ become:

$$K(s) = \begin{bmatrix} 52.806 & -1.455411 \\ -6.398245 & 30.169 \end{bmatrix} \quad 5.15$$

$$H(s) = \begin{bmatrix} -3.1954\times10^{-2} & 55.03 \\ -55.02 & 3.075\times10^{-2} \end{bmatrix} \quad 5.16$$

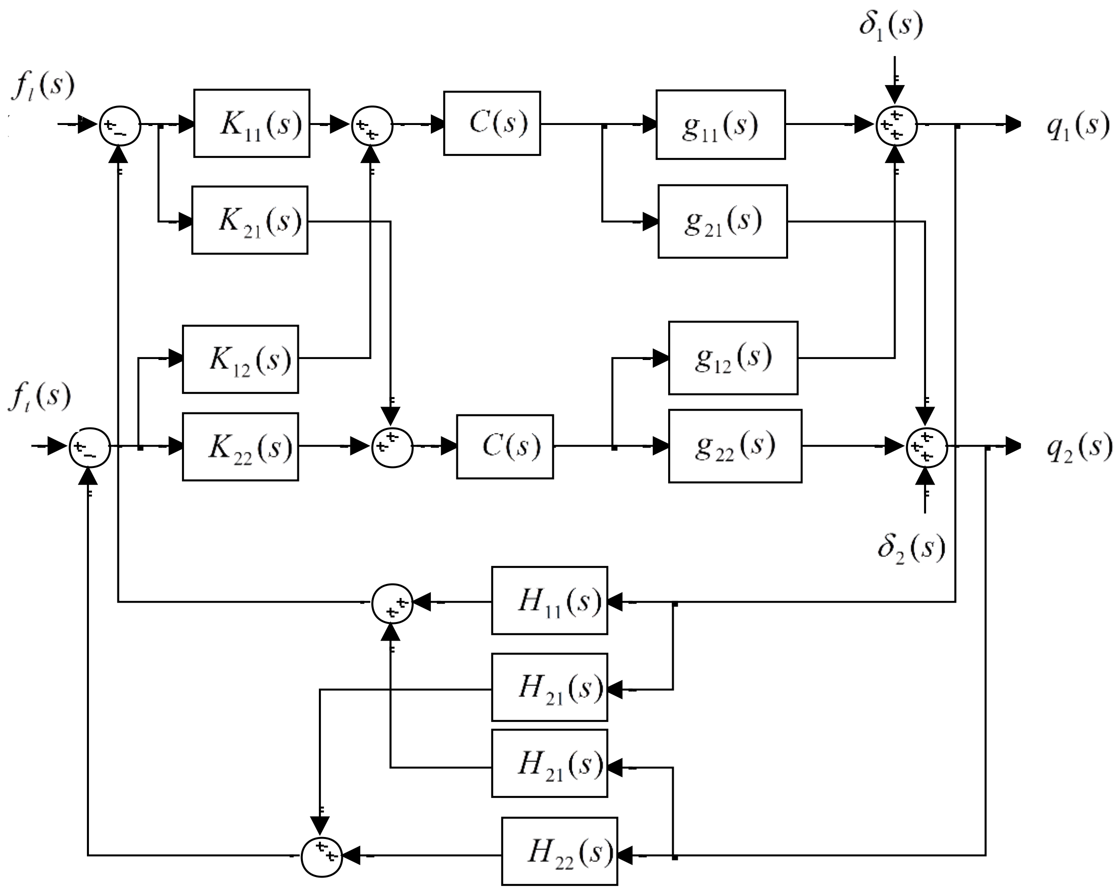

Figure 5.6, Conventional multivariable feedback structure block diagram

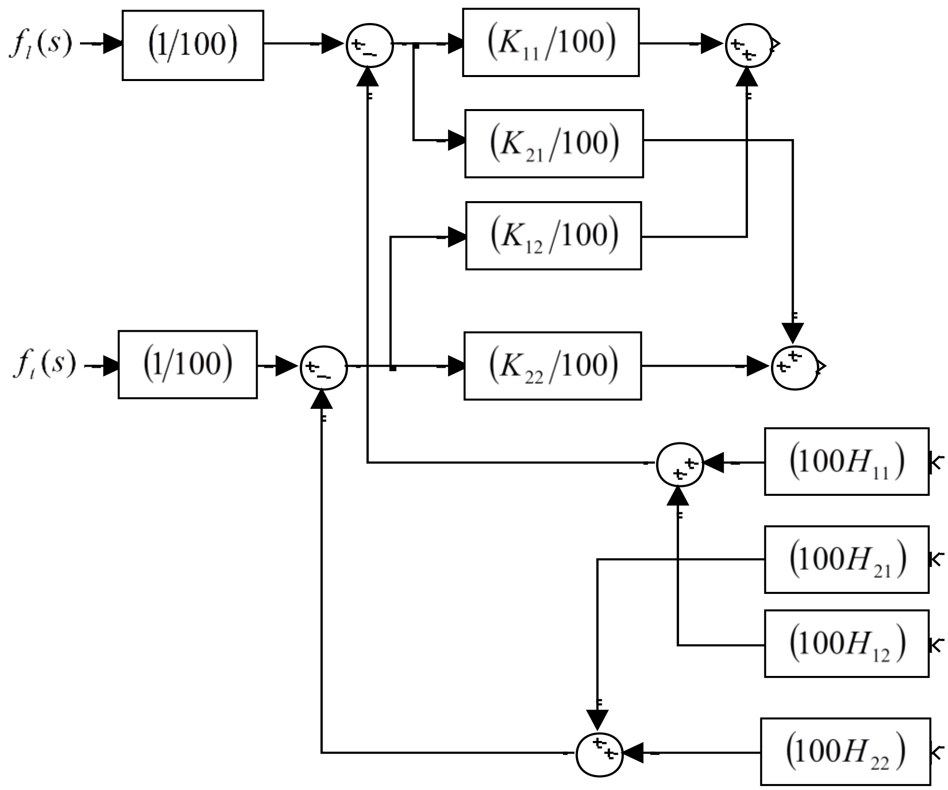

Figure 5.7, The block diagram changes in figure 5.6 for implementation purposes

Chapter 6

Nyquist Array Method

In this chapter, Nyquist array method is applied to this wing arrangement to be compared to the earlier method discussed in previous chapter. The fundamental objective of this method is to decrease system output interaction so that the closed loop system design problem reduces to a set of independent single loop designs and this happens when the system is diagonally dominant.

From previous chapters, the reduced transfer function matrix of this wing arrangement at zero velocity is given by:

$$G_0(s) = \frac{\begin{bmatrix} 9s + 1487.7 & 9s + 614.7 \\ 9s + 614.7 & 29s + 2502.7 \end{bmatrix}}{\Delta_0(s)}$$

where

$$\Delta_0(s) = 17.365s^4 + 238.86s^3 + 2.372\times10^4 s^2 + 5.46\times10^4 s + 3.456\times10^6 \qquad 6.1$$

As mentioned earlier, the first step is to obtain row or column diagonally dominant system transfer function. The Nyquist array for the equation 6.1 could be plotted with Gershgorin's bands superimposed. According to Gershgorin's bands theorem, the system is diagonally row dominant if the union of Gershgorin's bands does not enclose the complex plane's origin. Additionally, the closed loop system stability is attained if the Gershgorin's bands does not enclose the (-1,0) point (Munro, 1972).

The Gershgorin's bands for the first row of $G_o(s)$ were imposed for the Nyquist diagram of the element $g_{o11}(s)$ in figure 6.1 below. It can be clearly seen that none of the bands include the origin, therefore, diagonally dominance of the system (first row) is achieved.

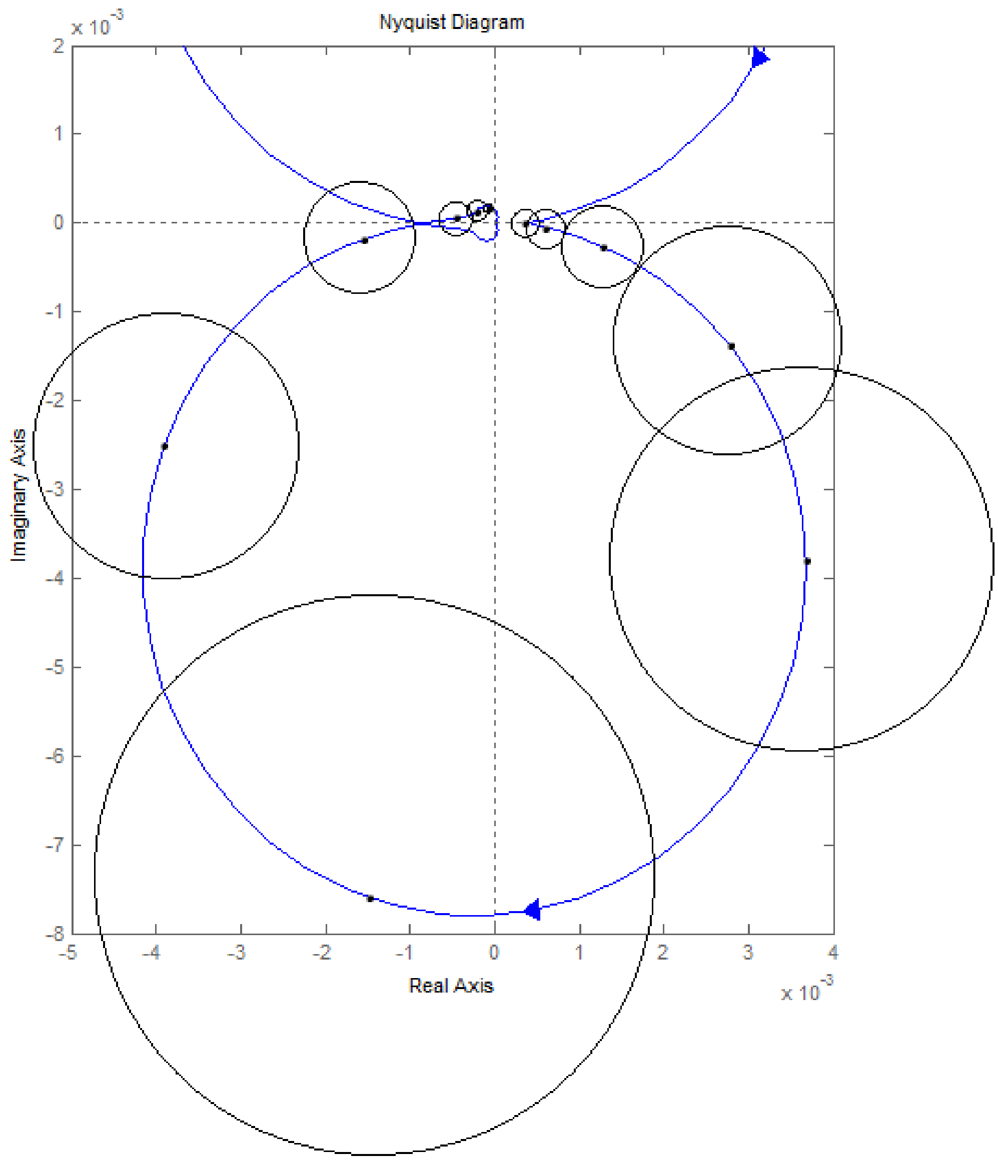

Figure 6.1, Nyquist diagram of $g_{o11}(s)$ with Gershgorin's bands (first row)

Similarly, from figure 6.2 below, imposed Gershgorin's bands for the second row ofr the Nyquist diagram of the element $g_{o22}(s)$, shows clearly none of the bands include the origin of the complex plane, hence the system is completely row dominant.

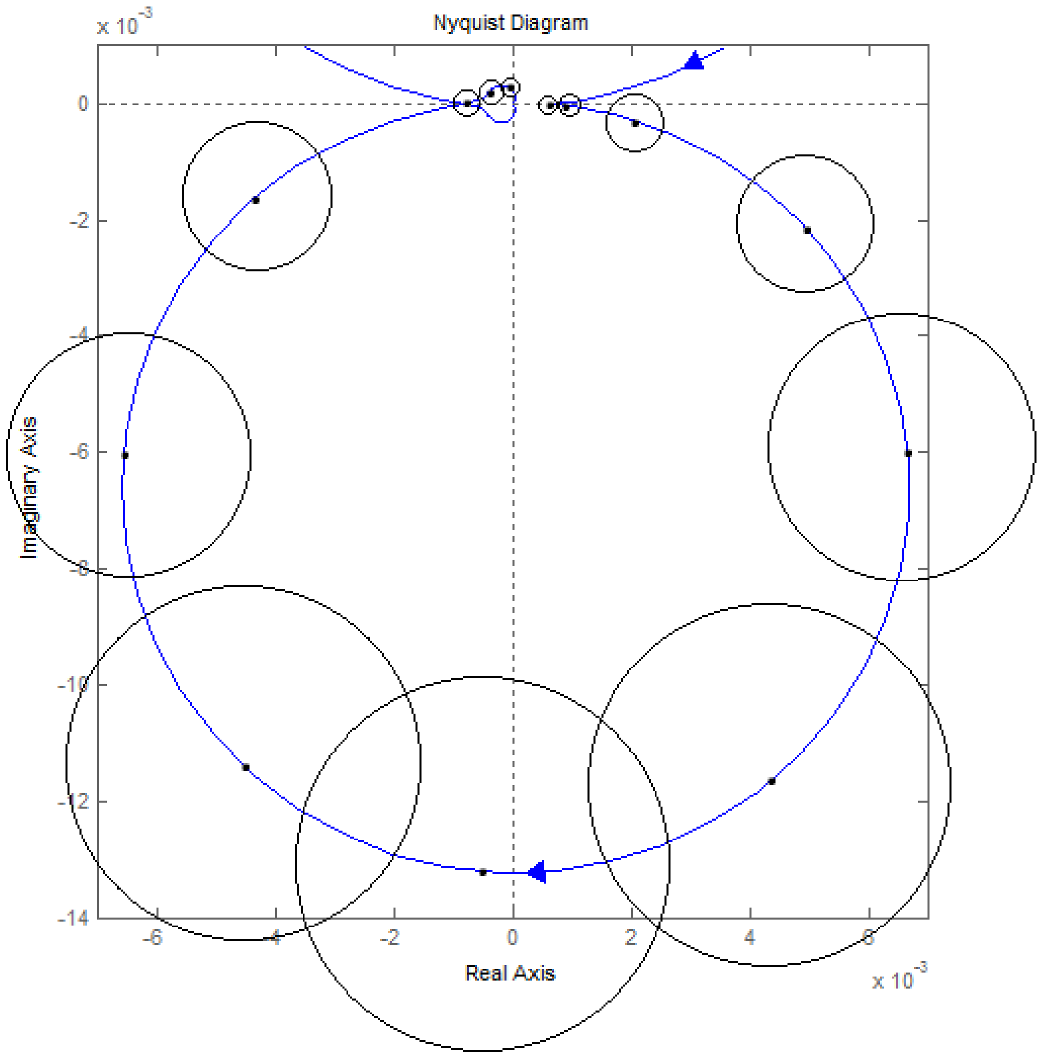

Figure 6.2, Nyquist diagram of $g_{o22}(s)$ with Gershgorin's bands (second row)

A pre-compensator is designed as $G_o(0)^{-1}$, equation 6.2, to produce the desired dominance condition. A controller for each loop could be designed independently, as diagonal dominance is achieved by this pre-compensator (Taher Khalifa, 2012).

$$G_0^{-1}(0) = \begin{bmatrix} 2502.7 & -614.7 \\ -614.7 & 1487.7 \end{bmatrix} \tag{6.2}$$

Figure 6.3 shows the block diagram of the system using controllers and pre-compensators. Additionally, unity feedback is proposed with independent loops.

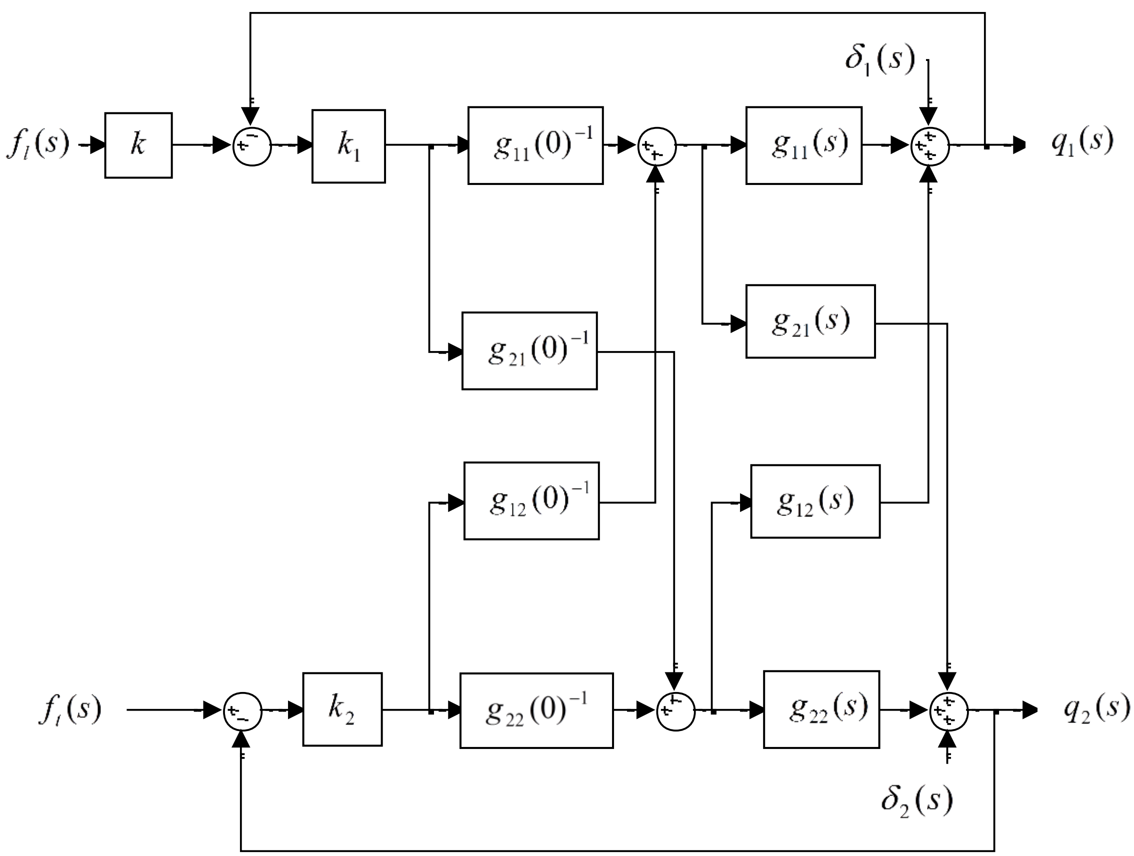

Figure 6.3, Block diagram of the system with pre-compensator and controllers (Nyquist array method)

Proportional controllers are designed for both outputs. The controllers are given by:

$$k_1 = 0.1, \quad k_2 = 0.1, \quad k = 11 \qquad 6.3$$

The simulation models are shown in The Appendix. The responses for this model will be shown and discussed in next chapter. Additionally, the disturbance recovery and energy consumption by the controllers will be examined.

Chapter 7

Simulation Results and Discussion

7.1. Least Effort Control Strategy Results

The transformed wing transfer function matrix was obtained and calculated for different velocities. As it was seen, the numerator of the transfer function is now of second degree polynomial form. To apply the least effort method to this system, the factors having s^2 were neglected. Equations 3.8 and 3.9 are the transfer function matrix equations before and after eliminating the factors having s^2. The open loop system models, figures A.1 and A.2 in The Appendix, were simulated in MATLAB. Figures 7.1 and 7.2 show that the behaviour of the open loop system after approximation, at zero velocity, have been changed only slightly. Therefore equation 3.9 for the system model was used to apply the least effort control method.

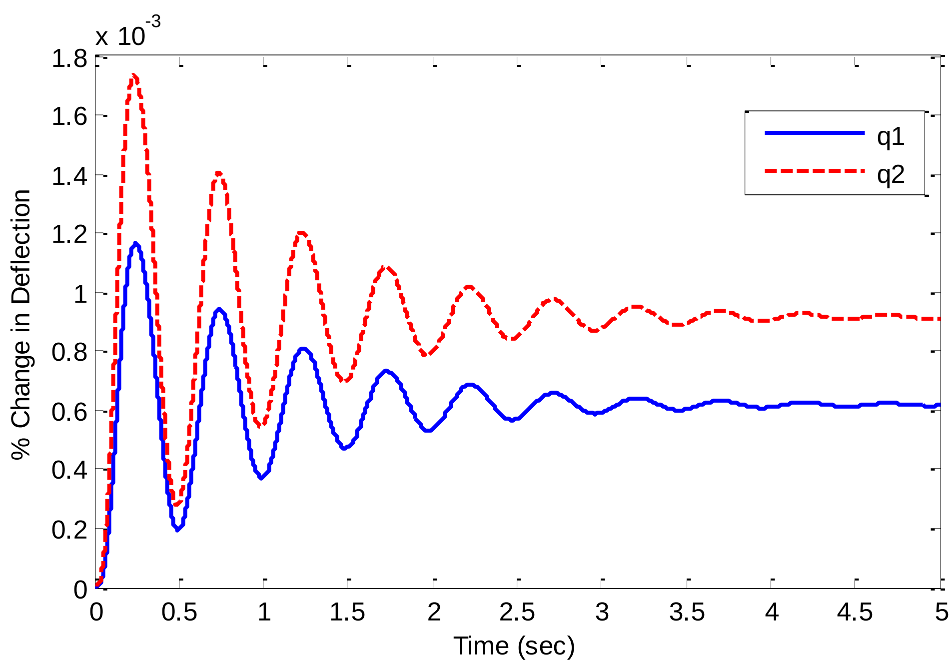

Figure 7.1, Open loop step responses for transfer function in equation 3.8

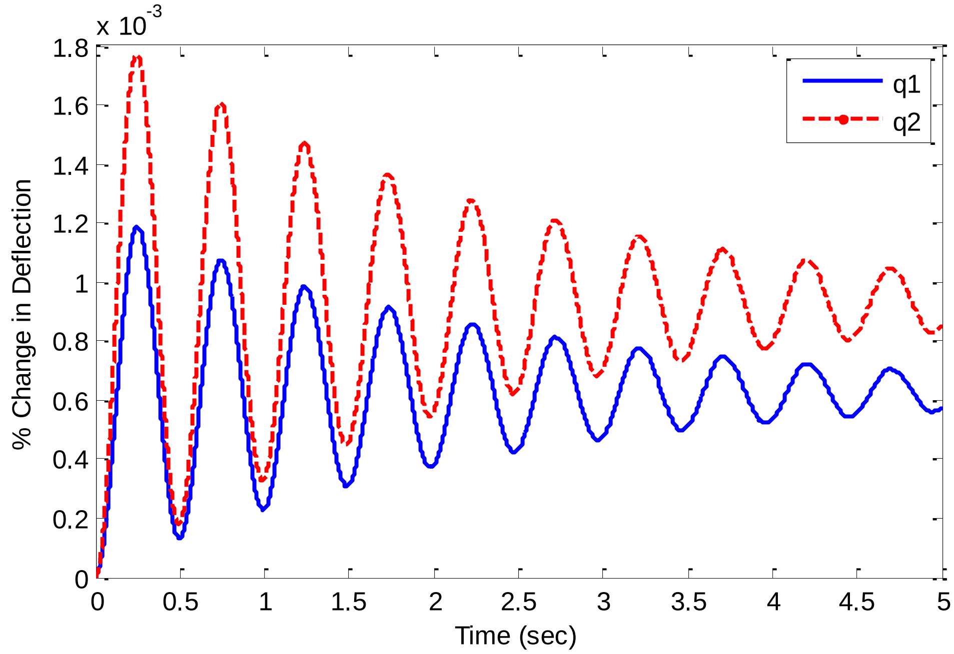

Figure 7.2, Open loop step responses for transfer function in equation 3.9

As stated in the previous sections, designing the Least effort, optimum control system includes two steps: Inner loop design and Outer loop design. In the inner loop design, the Root Locus for the equation 4.12 was plotted using MATLAB and shown in figure 4.5. In figure 4.6, the controller generated $b(s)$ has been selected to improve the dynamics of the closed loop system. The gain was selected as $b_{\circ} = 1.0969 \times 10^{4} / 0.0575875$ and a controller generated zero was generated at $(s = 0.1)$. Other places for the controller generated zero were tested but the responses were either highly oscillatory or had very high overshoots. It can be seen from the same figure that the selected gain has a damping ratio of (0.456) which is acceptable.

To find the gain ratio n for the inner loop controllers $h(s)$ and $k(s)$, the absolute minimum control effort was detected. For this purpose, the graph of the Performance Index $J(n)$ against gain ratio n was plotted in figure 4.7. It was calculated that the function of $J(n)$ has an absolute minimum at $(n = 0.3298)$. Thus this value has been chosen for the gain ratio of the inner loop controllers.

After finding the inner loop controllers $h(s)$ and $k(s)$ in equations 4.15 and 4.16, the inner loop system shown in figure 4.1 was simulated using MATLAB. Figure 7.3 shows the inner loop response for the trailing and leading edge deflection at zero velocity. As it can be seen, the responses have been improved comparing them to the open loop responses shown in figures 7.1 and 7.2. The rise time has been reduced to $(0.1\sec)$ and the responses are underdamped and well behaved whereas the open loop responses had large oscillations as indicated in figures 7.1 and 7.2. Moreover, the overshoots for leading and trailing edge have been decreased from 1.3×10^{-3} and 1.8×10^{-3} to 6.2×10^{-4} and 5.2×10^{-4} which is good. There are still small oscillations which rapidly disappear and are acceptable compared to the open loop responses. Essentially, the controlled flutter amplitude oscillation has been reduced by almost a factor of 10.

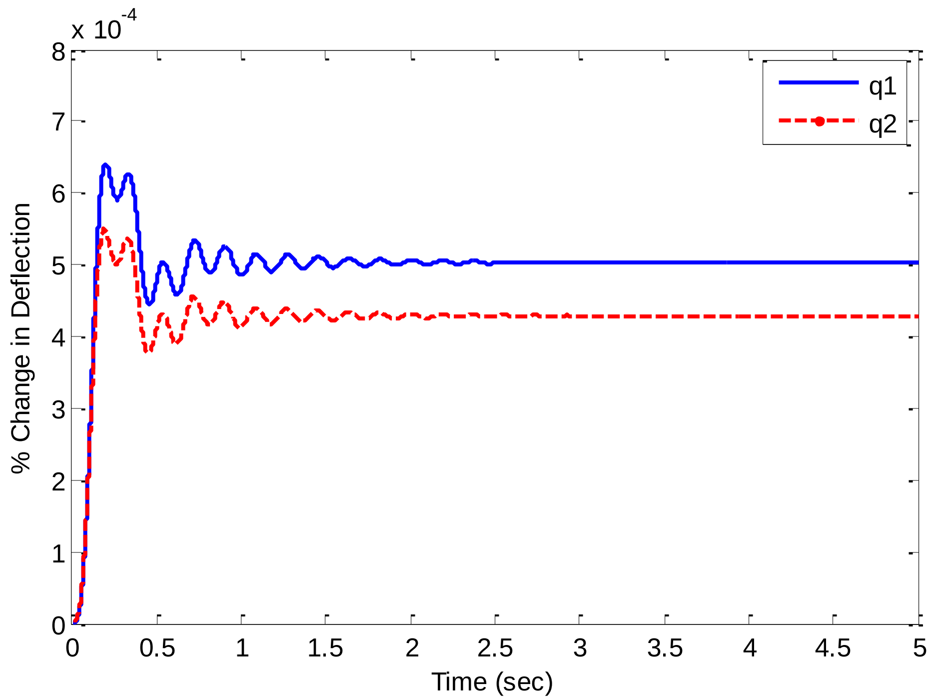

Figure 7.3, Inner loop step responses for the trailing and leading edge deflection at zero velocity

As the responses were acceptable for inner loop design at zero velocity, the outer loop controllers were calculated. For the outer loop design, the steady-state output interaction was assigned to be (0.1). As it can be seen in equation 4.18, the value for P when $(f = 0.5)$ is high. Figure 7.4 shows the transient responses for the leading and trailing edge deflection when $(f = 0.5)$ and unity signal is applied to the first reference input by simulating the model in figure 4.2. The responses are not satisfactory at all.

The same model has been simulated when $(f = 0)$. Figure 7.5 shows the time responses for the leading and trailing edge deflection following unity step change in the first reference input when $(f = 0)$. It was anticipated to get the similar responses as the inner loop responses in figure 7.3 when $(f = 0)$ but the input at leading edge force would play the role of a disturbance at the inner loop reference input. However, the responses are very oscillatory. This was unexpected because the responses show the poles of the system have been changed due to a high gain for the inner and outer loop controllers.

The other reason that caused oscillations is the poles of the system. The characteristic equation for the wing model has four complex poles at $(s = -0.4475 \pm 12.6991i)$ and $(s = -6.4301 \pm 33.9359i)$. The dominant complex poles at $(s = -0.4475 \pm 12.6991i)$ are very close to the imaginary axis and they cause closed loop oscillations. Thus the use of compensator for this system was necessary to compensate the effect of the 2 poles close to the imaginary axis that are causing the oscillations, in the system model.

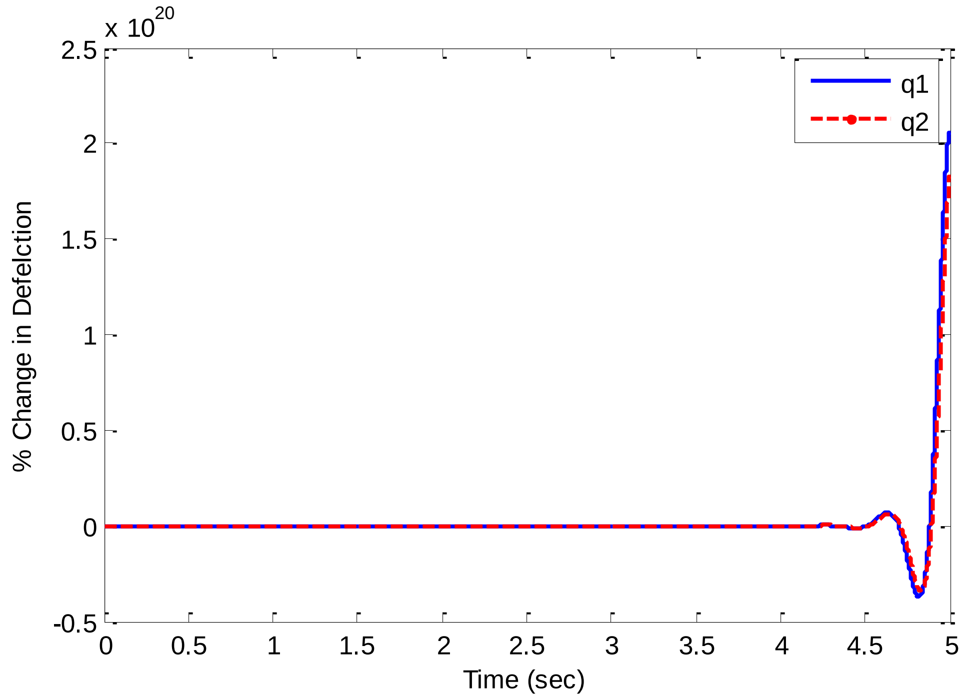

Figure 7.4, Outer loop time responses for system model at zero velocity when $(f = 0.5)$ following unity step change at Leading edge force

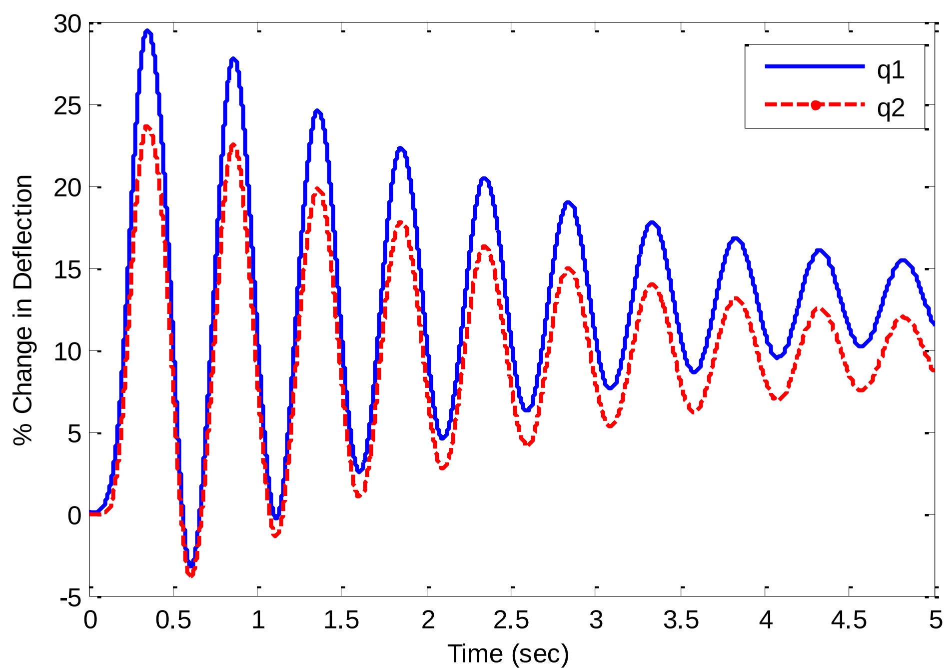

Figure 7.5, Outer loop time responses for system model at zero velocity when $(f = 0)$ following unity step change at Leading edge force

As it was seen in figure 7.4, the system time responses were unstable. Therefore, designing a compensator was essential for this wing model.

The open loop wing model characteristic equation has four complex poles at:

$$\begin{cases} s = -0.4475 \pm 12.6991i \\ s = -6.4301 \pm 33.9359i \end{cases}$$

The poles at $(s = -0.4475 \pm 12.6991i)$ are the dominant poles which cause the oscillations. Thus, the compensator $C(s)$ was designed, to produce the effect of equation 5.1, in order to cancel the influence of these poles. Therefore, the numerator of the compensator has zeros at $(s = -0.4475 \pm 12.6991i)$. The denominator was designed according to the second order active filter network in equation 5.2. The circuit diagram of this network, was shown in figure 5.1. The parameters for this network were calculated as in table 1.

After designing the compensator $C(s)$, the new transfer function was generated in equation 5.5. The inner loop design procedure was applied for the new system model. The inner loop controllers were designed and calculated according to the performance index graph, equation 5.7 in figure 5.3. The controller which generates the zero for the system was chosen at $(x = -6)$ and with a gain of $(b_{\circ} = 1)$ in order to increase the separation from the imaginary axis. The inner loop controllers were calculated in equation 5.8.

velocity (m/s)	Open loop transfer function
$v=0$	$G_0(s)=\dfrac{\begin{bmatrix} 9s+1487.7 & 9s+614.7 \\ 9s+614.7 & 29s+2502.7 \end{bmatrix}}{\Delta_0(s)}$ $\Delta_0(s)=17.365s^4+238.86s^3+2.372\times10^4 s^2+5.46\times10^4 s+3.456\times10^6$
$v=5$	$G=\dfrac{\begin{bmatrix} 13.032s+1491.3 & 4.462s+598.875 \\ 10.728s+611.1 & 31.233s+2486.9 \end{bmatrix}}{\Delta(s)}$ $\Delta(s)=17.365s^4+264.68s^3+2.3803\times10^4 s^2+6.9516\times10^4 s+3.456\times10^6$
$v=10$	$G=\dfrac{\begin{bmatrix} 17.064s+1502.1 & -0.076s+551.4 \\ 12.456s+600.3 & 33.466s+2439.4 \end{bmatrix}}{\Delta(s)}$ $\Delta(s)=17.365s^4+290.5s^3+2.3736\times10^4 s^2+84658s+3.3169\times10^6$
$v=15$	$G=\dfrac{\begin{bmatrix} 21.096s+1520.1 & -4.614s+472.275 \\ 14.184s+582.3 & 35.699s+2360.3 \end{bmatrix}}{\Delta(s)}$ $\Delta(s)=17.365s^4+316.32s^3+2.3518\times10^4 s^2+1.0011\times10^5 s+3.2818\times10^6$
$v=20$	$G=\dfrac{\begin{bmatrix} 25.128s+1545.3 & -9.152s+361.5 \\ 15.912s+577.1 & 37.932s+2249.5 \end{bmatrix}}{\Delta(s)}$ $\Delta(s)=17.365s^4+342.14s^3+2.3151\times10^4 s^2+115952s+3.2327\times10^6$

Table 2, Computation of the transfer function of the system model at different air velocities

The system model in figure 7.2 was simulated using the inner loop controllers found in equation 5.8. Figure 7.6a shows the inner loop time response for the system model with the compensator, for zero air flow velocity. The transfer functions for different velocities were computed in table 2. The inner loop responses were obtained for other air velocities at 5, 10, 15 and 20 (m/s) as well shown in figures 7.6b, 7.6c, 7.6d and 7.6e using the transfer functions in table 2, in the simulation model in figure 5.2. The responses are acceptable enabling the outer loop controller to be determined.

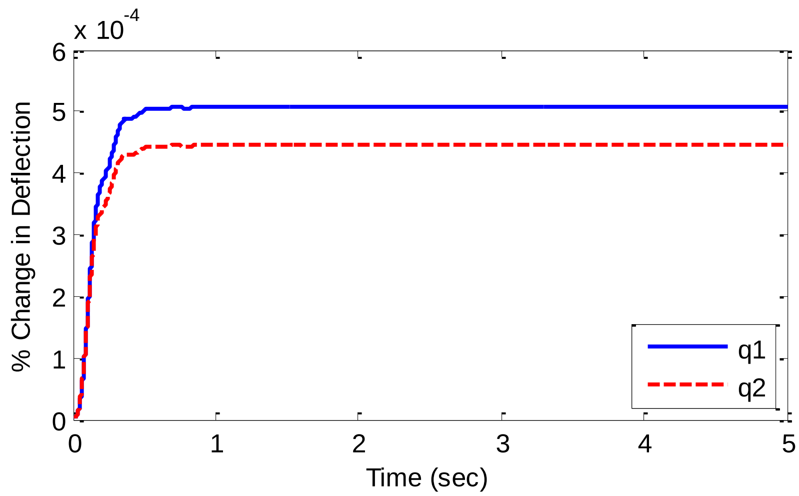

Figure 7.6a, Inner loop responses for the system model at $v = 0$ (m/s)

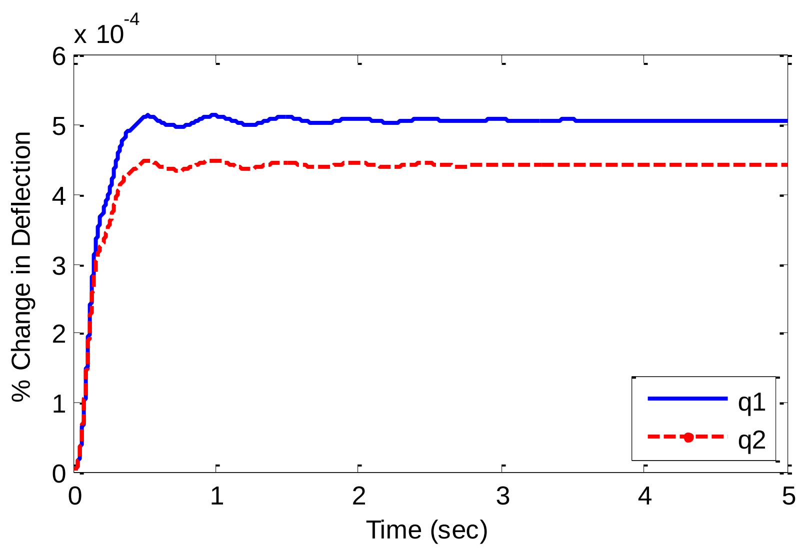

Figure 7.6b, Inner loop responses for the system model at $v = 5$ (m/s)

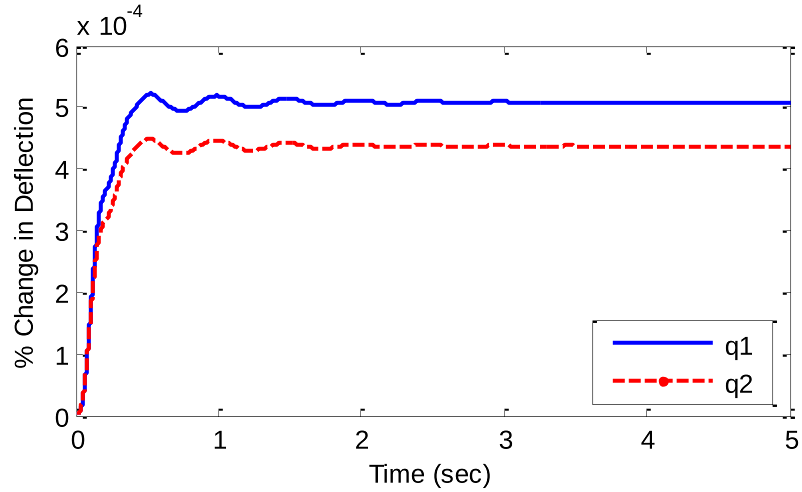

Figure 7.6c, Inner loop responses for the system model at $v = 10$ (m/s)

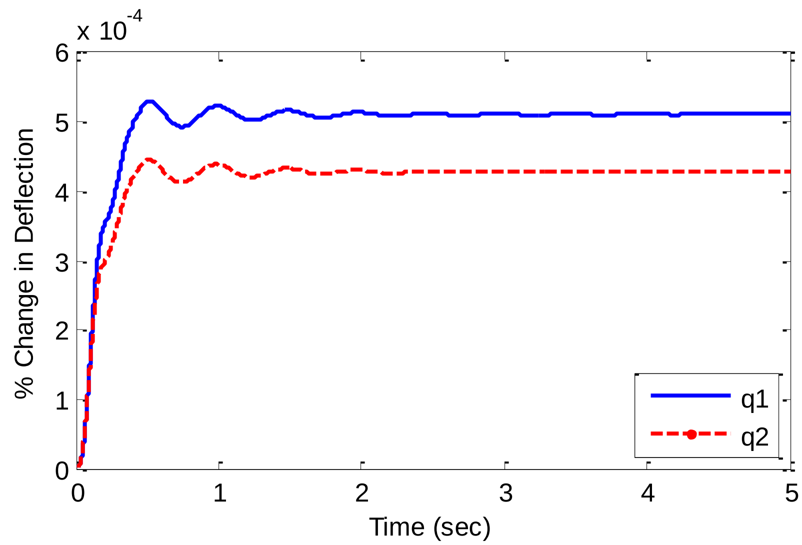

Figure 7.6d, Inner loop responses for the system model at $v = 15$ (m/s)

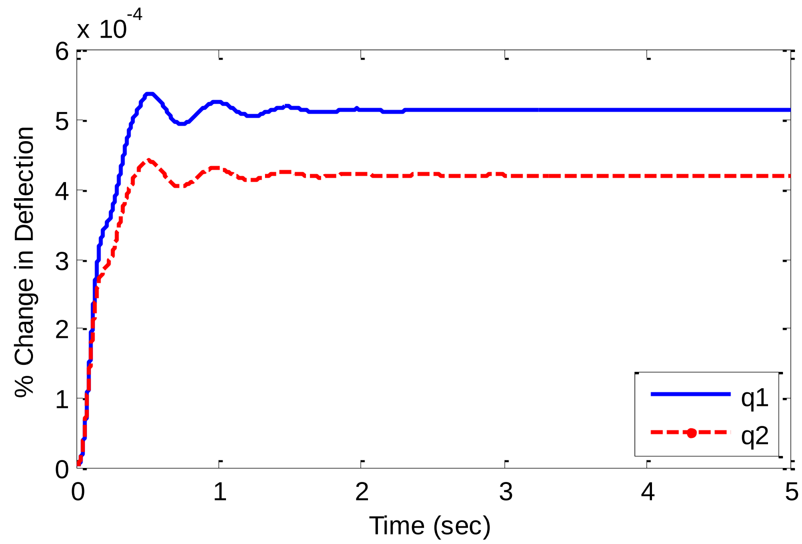

Figure 7.6e, Inner loop responses for the system model at $v = 20$ (m/s)

For the outer loop design, the steady-state matrix S_s was chosen in order to limit the steady-state output interaction to 10% and the outer loop feedback gains to (0.1). The outer loop controller P was obtained from equation 5.10 by applying the same procedure of previously. It is noticeable that the numerical values for this controller are high. In order to distribute these values for P, the gains were dispersed between the forward path gain P and the feedback gain f. This follows as shown in figure 5.5.

The outer loop model in figure 5.4 was simulated for different velocities for $(f = 0.55)$ following a step change of unity on $f_l(t)$ and then on $f_t(t)$. Figure 7.7 shows the outer loop responses following step change on the leading and trailing edge forces. Noticeably, from figure 7.7, the steady state values are almost (1) and (0.1), as designed. As the velocity increases, the responses become more oscillatory with less overshoots. The responses have rise time less than (0.1sec) which compared to open loop responses, are faster.

Finally, conventional pre and feedback compensator structure was achieved using simple transformation. The block diagram for $(f = 0.55)$ and calculated values for the pre and feedback compensators $K(s)$ and $H(s)$ can be found in figure 5.6 and equations 5.13 and 5.14 respectively. As the numerical values for $K(s)$ are high, the same procedure was applied to distribute these gains. Equations 5.15 and 5.16 are the new values for $K(s)$ and $H(s)$. The block diagram is shown in figure 5.7 after distributing the gains.

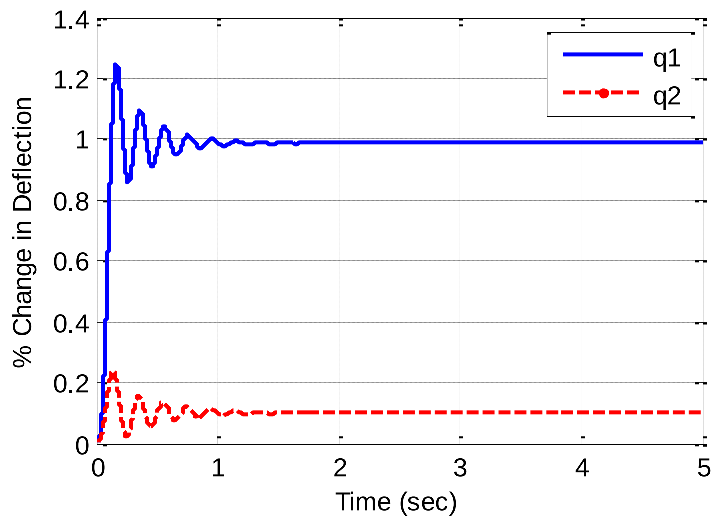

Figure 7.7a, Closed loop system responses following a step change on leading edge force when $v = 0$ m/s

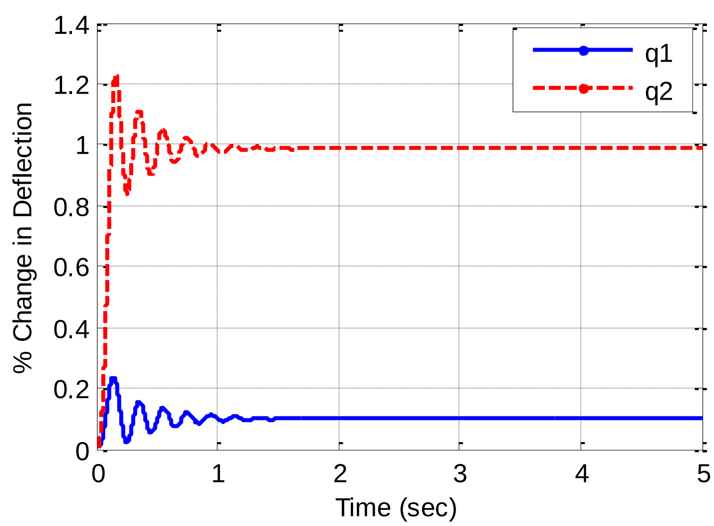

Figure 7.7b, Closed loop system responses following a step change on trailing edge force when $v = 0$ m/s

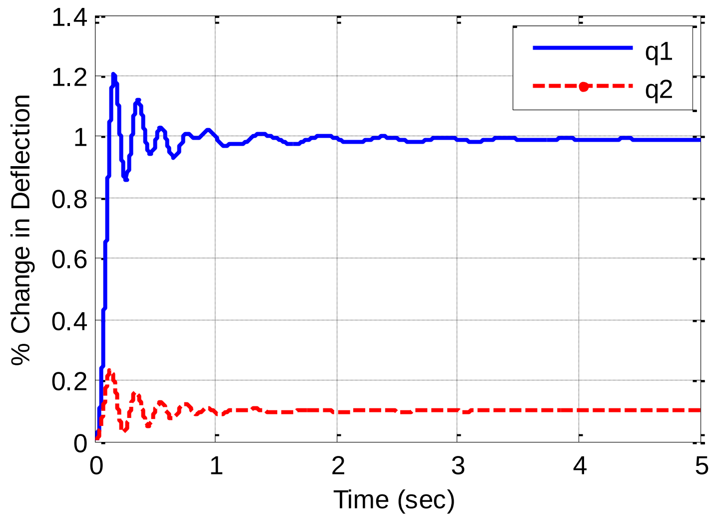

Figure 7.7c, Closed loop system responses following a step change on leading edge force when $v = 5$ m/s

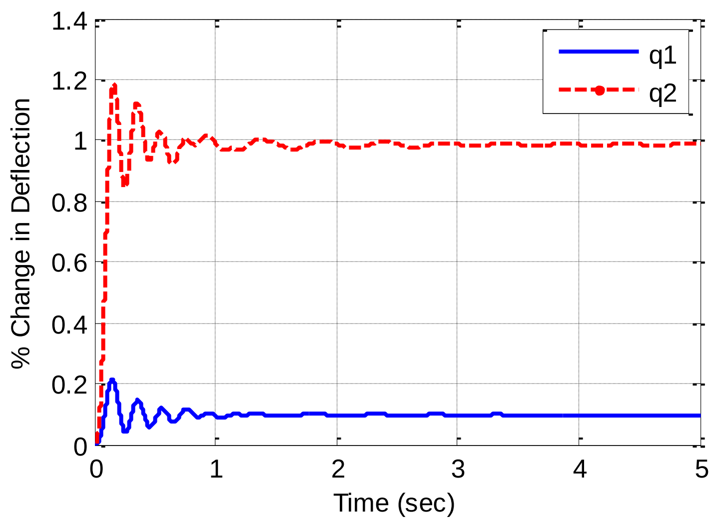

Figure 7.7d, Closed loop system responses following a step change on trailing edge force when $v = 5$ m/s

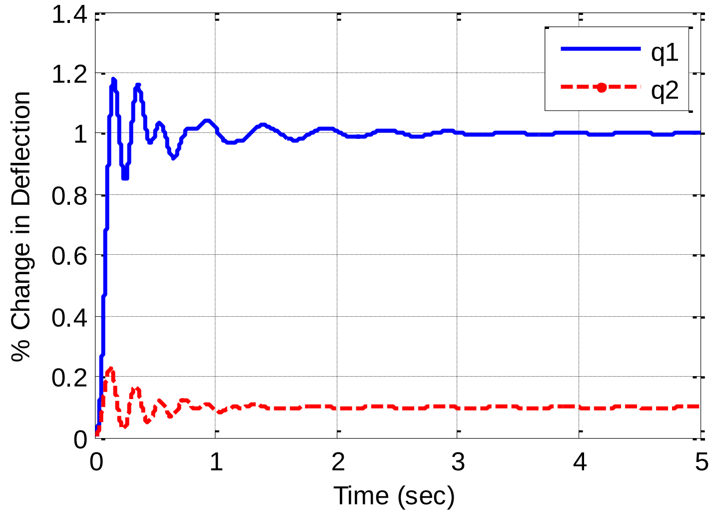

Figure 7.7e, Closed loop system responses following a step change on leading edge force when $v = 10$ m/s

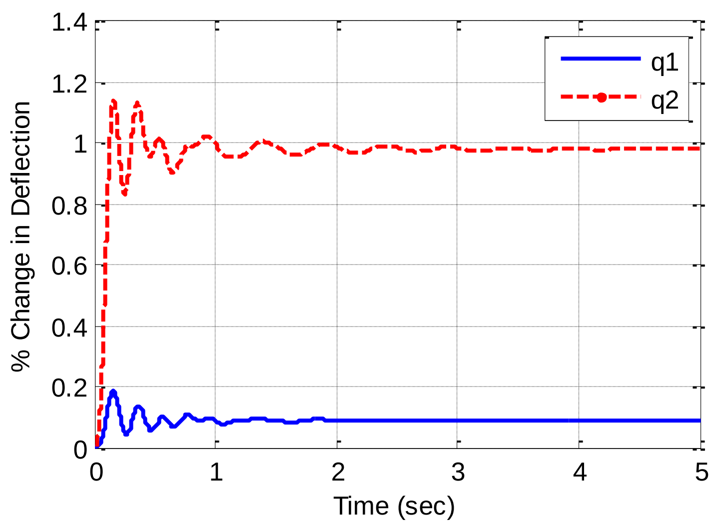

Figure 7.7f, Closed loop system responses following a step change on trailing edge force when $v = 10$ m/s

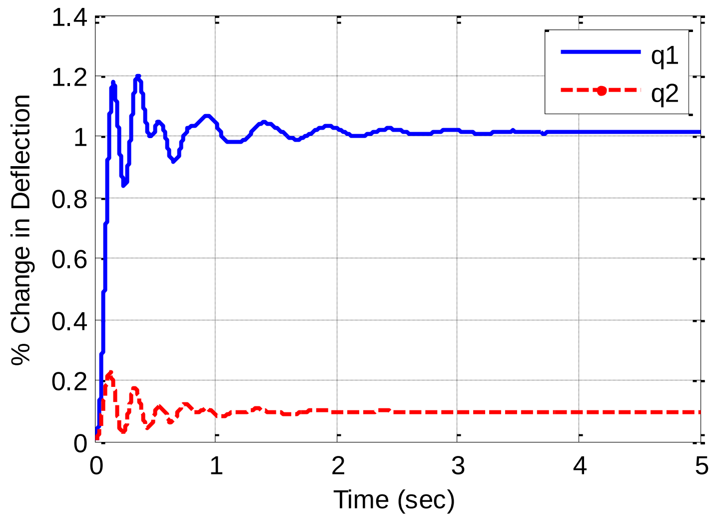

Figure 7.7g, Closed loop system responses following a step change on leading edge force when $v = 15$ m/s

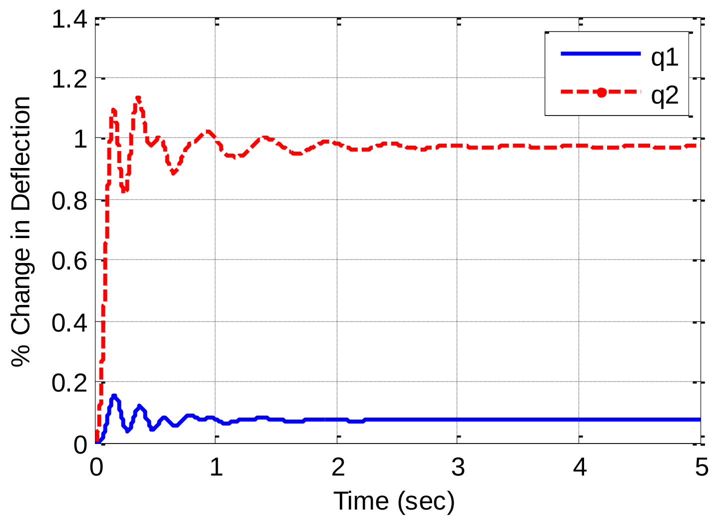

Figure 7.7h, Closed loop system responses following a step change on trailing edge force when $v = 15$ m/s

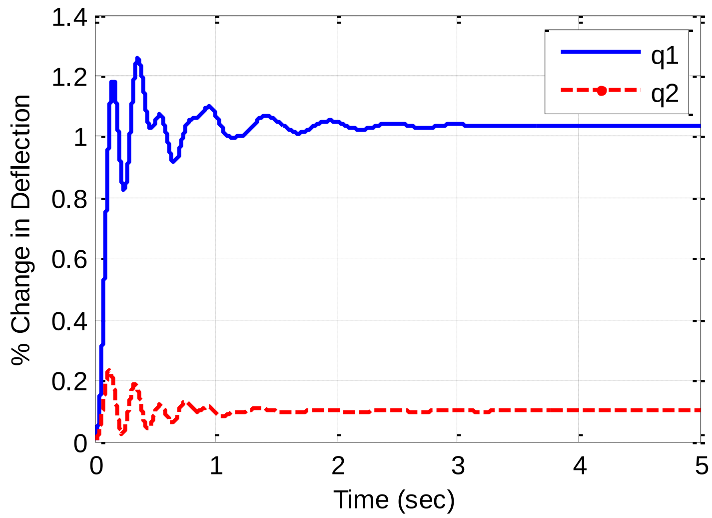

Figure 7.7i, Closed loop system responses following a step change on leading edge force when $v = 20$ m/s

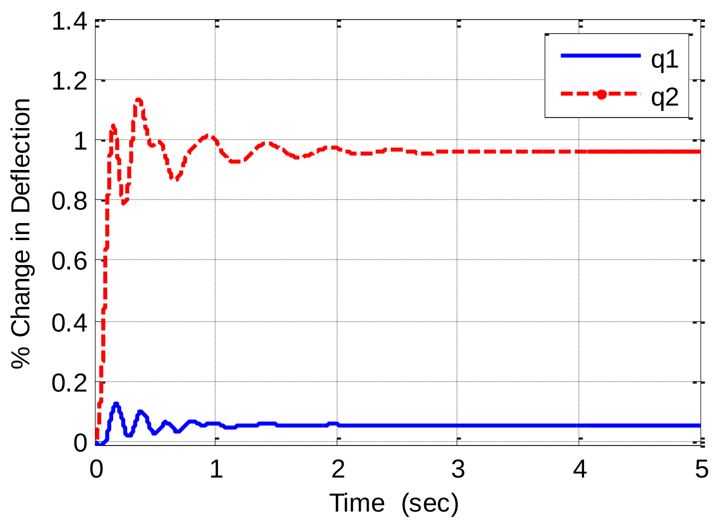

Figure 7.7j, Closed loop system responses following a step change on trailing edge force when $v = 20$ m/s

Chapter 8

Disturbance Suppression Results

"Disturbances coming from the environment often constitute an annoyance in the operation of dynamic systems. Disturbance rejection control (DRC), in which the controller is designed to suppress the disturbance's effect, is the major concern in the design of feedback control systems. Since external disturbances are usually not accessible for measurement, in the early development of disturbance rejection control, high gain control is used to suppress the unknown disturbance." (Jeang-Lin Chang, 2011

The closed loop system time responses when $f = 0.55$ following a step change of unity on disturbances $\delta_1(t)$ and then $\delta_2(t)$ for different velocities, setting references inputs to zero, are shown in figure 8.1. From figures 8.1a and 8.1b at least 55% disturbance suppression is achieved when $v = 0$ (m/s). As the velocity increases, the disturbance recovery increases slightly as well. For example, the disturbance suppression is 57% when $v = 20$ (m/s) as it shows in figures 8.1i and 8.1j with quiescence being achieved in less than 1 sec.

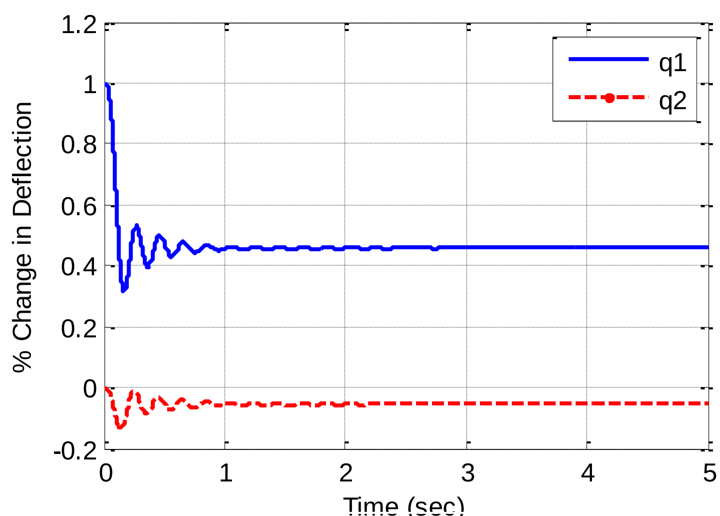

Figure 8.1a, Closed loop system responses following 1% step change on $\delta_1(t)$ when $v = 0$ m/s

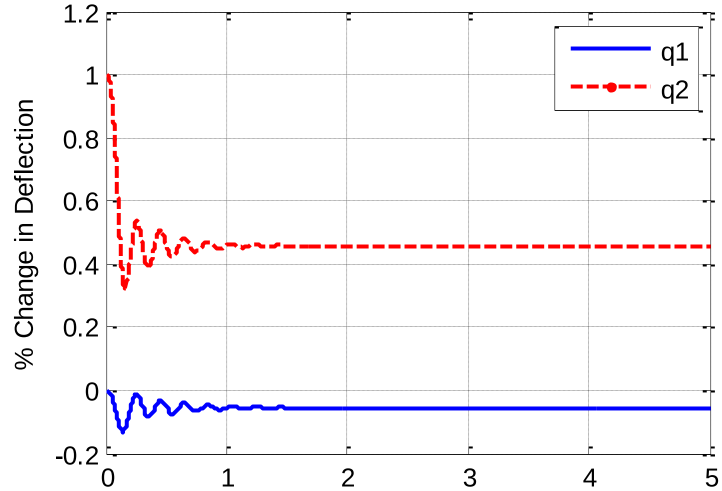

Figure 8.1b, Closed loop system responses following 1% step change on $\delta_2(t)$ when $v = 0$ m/s

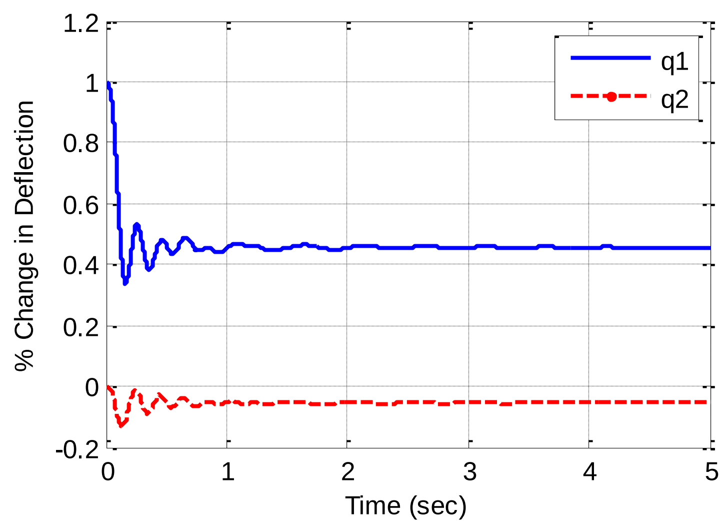

Figure 8.1c, Closed loop system responses following 1% step change on $\delta_1(t)$ when $v = 5$ m/s

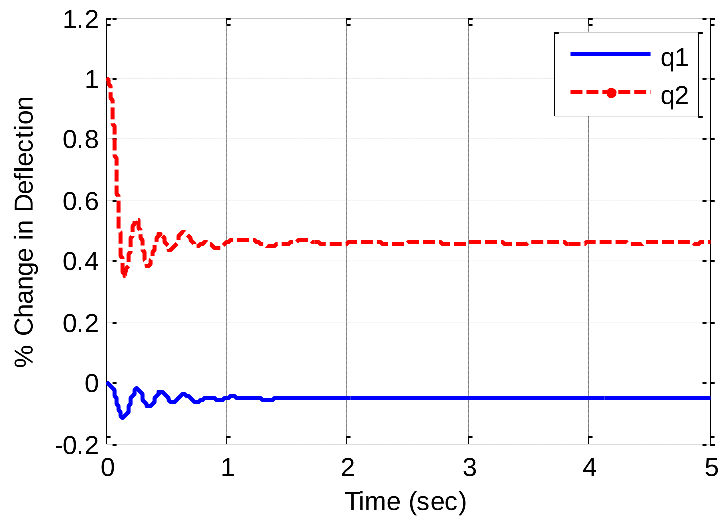

Figure 8.1d, Closed loop system responses following 1% step change on $\delta_2(t)$ when $v = 5$ m/s

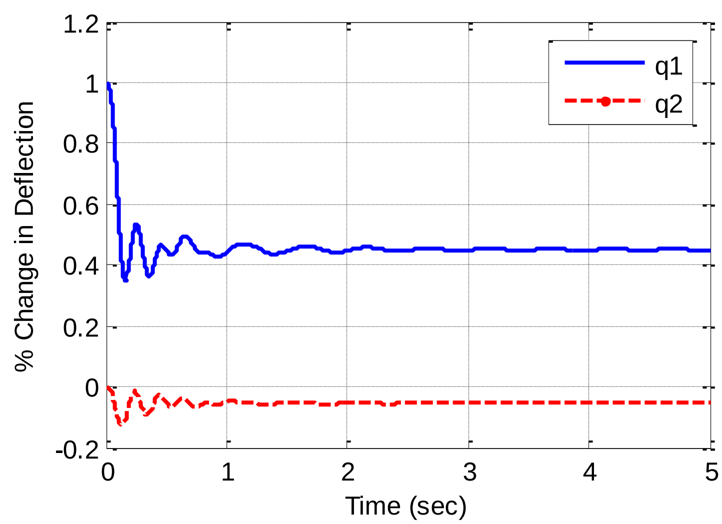

Figure 8.1e, Closed loop system responses following 1% step change on $\delta_1(t)$ when $v = 10$ m/s

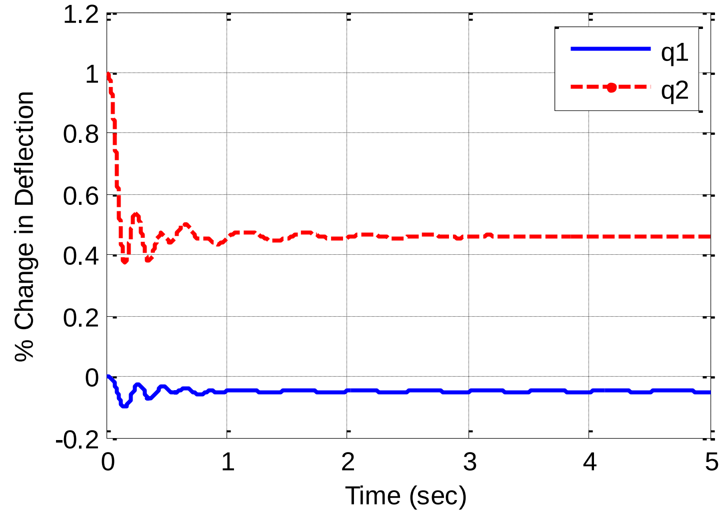

Figure 8.1f, Closed loop system responses following 1% step change on $\delta_2(t)$ when $v = 10$ m/s

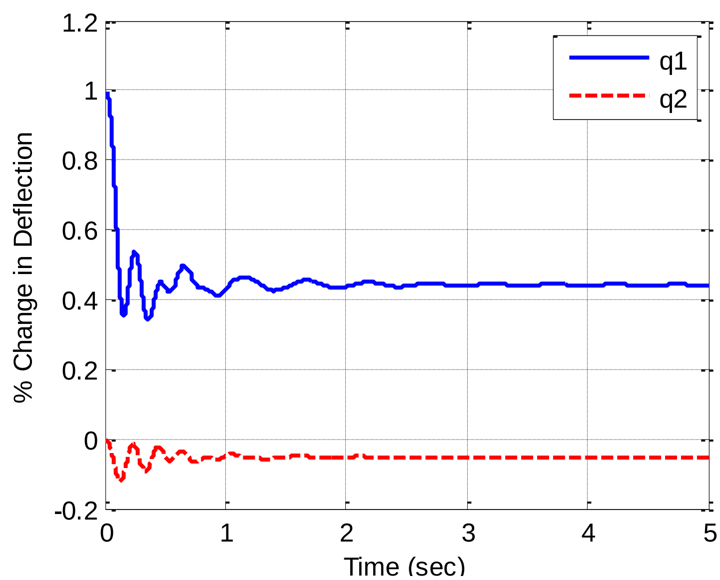

Figure 8.1g, Closed loop system responses following 1% step change on $\delta_1(t)$ when $v = 15$ m/s

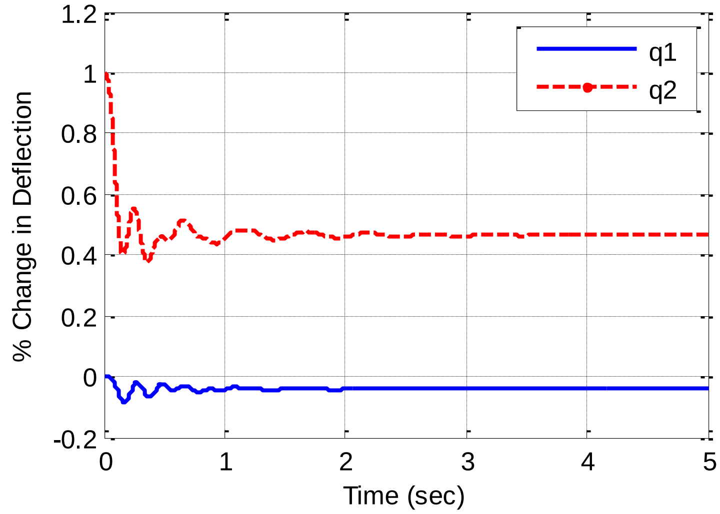

Figure 8.1h, Closed loop system responses following 1% step change on $\delta_2(t)$ when $v = 15$ m/s

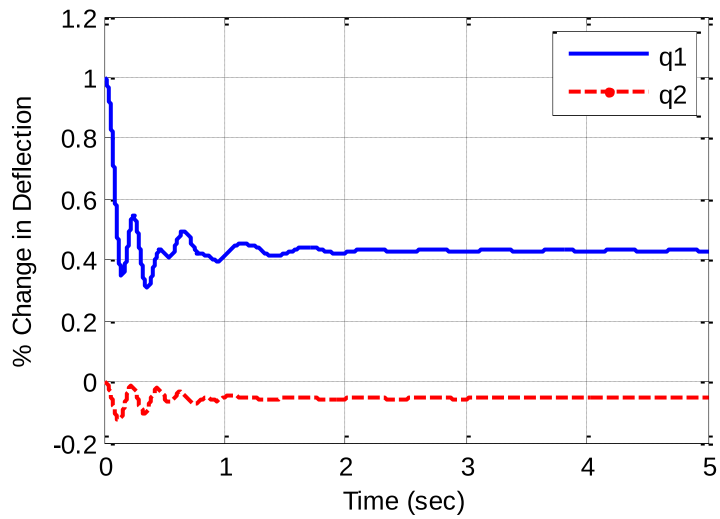

Figure 8.1i, Closed loop system responses following 1% step change on $\delta_1(t)$ when $v = 20$ m/s

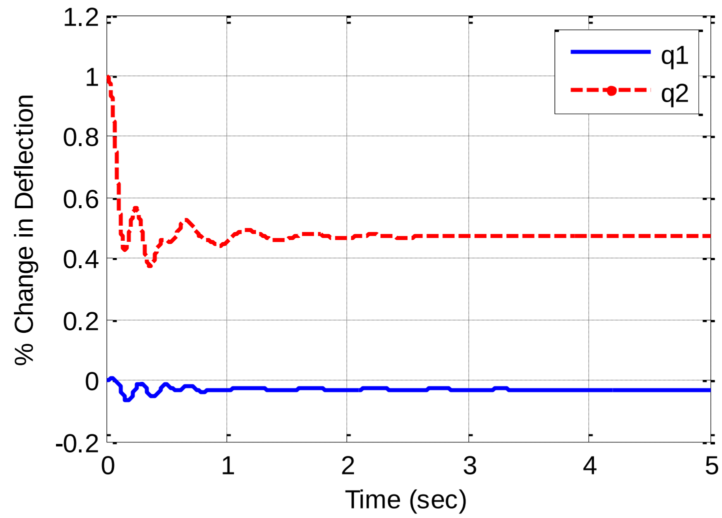

Figure 8.1j, Closed loop system responses following 1% step change on $\delta_2(t)$ when $v = 20$ m/s

In order to prove that the Least effort method dissipates the least energy, different gain ratios were chosen and simulated using the model shown in figure 4.4. Figure 8.2 shows control energy dissipation for different gain ratios following random changes on disturbances $\delta_1(t)$ and $\delta_2(t)$, for $(f = 0.55)$ with the reference inputs set to zero. It can be seen from these graphs that the energy required increases. The graph with the gain ratio of $(n = 0.3521)$ gives least effort control, as predicted, with least energy requirements, compared to the other two gain ratios of $(n_1 = 0.3)$ and $(n_2 = 0.4)$. This energy dissipation difference is proportional to the area difference under these curves which is monotonically increasing with time.

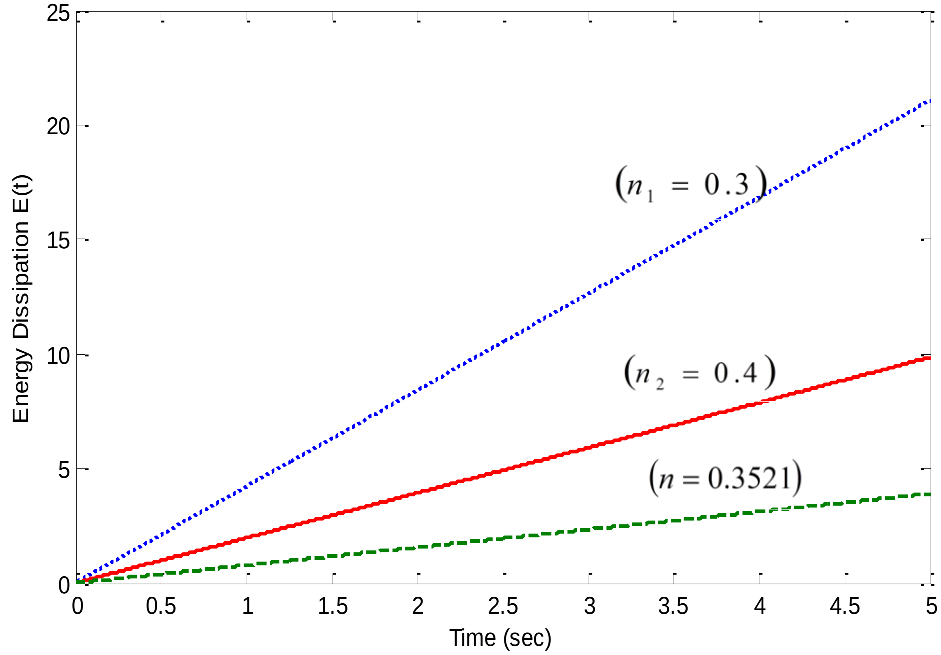

Figure 8.2, Energy dissipation following random disturbances on $\delta_1(t)$ and $\delta_2(t)$ when gain ratio of $(n = 0.3521)$, $(n_1 = 0.3)$ and $(n_2 = 0.4)$

Chapter 9

Nyquist Array Method Results

For comparison purposes, Nyquist array method was also applied to the same wing arrangement. As mentioned in previous chapter, according to Gershgorin's bands in figures 6.1 and 6.2, the system transfer function matrix was row diagonally dominance. To produce desired diagonal dominant conditions, pre-compensator $G_o^{-1}(0)$ was added to the system. The proportional controllers k, k_1 and k_2 were designed as given by equation 6.3.

The model in figure A.5 in the Appendix was simulated following a step input on leading edge force using MATLAB software. Figure 9.1 shows the transient response for this wing assembly at zero velocity using Nyquist array method. It is obvious that the system response requires much more time to settle and to reach steady state compared to the system response using the Least effort strategy in figure 7.7a. The complete decoupled system can be seen at steady state.

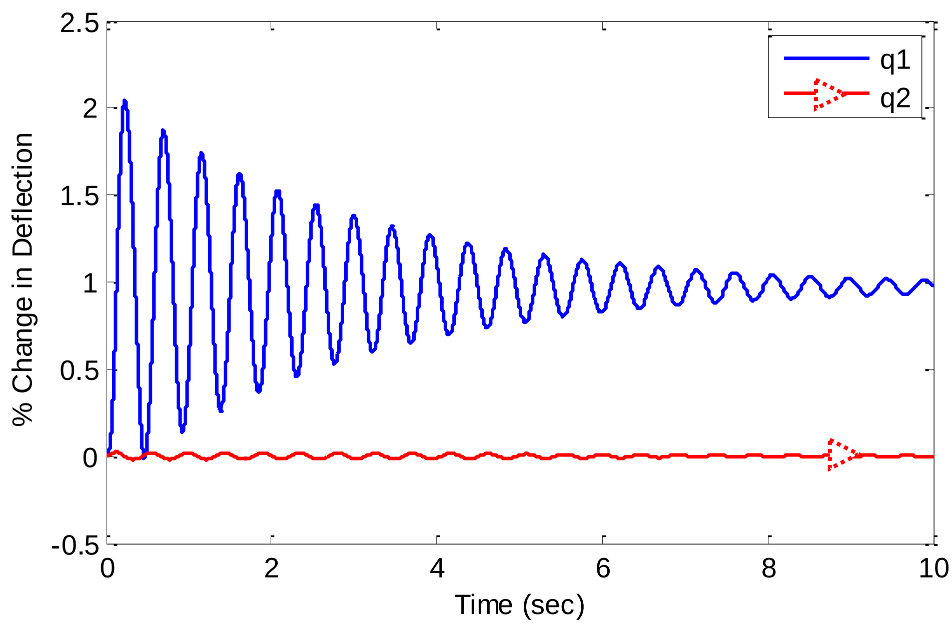

Figure 5.10, Closed loop system responses following 1% step change on leading edge force when $v = 0$ m/s

Additionally, following a unit step change on leading force when $v = 20$ m/s in simulation model, figure A.6 in The Appendix, results in the response shown in figure 9.2. Similar to the system response at zero velocity, the settling time is much more when $v = 20$ m/s compared to the response using the Least effort strategy in figure 7.7i. It is noticeable that the system is completely decoupled in steady state.

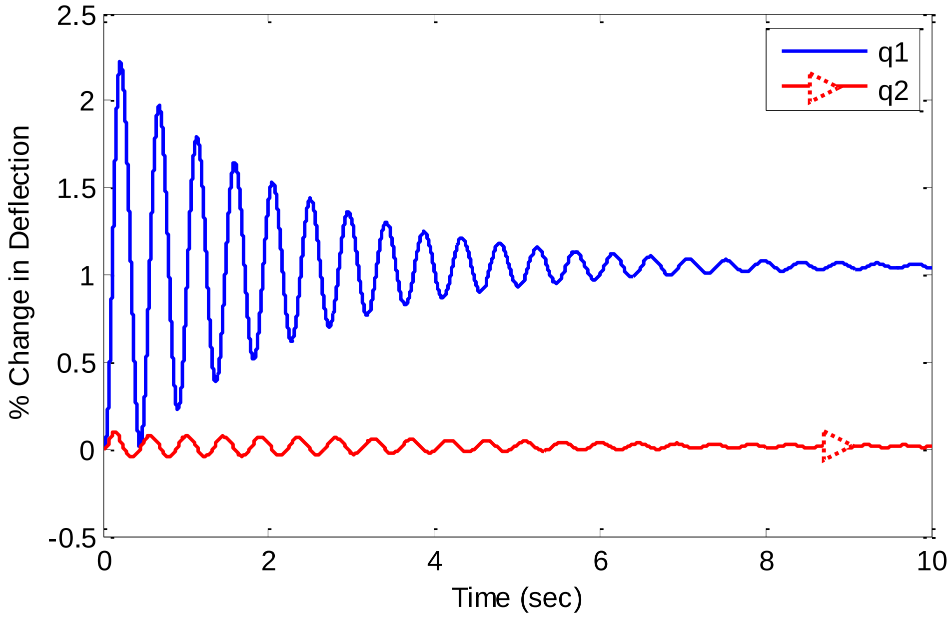

Figure 9.2, Closed loop system responses following 1% step change on leading edge force when $v = 20$ m/s

The models in figures A.7 and A.8 in the Appendix were simulated following a step input on first and second disturbances using MATLAB software. From figures 9.3a, 9.3b, 9.4a and 9.4b at least 10% disturbance suppression was achieved when $v = 0$ and 20 (m/s) which is poor.

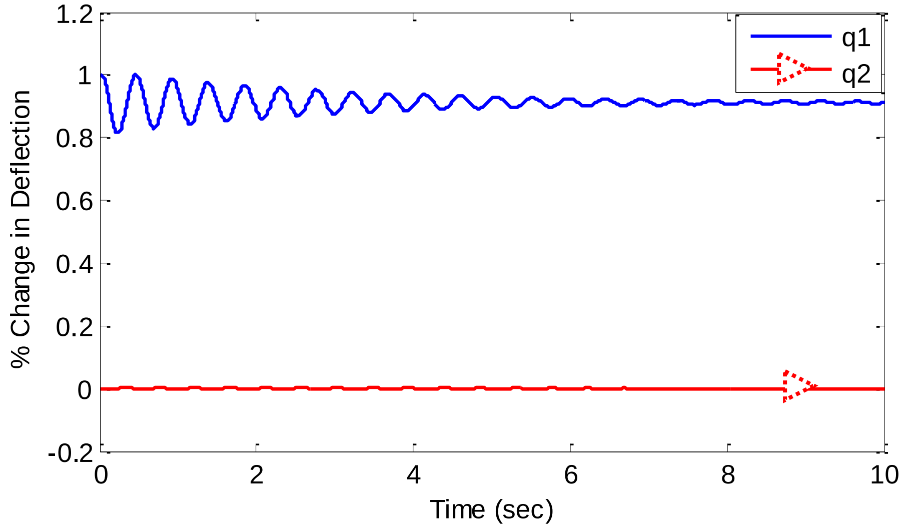

Figure 9.3a, Closed loop system responses at zero velocity following 1% step change on disturbance $\delta_1(t)$

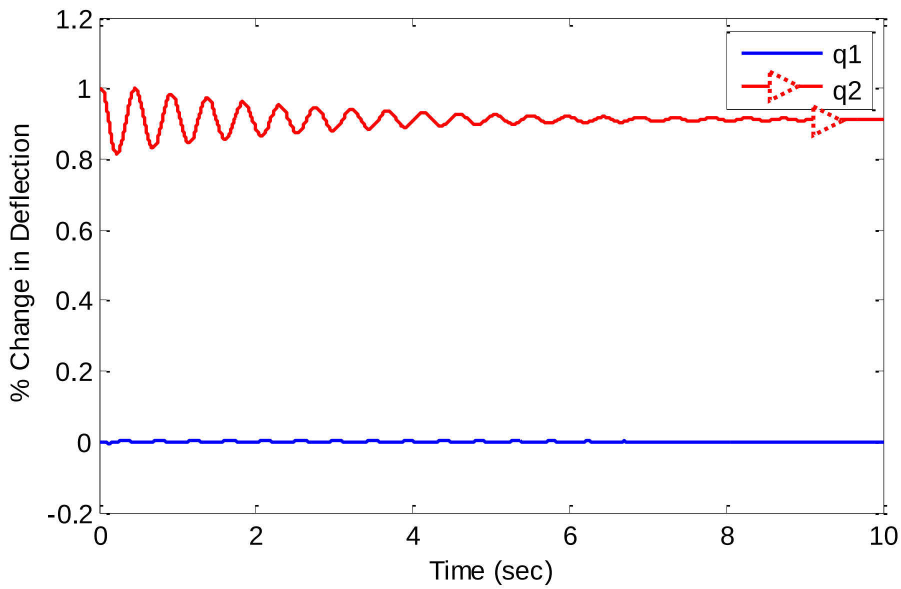

Figure 9.3b, Closed loop system responses at zero velocity following 1% step change on disturbance $\delta_2(t)$

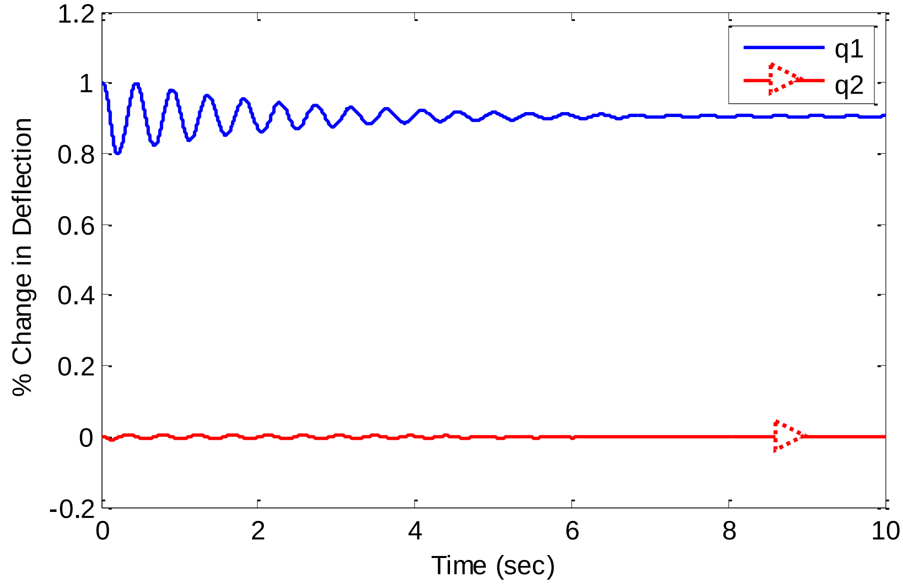

Figure 9.4a, Closed loop system responses following 1% step change on disturbance $\delta_1(t)$ when $v = 20$ m/s

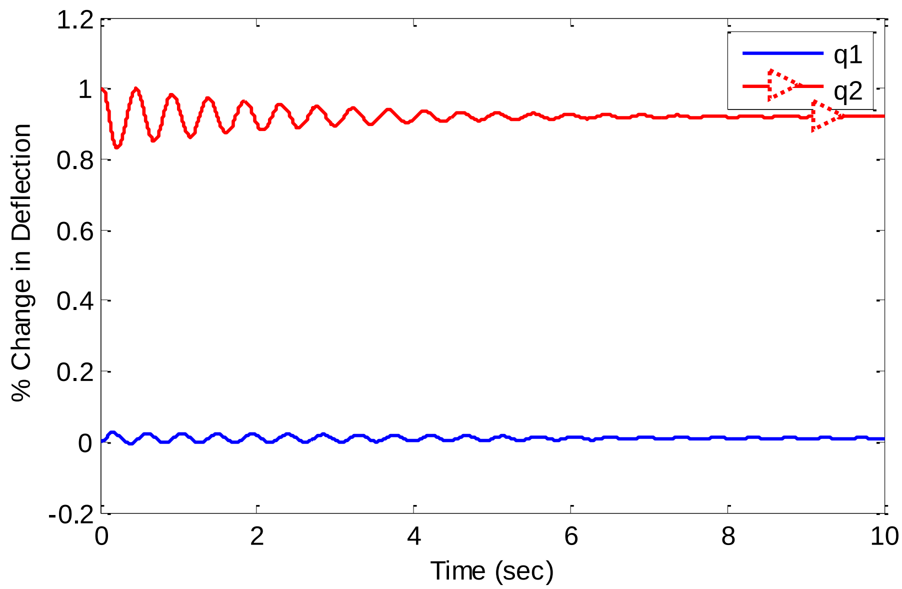

Figure 9.4b, Closed loop system responses following 1% step change on disturbance $\delta_2(t)$ when $v = 20$ m/s

Finally, control energy dissipation following random changes on disturbances $\delta_1(t)$ and $\delta_2(t)$ was computed. Figure 9.5 shows that controllers using Nyquist array method consumes substantial energy whereas the Least effort controller is very frugal, almost occupying the zero energy dissipation level.

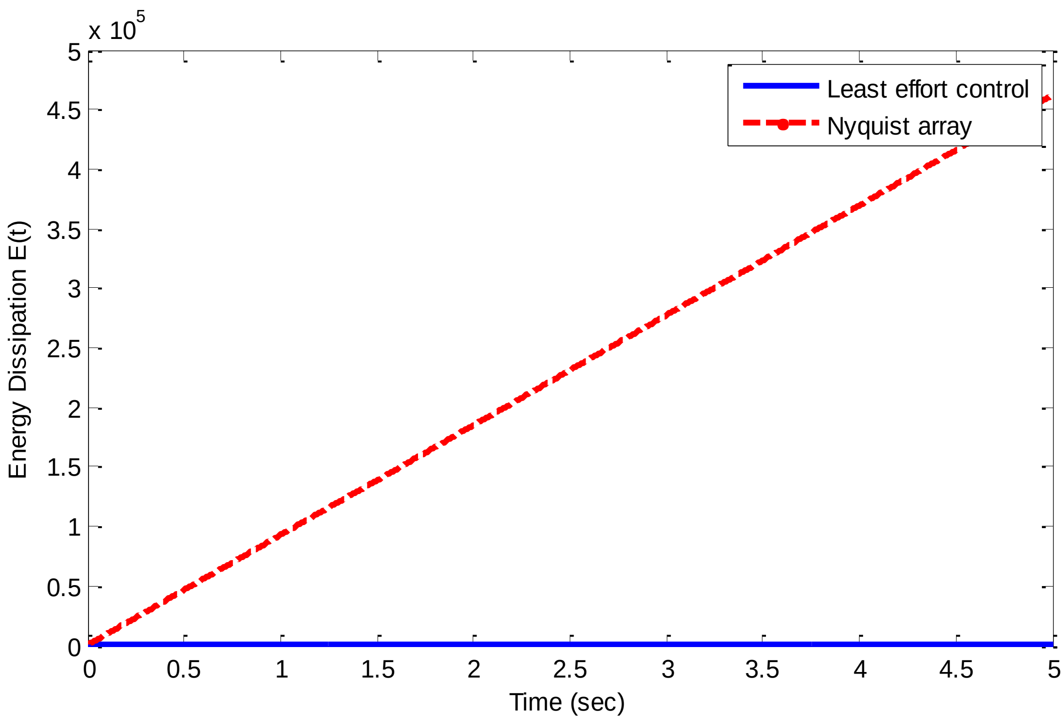

Figure 9.5, Energy dissipation following random disturbances on $\delta_1(t)$ and $\delta_2(t)$ using Nyquist array method

Chapter 10

Comparison study

Each technique for designing a multivariable controller has its own advantages, disadvantages and difficulties. There are four factors which are important:

1. Difficulties of applying the techniques and its practicality
2. Evaluating the closed loop response following a unit step change on each input independently
3. Achieving acceptable disturbance rejection
4. Using minimum energy to obtain 1, 2 and 3

Designing a controller for the system transfer function in the Laplace domain is required for applying the Least effort control strategy. However, to be suitable for designing purposes, the transfer function numerator should be approximated. The reduced transfer function transient and steady state values must be approximately same as the original one. Thus, this method can be applied to complicated systems with multiple of inputs and outputs.

On the other hand, the difficulty of the Nyquist array method lies in achieving diagonal dominance, to reduce the system output coupling, before applying the single-input single-output design techniques. There is no special technique for finding a pre-compensator which would induce this condition. Moreover, the question remaining is that there is the possibility of none or many pre-compensators which could be used to achieve this.

According to each controller, closed loop responses following a unit step changes on first reference input are compared. From figures 7.7, 9.1 and 9.2, it is clearly seen that the Least effort control results in superiour transient response and steady state performance compared to Nyquist array method. Moreover, the responses using the Least effort control strategy have desirable transients, in comparison to the ones obtained using the Nyquist array method.

Furthermore, the closed loop responses following a unit step disturbance change, from the simulation models of figures A.7 and A.8 in the Appendix are compared according to each controller. As discussed earlier, from figures 8.1a and 8.1b at least 55% disturbance suppression is achieved when $v = 0$ (m/s) using Least effort control strategy whereas from figure 9.3, the disturbance suppression is only 10% when $v = 0$ (m/s) using the Nyquist array method. Additionally, the disturbance suppression is 57% when $v = 20$ (m/s) using the Least effort control as it shows in figures 8.1i and 8.1j whilst for the Nyquist array method is only 10% when $v = 20$ (m/s) as it shows in figure 9.4. Hence, it can be clearly seen that the Least effort controller results in much better recovery responses disturbances for deterministic disturbances on the outputs.

Finally, the energy consumed by each controller is computed and compared according to equation 4.10. It can be clearly seen from figures 9.5 that the controller using Nyquist array method dissipates much more energy compared to the Least effort method as the range of the energy for the Nyquist array is proportional to 10^5 whereas for the Least effort, it is almost zero. This concludes that Least effort controller consumes the least control energy as pridicted.

Chapter 11

Conclusion and Future Work

In this paper, the analysis and design processes for an aircraft wing, flutter suppression at low-velocities, were presented. Measured data were used to construct the multiple input multiple output wing model from relating the wing deflections and applied forces, as given by Frazer *et al.* (1963).

In the beginning, the open loop transfer function models for this wing assembly were simplified in order to apply the Least effort control strategy. This had virtually no effect on the predicted wing performance. The Least effort control method was applied to the simplified transfer function. The inner loop design was applied to the system by plotting the Root Locus, (figure 4.5), for the equation 4.12 using MATLAB. In figure 4.6, the controller generated zero given by $b(s)$ was selected to improve the dynamics of the closed loop system. However, the results for the uncompensated system were not satisfactory as the input force at the leading edge played the role of a disturbance at the inner loop reference input when $(f = 0)$. This was unexpected because the responses, figure 7.5, show the poles of the system had been changed due to a high gain for the inner and outer loop controllers.

Thus, a second order active filter network was employed as the compensator for this system. Following the applications of this compensator, Least effort control was applied to the system model. Dual of inner and outer loops were employed as required by the theory. The Least effort performance index was minimised by minimising the sum of the squared gain elements to find the appropriate gain ratio n for the inner loop controller.

It is worth noting that, finding the appropriate gain ratio n was essential to give minimum energy dissipation. As shown in figure 8.2, the energy required, for the selected gain ratio n, is much smaller in comparison to all other gain ratios.

To maintain the desired steady state performance of the system whilst retaining energy consumption properties and the loop gains, the outer loop controller was computed. The outer loop gains were distributed between the forward path gain P and the feedback gain, as the gains were high. For implementation purposes, simple transformation techniques enabled the establishment of a conventional pre and feedback compensator structure.

Consequently, the transient behaviour of the system, leading and trailing edge deflections, for various values of velocity were presented and discussed. The responses were no longer highly oscillatory. The rise time and settling time were improved significantly. The desired steady state performance was virtually achieved. The disturbance recovery of approximately 55% was obtained. The control of the flutter vibrational problem for this wing arrangement was successfully achieved.

For comparison purposes, the Nyquist array method was also applied to the same wing arrangement. In order to apply single-input single-output control method, diagonal dominant conditions were achieved for this wing system model by using Gershgorin's bands theorem with adding a series, open loop pre-compensator. Proportional controllers were designed and applied to the system model, as indicated by equation 6.3. Although the transient responses were oscillatory, but the system was completely decoupled at steady state, as predicted.

Outer 10% disturbance suppression was achieved when $v = 0$ and 20 (m/s) which was very poor for this system using the Nyquist array method compared to the Least effort control method.

Finally, the energy dissipation for both controllers using the Least effort control and Nyquist array method were computed and compared. The model configuration used for computing the energy consumption considered the components of $u_1(s)$ and $u_2(s)$ negative. Squaring and adding these factors gave the dissipation required. It was evident that the calculated optimum gain ratio for Least effort controller dissipated the least control energy.

The Least effort control technique satisfied all the research objectives. There are many advantages when using this method. First, it is simpler and easier for implementation purposes. Second, the outer loop gains controls the disturbance recovery of the system. Third, the gains for this controller can be designed so that it will have the least energy consumption. Forth, it requires less electrical power and this leads to less wear, actuator activity, heat generation and noise. In order to apply this method, approximations may be essential to reduce the transfer function matrix numerator order. However, as demonstrated, remote zeros have little effect on the system response, giving excellent correspondence with the original dynamic descriptions.

Future work may include applying alternative control strategies to this flexible wing arrangement for purpose of comparison. However, the high gains required arise from the wing stiffness characteristics which cannot be altered.

Least effort control strategy is recommended for other system models. For higher dimensional 3 input - 3 output models, numerical minimisation methods would be appropriate.